Analysis of the peroxisomal malate/aspartate and lactate/pyruvate shuttle components and their metabolic function

Dissertation
for the award of the degree
"Doctor rerum naturalium" (Dr.rer.nat.)
of the Georg-August-Universität Göttingen

within the doctoral program Molecular Medicine
of the Georg-August University School of Science (GAUSS)

submitted by
Ignacio Felipe Lobos Matthei
from Santiago, Chile
Göttingen, 2021

Thesis Committee

Prof. Dr. Sven Thoms
Department of Child and Adolescent Health, University Medical Center Göttingen
Biochemistry and Molecular Medicine, Bielefeld University

Prof. Dr. Ralph Kehlenbach
Department of Molecular Biology, University Medical Center Göttingen

Prof. Dr. Michael Müller
Department of Neurophysiology and Sensory Physiology, University Medical Center Göttingen

Members of the Examination Board

Reviewer: **Prof. Dr. Sven Thoms**
Department of Child and Adolescent Health, University Medical Center Göttingen
Biochemistry and Molecular Medicine, Bielefeld University

Second Reviewer: **Prof. Dr. Ralph Kehlenbach**
Department of Molecular Biology, University Medical Center Göttingen

Further members of the Examination Board:

Prof. Dr. Michael Müller
Department of Neurophysiology and Sensory Physiology, University Medical Center Göttingen

PD Dr. Laura Zelarayán-Behrend
Institute of Pharmacology and Toxicology, University Medical Center Göttingen

Prof. Dr. Tiago Outeiro
Department of Experimental Neurodegeneration, University Medical Center Göttingen

Dr. Dieter Klopfenstein
Third Institute of Physics, Georg-August-Universität

Date of the oral examination: 28th of January 2022

Table of contents

Table of contents I
Abstract IV
List of figures V
List of tables VI
Introduction 1
Biology of peroxisomes 1
Peroxisome biogenesis 1
Import of proteins into peroxisomes 1
Metabolic processes within peroxisomes 2
Fatty-acid oxidation 2
Transport of metabolites 3
Transport of fatty acids 4
Export of products 4
Transport of cofactors 5
Functional translational readthrough 5
Shuttle of metabolites in peroxisomes 7
Lactate/pyruvate shuttle 7
Malate/aspartate shuttle 8
Aims of the project 10
Materials and methods 11
Materials 11
Bacterial strains 11
Mammalian cell lines 11
Materials and chemicals 11
Solutions 16
Methods 19
Cell culture 19
Differentiation of iPSCs into cardiomyocytes 19

CRISPR-Cas9 20
Immunofluorescence 21
Imaging and image analysis 22
siRNA transfection 24
Western blot 24
Glutathione Assay 25
Catalase Assay 26
Mitochondrial respiration 26
Metabolite quantification 27
Plasmid generation 28
Transfections 30
Proximity ligation assay 30
Results 32
Peroxisomal presence of MDH1 and LDHB is inducible by geneticin 32
Generation of cells lacking MDH1x and LDHBx 35
Deletion of MDH1x lowers the peroxisomal presence of MDH1 in HEK cells 37
Lack of MDH1x in iPSCs decreases MDH1 presence in peroxisomes 38
Effect of the lack of LDHBx in the presence of LDHB in peroxisomes of iPSCs 41
ROS levels increase in iPSCs lacking MDH1x and LDHBx 43
Mitochondrial respiration in iPSC MDH1Δx and LDHBΔx 44
Fatty acid metabolism in cells lacking MDH1Δx 47
Expression of AGC1, AGC2 and OGC with fluorescent tags indicates their presence in peroxisomes 48
Validation of antibodies against AGC1 51
Assessment of the peroxisomal localization of MAS transporters in HeLa 53
Evaluation of the peroxisomal presence of MAS transporters in iPSC-CM 56
Proximity between peroxisomal marker and AGC1, AGC2 and OGC supports their presence in peroxisomes 58
Discussion 61

Induction of readthrough leads to higher import of MDH1 and LDHB into peroxisomes 61

Deletion of its extension reduces the peroxisomal import of MDH1, but not of LDHB 63

Lack of MDH1x and LDHBx increase ROS levels in iPSCs.....65

Deletion of MDH1x and LDHBx has an effect on mitochondrial respiration 67

Peroxisomes in HeLa contain AGC1, AGC2 and OGC, while only AGC2 is present in peroxisomes of iPSC-CMs 69

References 74

Acknowledgments.....83

Curriculum vitae.....**¡Error! Marcador no definido.**

Abstract

Peroxisomes are responsible for several metabolic processes. Among the best known functions are the breakdown of peroxides like H_2O_2 and the catabolism of fatty acids by α- and β-oxidation.

The proper function of these pathways relies on the transport of not only the enzymes responsible of these processes, but also of the metabolites in play. Small molecules, up to 400 Da, can freely move through the peroxisomal membrane, but bulkier molecules like ATP, NAD^+, NADH, $NADP^+$ NADPH, and CoA, require of transporters to cross the peroxisomal membrane. So far, no protein responsible for the transport of NAD^+, nor NADH has been found.

In the last decade, two human proteins have been found to acquire a peroxisomal targeting signal by translational readthrough: malate dehydrogenase 1 (MDH1) and lactate dehydrogenase B (LDBH). Both these proteins are hypothesized to be part of independent shuttling systems, responsible of oxidizing NADH within peroxisomes, MDH1 as part of the malate/aspartate shuttle (MAS), and LDHB as part of the lactate/pyruvate shuttle (LS).

In this work, I showed evidence of the presence of both these shuttling systems within peroxisomes. First, by demonstrating an increase in peroxisomal colocalization of MDH1 and LDHB when readthrough levels are induced with antibiotics. Then, showing a reduction in the peroxisomal levels of MDH1 in cells lacking the extended MDH1 (MDH1x), which contains a PTS1 at the very C-termini. For LDHB, no reduction in the peroxisomal levels of LDHB were found in cells lacking LDHBx. Nevertheless, cells lacking both MDH1x and LDHBx showed metabolic differences than the wild type, with higher glutathione (GSH) levels and higher catalase activity levels.

Additionally, the presence of the carriers AGC1, AGC2 and OGC, responsible for the metabolite transport through the peroxisomal membrane in the MAS, was confirmed in HeLa cells, whereas in differentiated cardiomyocytes (iPSC-CM) only AGC2 was detected in peroxisomes.

Altogether, the evidence gathered in this work supports the hypothesis of a MAS shuttle in human peroxisomes, suggesting a mechanism for the reoxidation of NADH within peroxisomes.

List of figures

Figure 1 – Translational readthrough as means for increasing the peroxisomal protein diversity 7
Figure 2 – Proposed peroxisomal lactate/pyruvate shuttle 8
Figure 3 – Proposed peroxisomal malate/aspartate shuttle.....9
Figure 4 – Geneticin treatment induces the peroxisomal import of MDH1 and LDHB in in HEK and HeLa cells 34
Figure 5 – Deletion of the MDH1 and LDHB extensions does not affect their protein expression 36
Figure 6 – MDH1 shows less peroxisomal colocalization in HEK cells lacking MDH1x 38
Figure 7 – MDH1 colocalizes less with peroxisomes in iPSCs lacking MDH1x..... 40
Figure 8 – Effect of LDHB colocalization with peroxisomes in cells lacking LDHBx..... 42
Figure 9 – iPSC mutants MDH1Δx and LDHBΔx show higher glutathione levels and catalase activity than wild type..... 44
Figure 10 – The lack of peroxisomal MDH1 and LDHB has small but significant effects on mitochondrial respiration ……46
Figure 11 – Catabolism of dodecanoic acid in cells lacking MDH1x 48
Figure 12 – Plasmid-borne expression of AGC1, AGC2 and OGC demonstrates their presence at the peroxisome of HeLa cells 50
Figure 13 – Antibodies produced in rabbit and mouse against AGC1 are suitable for western blot, but only anti-AGC1 (rabbit) for immunofluorescence 52
Figure 14 – Antibodies against AGC1, AGC2 and OGC were validated with their GFP-tagged counterparts……53
Figure 15 – LAMP1, COX4 and PEX14 serve as peroxisomal colocalization controls in HeLa HeLa cells were immunostained against LAMP1, COX4, or PEX14, together with PMP70..... 55
Figure 16 – AGC1, AGC2 and OGC are present in peroxisomes of HeLa cells..... 56
Figure 17 – LAMP1, COX4 and PEX14 serve as controls for peroxisomal colocalization in iPSC-CM..... 57
Figure 18 – AGC2 is present in the peroxisomes of iPSC-CMs 58
Figure 19 – Proximity between MAS transporters and PMP70 adds evidence to their presence in peroxisomes 60

List of tables

Table 1 – Disposables 11
Table 2 – Equipment and instruments 12
Table 3 – Reagents 13
Table 4 - Enzymes 16
Table 5 – Primary antibodies used in Immunofluorescence 22
Table 6 – Secondary antibodies used in immunofluorescence 22
Table 7 – Primary antibodies used for western blot 25
Table 8 – Secondary antibodies used for western blot 25
Table 9 – Mass spectrometer settings 28
Table 10 – Antibodies for PLA 31

Introduction

Biology of peroxisomes

Peroxisomes are ubiquitous single-membrane organelles, which are present in almost all eukaryotic cells. They are dynamic structures that contain over 50 different enzymes in mammals, and are able to modulate their number, size, and content, in response to cellular requirements (Wanders and Waterham, 2006). Peroxisomes were first discovered in the fifties, through the analysis of mouse kidney sections by electron microscopy (Rhodin, 1954). Yet, they were first biochemically characterized during the sixties, and then the name “peroxisome” was coined, since its main function at the time was thought to be its involvement in the peroxidase metabolism (De Duve and Baudhuin, 1966).

Peroxisome biogenesis

Peroxisomes are formed following two distinct routes, either by the fission of already mature peroxisomes, or *de novo*, which starts in the ER and continues through the acquisition of matrix proteins from the cytosol. In biogenesis through fission, activated peroxisomes are first elongated, followed by constriction and division of the now tubular organelle, and finalizes with the import of matrix and membrane proteins (Schrader et al., 2016). Interestingly, most proteins of the fission machinery are shared between peroxisomes and mitochondria (Fujiki et al., 2020). For biogenesis *de novo*, two kinds of preperoxisomal vesicles are produced in the ER, each containing different portions of the peroxisomal transport machinery. Then, these two types of vesicles fuse in a heterotypic manner in the cytosol, producing peroxisomes with a functional transport machinery that can now import the peroxisomal matrix proteins translated in the cytosol (van der Zand et al., 2012).

Import of proteins into peroxisomes

The production of the peroxisomal matrix proteins takes place in the cytosol, where they are translated by free ribosomes before being imported into peroxisomes. Most of the peroxisomal proteins contain one of two peroxisomal signals, a peroxisomal targeting signal 1 (PTS1) at the C-terminal portion, or a PTS2 at the N-terminal region of the protein (Gould et al., 1989; Smith and Aitchison, 2013; Walton et al., 1995). The consensus sequence of PTS1 is the tripeptide serine-lysine-leucine (SKL), but, since peroxisomal import is possible with a more varied combination of tripeptides, the definition can be expanded to [S/A/C]-[K/R/H]-L (Brocard and Hartig, 2006). For

PTS2, the nine-peptide consensus sequence, [R/K]-[L/V/I]-[X]5-[H/Q]-[L/A], is looser than in PTS1, and its distance from the start varies from gene to gene (Rachubinski and Subramani, 1995). In mammals, proteins containing a PTS1 are recognized and bound by the peroxisomal biogenesis factor 5 (PEX5), while in proteins with a PTS2 this is done by PEX7 (Braverman et al., 1997; Dodt and Gould, 1996). Interestingly, some nucleotides upstream of PTS1 influence the strength of the interaction between PEX5 and the PTS1-holding proteins (Lametschwandtner et al., 1998).

After binding the cargo, these chaperones move to the peroxisomal membrane where they dock to a portion of the protein complex known as importomer. This complex translocates then the cargo together with the chaperone into the peroxisomal lumen, where it releases them both (Brown and Baker, 2008). Impressively, this system is also capable of importing fully folded proteins, as well as oligomers (Léon et al., 2006). The ability to transport fully functional oligomers allows for piggy-back import to happen. That is, the co-recruitment of a protein that lacks a peroxisomal signal, through prior oligomerization with a PTS-containing protein (Thoms, 2015).

Metabolic processes within peroxisomes

The recruitment of proteins within the peroxisomal matrix is necessary for the several metabolic processes it harbors. Among these are the β-oxidation of long- and very long-chain fatty acids (LCFA and VLCFA), the α-oxidation of branched-chain fatty acids like phytanic acid, and the biosynthesis of ether-phospholipids. In addition, peroxisomes bear the metabolism of glyoxylate, which prevents the accumulation of the toxic metabolite oxalate, as well as the catabolism of amino acids, and the generation of NADPH within peroxisomes through the pentose phosphate pathway. Finally, the metabolism of reactive oxygen and nitrogen species (ROS and NOS) also takes place in peroxisomes, as well as the oxidation of polyamines (Wanders and Waterham, 2006).

Fatty-acid oxidation

Through the wide variety of metabolic pathways they harbor, peroxisomes consume over 10% of the oxygen in the cell (Legakis et al., 2002). Most of the oxygen they consume is converted into H_2O_2, while a small amount is converted into superoxide anions, both of which increase the ROS stress within peroxisomes (Singh, 1996). Among the enzymes responsible for ROS metabolism within peroxisomes, the one with higher expression levels is catalase, able to decompose H_2O_2 catalytically into H_2O and O_2, or through a peroxidatic reaction into H_2O and an oxidized proton donor (Fransen et al., 2012). Other peroxisomal matrix enzymes like glutathione S-transferase (GST), superoxide dismutase 1 (SOD1), epoxide hydrolase 2 (EPHX2),

and peroxiredoxin 5 (PRDX5), also contribute in the removal of ROS (Fransen et al., 2012).

In order to be imported into peroxisomes, fatty acids are first converted into acyl-CoAs by peroxisomal proteins (Watkins and Ellis, 2012). Within peroxisomes, fatty acids can be catabolized in different pathways according to their nature. For example, β-oxidation is reserved for saturated unbranched and 2-methyl-branched fatty acids. These fatty acids go through the steps of dehydrogenation, hydratation, dehydrogenation and thiolysis, resulting in the shortening of two carbons while generating one molecule of H_2O_2 from O_2, and a molecule of NADH through the reduction of NAD^+ (Wanders and Waterham, 2006). Additionally, if a fatty acid contains a methyl group at the third carbon, catabolism will first occur through α-oxidation. In this pathway, fatty acids undergo a step of 2-hydroxylation, a decarboxylation and a dehydrogenation, resulting in a shortening in length of one carbon of the fatty acid, with the production of CO_2, succinate and NADH (Jansen and Wanders, 2006). Interestingly, α-oxidation is not stereo-selective, so fatty acids are catabolized in the (*S*)- and (*R*)-configuration, while β-oxidation only accepts fatty acids in (*S*)-configuration, meaning that (*R*)-configured fatty acid will have to be isomerized by a racemase for further β-oxidation (Ferdinandusse et al., 2000).

Transport of metabolites

To function properly, the various metabolic pathways within peroxisomes require of metabolites and cofactors that need to be transported through the peroxisomal membrane. The peroxisomal membrane allows the free movement of molecules up to 400 Da. Yet, bulky molecules such as the cofactors ATP, NAD^+, NADH, $NADP^+$, NADPH, and CoA, are not able to cross freely (Antonenkov et al., 2004; Antonenkov and Hiltunen, 2012). Therefore, it is thought that small solutes cross the peroxisomal membrane through channels, while larger metabolites require of specific transporters (Antonenkov and Hiltunen, 2012). So far, one pore-forming channel has been reported in mammals, PXMP2 (PMP22), which is able to transport metabolites up to 300 Da, such as glycerol-3-phosphate (G3P) and dihydroxyacetone phosphate (DHAP), both metabolites required in ether phospholipid biosynthesis (Rokka et al., 2009). Additionally, in yeast, PMP11 was reported to form non-selective channels for metabolites under 400 Da (Mindthoff et al., 2016).

Among the metabolite-specific transporters, the peroxisomal presence of the monocarboxylate transporter 1 (MCT1, SLC16A1) and 2 (MCT2, SLC16A7), both part of the solute carrier (SLC) family, has been reported in rat liver (McClelland et al., 2003). MCT1 is ubiquitously expressed and is mainly located in the plasma membrane

and nucleus, while MCT2 is localized in the plasma membrane, but unlike MCT1, its expression is tissue specific (Chornyi et al., 2021). Functionally, both MCT1 and MCT2 can transport monocarboxylates like lactate, pyruvate and acetoacetate (Felmlee et al., 2020). Another transporter of this family in peroxisomes is PMP34 (SLC25A17), which was first thought to be an ATP transporter, but later studies suggested its ability to transport CoA, FAD, and to a lesser extent NAD^+ (Agrimi et al., 2012; Visser et al., 2002).

Transport of fatty acids

The import of fatty acids into peroxisomes is crucial for their catabolism. In this respect, three members of the ATP-binding cassette (ABC) superfamily are responsible for the import of fatty acids: ABCD1 (also known as ALDP), ABCD2 (also known as ALDR), and ABCD3 (also known as PMP70). These three transporters possess overlapping substrate specificities, especially between ABCD1 and ABCD2, but they all differ in their substrate preference. While ABCD1 prefers to transfer C24:0 and C26:0, ABCD2 is more prone to take C22:0, in addition to the poly unsaturated fatty acids C22:6 and C24:6. Finally, ABCD3 prefers C16:0, pristanic acid, dicarboxylic fatty acids, and the unsaturated fatty acids C18:1, C18:2, C20:5 and C22:6 (Kemp et al., 2011; Morita and Imanaka, 2012; Roermund et al., 2008; van Roermund et al., 2014, 2011).

Export of products

The export of the products of the peroxisomal metabolic pathways like β-oxidation is also key for their utilization in other organelles and processes. Importantly, the products of β-oxidation are CoA-derivatives, which due to their size remain held in the peroxisomal lumen. Because of this, their CoA moiety needs to be removed or exchanged for further transport. Different routes are available in peroxisomes for this purpose, for example, the carnitine system is responsible for converting acetyl-, propionyl- and acyl-CoA; exchanging the CoA for carnitine, which is small enough to cross the membrane (Farrell et al., 1984; Ferdinandusse et al., 1999). Other example are the acyl(acetyl)-CoA thioesterases (ACOTs), which mediate the hydrolysis of acyl(acetyl)-CoA into CoA and free fatty acids (or acetic acid) with different specificities (Kirkby et al., 2010). In humans, ACOT4 hydrolyzes LCFA-CoAs, succinyl-CoA and glutaryl-CoA, while ACOT8 prefers medium- and long-chain fatty acyl-CoAs (Hunt et al., 2006; Jones et al., 1999). In the case of bile acids, the acid-CoA:amino adic N-acyltransferase (BAAT) mediates amidation of bile acids into tauro- and glycol-bile acids and free CoA by bile (He et al., 2003; Pellicoro et al., 2007). Nevertheless, even though is accepted that the removal of CoA is sufficient to able

fatty acids out of the peroxisome, it is not clear if this occurs through simple diffusion, or another transport mechanism (Antonenkov and Hiltunen, 2012).

Transport of cofactors

The import of cofactors is also essential for the correct functioning of several peroxisomal enzymes, although still not fully understood. For example, the cofactor flavin adenine dinucleotide (FAD) is proposed to enter peroxisomes either through PMP34, or through co-import with already fully folded proteins (Walton et al., 1995). As with the cofactor FAD, flavin mononucleotide (FMN) is also thought to be co-imported with the fully folded proteins in which it acts as a cofactor, the 2-hydroxyacid oxidases HAO1, HAO2, and HAO3 (Jones et al., 2000).

Even though the presence of NAD^+ is key for some of the peroxisomal processes mentioned above, it remains unclear how this cofactor, or its reduced version, NADH, crosses the peroxisomal membrane (Jansen and Wanders, 2006; Poirier et al., 2006). Yet, the import of two enzymes into peroxisomes might bring light to this issue, specifically, a subpopulation of malate dehydrogenase 1 (MDH1) and lactate dehydrogenase B (LDHB), which reach peroxisomes thanks to a C-terminal extension containing a PTS1.

Functional translational readthrough

Translational readthrough refers to the process in which a ribosome reads a stop codon as a sense codon, and continues translating until the next stop codon is met. In principle, such an event can be considered an error, with a chance of around 0.1% of occurring (Harrell et al., 2002; Namy et al., 2001). Yet, it has been shown that different organisms make use of such mechanism to expand their protein population without a great increase in their genome, cases in which the readthrough levels of the total expression of a particular protein increase up to 10% (Loughran et al., 2014). The propensity to which a ribosome by-passes a stop codon is influenced by factors like the stop codon context (SCC), which contemplates about 10 nucleotides surrounding the stop codon. Additionally, the stop codon itself plays a role in readthrough propensity, being UGA the stop codon with the highest propensity to undergo readthrough, followed by UAG and UAA with the lowest (McCaughan et al., 1995; Namy et al., 2001; Schueren and Thoms, 2016).

Furthermore, translational readthrough may be employed by the cell in order to achieve different biological goals, in which case is named functional translational readthrough (FTR). For example, in Moloney leukemia virus, a ratio between its polymerase (pol) and the group-specific antigen (gag) is achieved through FTR. Here,

the translation of the pol is produced only by readthrough of the protein gag, producing a gag-pol chimera that is later cleaved, making the levels of pol dependent on the expression of gag (Felsenstein and Goff, 1988; Yoshinaka et al., 1985). In astrocytes, aquaporin 4 (AQP4) undergoes FTR with a propensity of approximately 10%, resulting in the expression of an extended version of AQP4, which is associated with the formation of smaller and more homogeneous pores than its parental protein (De Bellis et al., 2017). In addition, a targeting signal can be added through FTR in order to direct a protein into a new organelle. Such is the case in *Ustilago maydis,* where a PTS1 is part of the extension of the FTR-version of its 3-phosphoglycerate kinase (PGK), D-ribulose-5-phosphate-3-epimerase, and aldehyde reductase (Freitag et al., 2012).

In humans, MDH1 and LDHB are the first enzymes described to gain a PTS1 signal through FTR. Both these proteins were identified with a combination of a PTS1 prediction and a genome-wide screening of the readthrough propensity from a total of 200,000 candidates, resulting in LDHB and MDH1 as the candidates with the highest score (Schueren et al., 2014). Experimentally, it was proven that a 1.6% of the translated LDHB mRNA undergoes FTR, resulting in the translation of 7 extra amino acids before the next stop codon is met, and thus, giving rise to the extended version of LDHB, LDHBx (Schueren et al., 2014). Interestingly, since LDHB forms tetramers, the addition of the PTS1 at the C-terminus allows the co-import of three isoenzymes lacking the targeting signal (Figure 1) (Thoms, 2015). In the case of MDH1, it was estimated that about 4% of its translated protein is the product of FTR, for which the translation of 19 amino acids before the second stop codon results in the generation of the extended MDH1x (Hofhuis et al., 2016). In addition, since MDH1 forms dimers, the co-import of just one isoform lacking the peroxisomal signal would be possible (Hall et al., 1992).

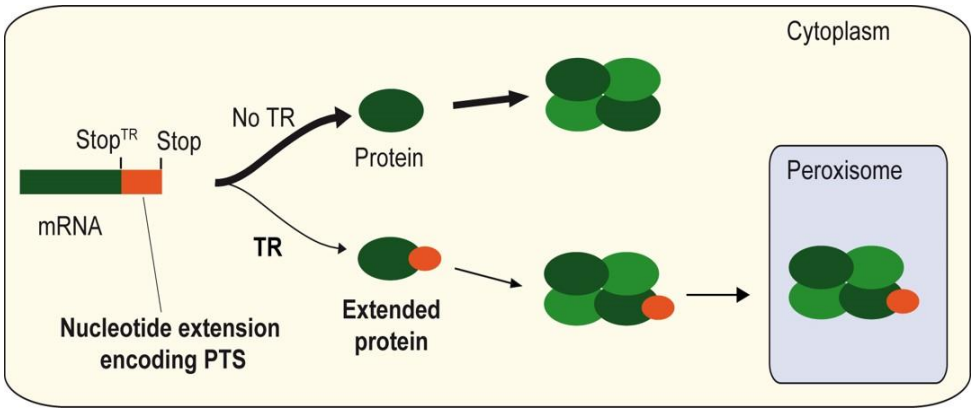

Figure 1 – Translational readthrough as means for increasing the peroxisomal protein diversity.
Translational readthrough (TR) of LDHB leads to the addition of a PTS1 signal in the C-terminal portion of the protein, producing LDHBx. The extended version can form tetramers in the cytosol, which will be transported into peroxisomes as a whole by the peroxisomal import machinery. Image from Bersch et al., 2018.

Shuttle of metabolites in peroxisomes

The presence of LDHB and MDH1 in peroxisomes supports the existence of shuttling systems that mediate the oxidation of NADH within peroxisomes.

Lactate/pyruvate shuttle

Lactate dehydrogenase mediates the reversible reduction of pyruvate into lactate, with the oxidation of the cofactor NADH into NAD^+ (Le et al., 2010). Humans harbor three genes coding for LDH: LDHA, which has higher levels in skeletal muscle and liver, LDHB, which is mostly present in cardiac muscle, and LDHC, which only present in testis (Chornyi et al., 2021). Interestingly, the presence of LDH in peroxisomes has been suggested since the seventies, when its activity was measured in rat liver and kidney (McGroarty et al., 1974). Also, indications of the involvement of LDH in the oxidation of peroxisomal NADH were suggested indirectly over the years, for example by the increase in activity of β-oxidation, when pyruvate was added in isolated rat peroxisomes (Osmundsen, 1982). Another indication was observed in medium of isolated peroxisomes from rat liver, in which pyruvate addition would lead to fully oxidation of NADH, oxidation which was also affected by the LDH-inhibitor oxamate (Baumgart et al., 1996). Using electron microscopy, the peroxisomal presence of $LDHA_4$ and $LDHA_3B$ was reported in sections of rat liver (Baumgart et al., 1996). Finally, by quantitative proteomics, the presence of LDHA was showed in human liver (Gronemeyer et al., 2013). All this evidence points to a peroxisomal lactate/pyruvate shuttling system in which lactate and pyruvate are transported through the membrane and NADH is oxidized into NAD^+ within the peroxisomal lumen and reduced in the cytosol by different LDH populations (Figure 2).

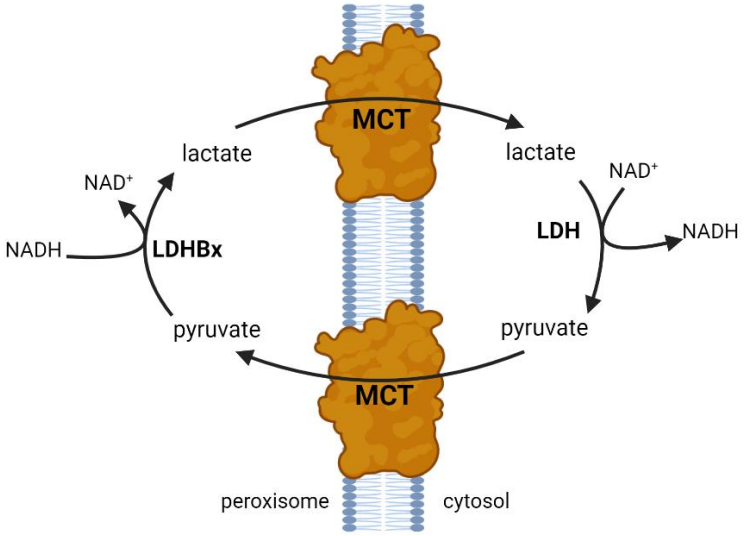

Figure 2 – Proposed peroxisomal lactate/pyruvate shuttle.
The lactate/pyruvate shuttle is a proposed mechanism for the oxidation of NADH within peroxisomes. Here, pyruvate is converted into lactate by LDH in a NADH-dependent manner within peroxisomes. Lactate is then exported into the cytosol by a monocarboxylate transporter (MCT), where LDH mediates its conversion into pyruvate, this time consuming NAD^+. Pyruvate can finally re-enter peroxisomes through a MCT, closing the cycle.

Malate/aspartate shuttle

Malate dehydrogenase catalyzes the conversion of oxaloacetate into malate, while it oxidizes NADH into NAD^+. In humans, two different genes give rise to MDH isomers with different locations: MDH1 being the cytosolic version, while MDH2 is directed to mitochondria (Chornyi et al., 2021). Additionally, as mentioned above, a third isomer is produced through the FTR of MDH1, event which adds a PTS1 signal and generates the peroxisomal MDH1x (Hofhuis et al., 2016). The peroxisomal presence of MDH1 has been previously reported by a proteomics analysis in human liver, as well as in mouse kidney and mouse liver (Gronemeyer et al., 2013; Wiese et al., 2007). Even though the presence of a peroxisomal malate/aspartate shuttle (pMAS), resembling mitochondria, was suggested already in the seventies as a way of oxidizing NADH within peroxisomes, there is still debate about its presence in mammals (McGroarty et al., 1974).

The mitochondrial MAS (mMAS), takes part within mitochondria and in the cytosol. Inside mitochondria, malate is converted into oxaloacetate while the cofactor NAD^+ is reduced, replenishing the NADH pool for its use in oxidative phosphorylation. Then, the enzyme glutamate oxaloacetate transaminase 2 (GOT2) mediates the transamination of oxaloacetate and glutamate into aspartate and 2-oxoglutarate.

Afterwards, aspartate is exported from the mitochondria in exchange for cytosolic glutamate by one of the aspartate-glutamate carriers, AGC1 (SLC25A12), or AGC2 (SLC25A13). In the cytosol, GOT1 catalyze the same reaction in the opposite direction, generating oxaloacetate and glutamate from aspartate and 2-oxoglutarate. Oxaloacetate is then converted into malate by MDH1 with the oxidation of NADH into NAD^+, which can support again glycolysis. Finally, malate is imported into mitochondria in exchange for 2-oxoglutarate by the 2-oxoglutarate/malate carrier (OGC, SLC25A11), closing the cycle (Amoedo et al., 2016). In this context, the presence of a pMAS would answer the question of how NADH is oxidized within peroxisomes, and explain the presence of MDH1x (Figure 3).

Altogether, the evidence points to the presence of shuttling systems within peroxisomes, which main function is the oxidation of peroxisomal NADH.

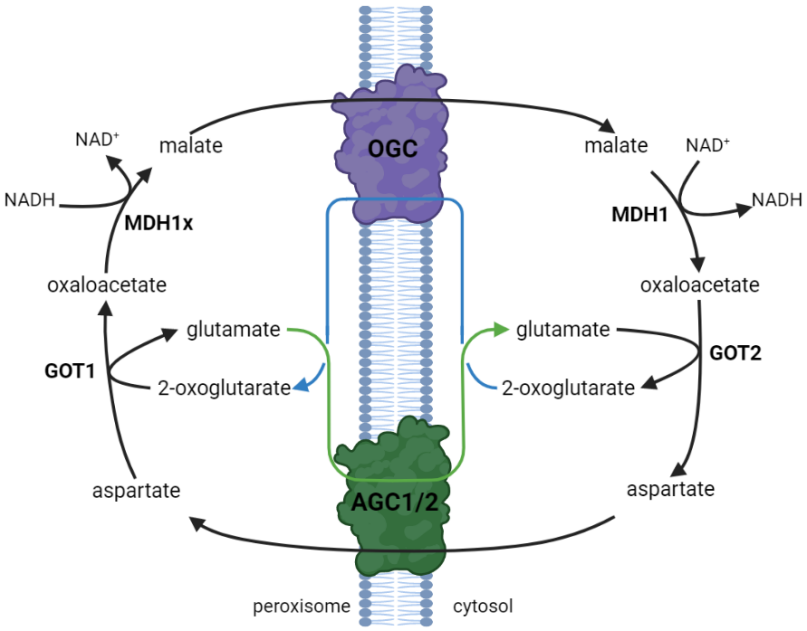

Figure 3 – Proposed peroxisomal malate/aspartate shuttle.
Resembling mMAS, although in the opposite direction, the presence of pMAS is presented as a mechanism for the oxidation of NADH within peroxisomes. Here, metabolites cross the peroxisomal membrane through transporters: malate against 2-oxoglutarate through OGC, and aspartate against glutamate through AGC1 or AGC2. Mirrored reactions between peroxisomes and cytosol replenish the peroxisomal NAD^+ pool, while increasing the cytosolic NADH pool.

Aims of the project

This project intends to gain evidence of the presence of a MAS and LS in peroxisomes. First, I will use colocalization measurements to analyze a possible correlation between FTR and the presence of MDH1 and LDHB in peroxisomes.

Then, in order to assess functional aspects of MDH1x, I will use CRISPR/Cas to generate cells lacking the readthrough-extension of this protein. Additionally, the metabolic effects of the lack of MDH1x and LDHBx will be assessed by measurement of catalase activity, glutathione levels, mitochondrial respiration, and fatty acid metabolism.

Finally, the cellular localization of the MAS metabolite carriers AGC1, AGC2 and OGC will be analyzed. I will use recombinant fluorescently tagged proteins, antibodies, and proximity ligation assay to study the peroxisomal colocalization of the MAS components.

Materials and methods

Materials

Bacterial strains

For plasmid generation Bio*Blue* Chemically Competent Cells (BIO-85036 ≥10^8 cfu/µg of pUC19) were used.

Mammalian cell lines

HeLa cells	Immortal human cell line from cervical carcinoma.
HEK293	Immortalized cell line derived from human embryonic kidney.
HEK293 MDH1Δx	Mutated HEK cell lacking the extension after the first stop codon of MDH1.
iPSC	Induced pluripotent stem cell derived from human skin fibroblasts.
iPSC MDH1Δx	Cell lacking the PTS1 extension after the first stop codon of MDH1.
iPSC LDHBΔx	Mutant cell line lacking the PTS1 at the readthrough extension of LDHB.
iPSC-CM	Cardiomyocytes derived from iPSCs.

Materials and chemicals

Table 1 – Disposables

Material	Product number	Manufacturer
Blotting paper sheets	FT-2-520-580600 K	Sartorius
Cell scrapers	83,183	Sarstedt
Combitips advanced®, 5 mL	0030 089.456	Eppendorf
Conical tubes, 15 mL, sterile	62.554.502	Falcon
Conical tubes, 50 mL, sterile	62.547.254	Falcon
Cryo 1°C freezing containers for cell culture	5100-0001	Nalgene
Cryo tubes, 1.8 mL	368632	Thermo Scientific
Cryotube 2ml	126263	Greiner
Filters, Minisart, pore size 0.2 µm	16534K	Sigma Aldrich
Flasks for cell culture, 75 cm^2	658175	Greiner Bio-One
Glass microscope slides	631-0411	Menzel-Gläser
Gloves	7696900	Labsolute
Microplate, 96-well, flat bottom	655101	Greiner Bio-One
Microscope cover glasses 12 mm Ø, No. 1.5H	117520	Marienfeld

Microscope cover glasses 18 mm Ø, No. 1.5H	117580	Marienfeld
Nitrocellulose blotting membrane, 0.45 µm	10600002	GE Healthcare
Parafilm®, M, laboratory film	PM996	Bemis
Pasteur pipettes	7691060	Labsolute
Petri dishes, 92x16 mm	82.1473.001	Sarstedt
Pipette filter tips 10 µL	70.111.4.210	Sarstedt
Pipette filter tips 100 µL	70.760.212	Sarstedt
Pipette filter tips 1250 µL	VT0270	Biozym
Pipette tips 10 µL	70,113	Sarstedt
Pipette tips 200 µL	70.760.002	Sarstedt
Plates for cell culture, 12-well	665 180	Greiner Bio-One
Plates for cell culture, 24-well	662 160	Greiner Bio-One
Plates for cell culture, 6-well	CC7672-7506	Starlab
Plates for cell culture, 6-well	353046	Falcon
Reaction tubes, Safe-Lock, 2 mL	30120094	Eppendorf
Safe-Lock tubes 1,5ml	30120086	Eppendorf
Safe-Lock tubes 2ml	30120094	Eppendorf
Seahorse XF24 V7 PS Microplates	100777-004	Agilent
Seahorse XFe24 FluxPak	102340-100	Agilent
Serological pipettes, 10 mL	86.1254.001	Sarstedt
Serological pipettes, 2 mL	86.1252.001	Sarstedt
Serological pipettes, 25 mL	86.1685.001	Sarstedt
Serological pipettes, 5 mL	86.1253.001	Sarstedt

Table 2 – Equipment and instruments

Instrument	**Manufacturer**
Analytical balance 2001MP2	Sartorius
Cell counting chamber, Neubauer	Brand GmbH + Co KG
Centrifuge, 5417R	Eppendorf
Centrifuge, Mikro 200R, rotor 2424-B	Andreas Hettich GmbH & Co.KG
Centrifuge, Universal 320, rotor 1619	Andreas Hettich GmbH & Co.KG
CO2 incubator, HeraCell VIOS 160i	Thermo Fisher
ECL and fluorescence imager, ChemoStar	Intas
Electrophoresis cell, Mini-PROTEAN Tetra Cell	Bio-Rad
Electrophoresis systems for agarose gels	Analytik Jena

Gel documentation system	BioDocAnalyze
Laminar flow hood, LaminAir HB 2448	Heraeus
Light microscopem, Nikon ECLIPSE TS100	Nikon
LUNA-FL™ Dual Fluorescence Cell Counter	Logos biosystems
Microplate reader, BioTek Synergy Mx	BioTek® Instruments
Pipette, manual, ErgoOne®, 2.5 µL	Starlab
Pipette, manual, ErgoOne®, 10 µL	Starlab
Pipette, manual, ErgoOne®, 200 µL	Starlab
Pipette, manual, ErgoOne®, 1000 µL	Starlab
Power supply, Standard PowerPack P25	Biometra
Rocking platform	Biometra
Seahorse XFe24 Analyzer	Agilent
Semi-dry blotting system, Biometra FasBlot	Biometra
Spectrophotometer, ND-1000	NanoDrop™
Thermo block, TB2m Biometra	Biometra
Thermo block, Thermomixer compact	Eppendorf
Thermocycler T3	Biometra
Thermocycler, labcycler	SensoQuest
Vortex mixer, Genie 2™	Bender & Hobein
Water bath	Memmert
Xevo G2-S mass spectometer	Waters
Zeiss Axio Observer 7 with Apotome.2	Carl Zeiss

Table 3 – Reagents

Reagent	**Product number**	**Manufacturer**
0.25% Trypsin-EDTA	25200056	Thermo Fisher
2-Propanol	1096341000	Merck
Agarose	Bio-41025	Bioline
Albumin, human recombinant	A9731	Sigma-Aldrich
Ammonium persulfate (APS)	113H0315	Serva Electrophoresis
Antimycin A	A8674	Sigma-Aldrich
B27 with Insulin	17504044	Thermo Fisher
BCA Assay Reagent A	UP95424A	Interchim
BCA Assay Reagent B	UP95425A	Interchim

Bovine serum albumin (BSA), Fraktion V	8076,2	Carl Roth
Bromophenol blue	8122-5g	Merck
CHIR99021	361559	Millipore
cOmplete™ Protease Inhibitor Cocktail Tablets	4693116001	Roche
Dimethyl sulfoxide (DMSO)	39757	Serva Electrophoresis
Disodium phosphate	T877	Carl Roth
DMSO	D2650	Sigma-Aldrich
Dulbecco´s phosphate buffered saline (PBS)	D8537	Sigma-Aldrich
Dulbecco's Modified Eagle Medium (DMEM), 4.5 g/L D-glucose	F 0445	Biochrom
Duolink® In Situ PLA® Probe Anti-Mouse PLUS	DUO92001	Sigma-Aldrich
Duolink® In Situ PLA® Probe Anti-Rabbit MINUS	DUO92005	Sigma-Aldrich
Duolink® In Situ Detection Reagents Red	DUO92008	Sigma-Aldrich
EDTA Solution pH 8,0	A3145.0500	Life technologies
Ethanol	1.00983.2500	Merck
Ethylene glycol tetraacetic acid (EGTA)	3054,2	Carl Roth
Ethylenediaminetetraacetic acid (EDTA)	CN06.1	Carl Roth
FCCP (Carbonyl cyanide 4-(trifluoromethoxy)phenylhydrazone)	C2920	Sigma-Aldrich
Fetal bovine serum (FBS) "GOLD"	A15-151	PAA Laboratories
Geltrex	A1413201	Gibco
GeneRuler™, DNA Ladder Mix	SM0331	Fermentas Life Science
Gentamicin	HN09.2	Carl Roth
GlutaMAX™ -I (100x)	35050-061	Gibco
HEPES Buffer (pH 7.0-7.6)	H3662	Sigma-Aldrich
Hydrochloric acid (HCl)	1003141000	Merck
Imidazole buffer solution 1 M	68268	Sigma-Aldrich
IWP2	681671	Millipore
Laminin from Engelbreth-Holm-Swarm murine sarcoma basement membrane	L2020	Sigma-Aldrich
L-aminocarnitine	A603400	Toronto Research Chemicals
L-Ascorbic Acid 2-Phosphate	A8960	Sigma-Aldrich
LB-Agar (lurial/Miller)	X969.1	Carl Roth
LDHB Silencer® select	4427038	ambion
Lipofectamine™ CRISPRMAX™ Cas9 transfection reagent	CMAX00001	Integrated DNA technologies
Lumi-Light Plus Western Blotting Substrate	12 015 196 001	Roche
LB medium	X968.1	Carl Roth

MDH1 Silencer® select	4427037	ambion
Methanol	8045	J.T. Baker
Methyl dodecanoate	20-1200	Larodan
Milk powder	T145.3	Carl Roth
Monopotassium phosphate (KH_2PO_4)	3904	Carl Roth
N,N,N′,N′-Tetramethylethan-1,2-diamin (TEMED)	2367,1	Carl Roth
Nonidet™ P (NP)-40	74385	Fluka Analytical
nuclease-free duplex buffer	11-01-03-01	Integrated DNA technologies
Oligomycin	O4876	Sigma-Aldrich
Opti-MeM	31985062	Thermo Fisher
PageRuler™ Prestained Protein Ladder	26616	Thermo Fisher
Paraformaldehyde (PFA), 4% in PBS	19943 1 LT	Affymetrics
Phenylmethane sulfonyl fluoride (PMSF)	A0999.0005	Applichem
Ponceau-S solution	P7170	Sigma-Aldrich
Potassium acetate	T874	Carl Roth
ProLong Gold antifade reagent with DAPI	P36935	Invitrogen
Rotenone	R8875	Sigma-Aldrich
Rotiphorese®NF-Acrylamide/Bis-solution 30 (29:1)	3029.1	Carl Roth
RPMI 1640 with HEPES with GlutaMax	72400021	Thermo Fisher
RPMI 1640 without HEPES without Glucose	11879020	Thermo Fisher
Seahorse XF Calibrant Solution	100840-000	Agilent
Seahorse XF RPMI medium, pH 7.4	103576-100	Agilent
siGENOME Human SLC25A12 siRNA	M-007471-01-005	Horizon
Sodium azide (NaN_3)	K305	Carl Roth
Sodium bicarbonate ($NaHCO_3$)	965	Carl Roth
Sodium cacodylate trihydrate	C4945	Sigma-Aldrich
Sodium chloride (NaCl)	3957.1	Carl Roth
Sodium dodecyl sulfate (SDS), 20% solution	1057	Carl Roth
Sodium hydroxide (NaOH)	6771.1	Carl Roth
StemFlex Medium	A3349401	Gibco
Thiazovivin	420220	Millipore
tracrRNA	1072532	Integrated DNA technologies
Tris	5429.3	Carl Roth
Triton X-100	T8787-100ML	Sigma-Aldrich

Titanium(IV) oxysulfate	13825-74-6	Sigma-Aldrich
Tryptan blue, 0.5% (w/v) in physiologocal saline	L2143	Biochrom
Tween® 20	8.22184.0500	Merck
β-Mercaptoethanol	M3148-25ml	Sigma-Aldrich

Table 4 - Enzymes

Enzyme	Product number	Manufacturer
AgeI	R0552S	Biolabs
Alt-R® S.p. HIFI Cas9 Nuclease V3	1081060	Integrated DNA technologies
HindIII-HF	R31045	Biolabs
KAPA HiFi DNA Polymerase	7958846001	Kapa Biosystems
KnpI	R3142L	Biolabs
PstI	R0140M	Biolabs
RNAse A	556746	Calbiochem
T4 DNA Ligase	EL0014	Thermo Fisher
Trypsin/EDTA solution, 0.05%/0.02% (w/v)	L2143	Biochrom

Solutions

Agarose gel (1%)

TBST buffer

1% (w/v) agarose

0.008% (v/v) GelRed

Catalase substrate

20 µM imidazole buffer (pH 7)

0.1% (w/v) BSA

0.001% (v/v) H_2O_2

Cardio culture medium

RPMI 1640 with HEPES and GlutaMax

2% (v/v) B27 supplement with insulin

Cardio digestion medium

Cardio culture medium

20% (v/v) Fetal bovine serum

2 µM Thiazovivin

CM differentiation supplement 100x

68 mM L-ascorbic acid 2-phosphate

5% (w/v) albumin, human recombinant

Cardio differentiation medium

RPMI 1640 with HEPES and GlutaMax

1% (v/v) CM differentiation supplement 100x

Cardio selection medium

RPMI 1640 without glucose nor HEPES

1% (v/v) CM differentiation supplement 100x

4 mM Lactate/HEPES

PBS - pH 7.4

2.7 mM KCl

1.8 mM KH2PO4

137 mM NaCl

8.1 mM Na2PO4

PBS-T

0.05% (v/v) Tween20 in PBS

Plasmid isolation buffer P1

50 mM Tris/HCl, pH 8.0

10 mM EDTA

100 µg/mL RNAse A

Plasmid isolation buffer P2

200 mM NaOH

1% (w/v) SDS

Plasmid isolation buffer P3

3 M Potassium acetate, pH 5.5

RIPA Buffer

2 mM EDTA, pH 8.0

5 mM EGTA

0.1% (w/v) SDS

1% (v/v) NP-40

150 mM NaCl

25 mM Tris/HCl, pH 7.4

1:25 Complete™ protease inhibitors

SDS-PAGE Buffer

1.92 M Glycine

25 mM Tris Base

1% (w/v) SDS

Stopping solution

0.34% (w/v) $TiOSO_4$

1 M H_2SO_4

Transfer Buffer

260 mM Glycine

20% (v/v) Methanol

25 mM Tris

TBST

150 mM NaCl

20 mM Tris

0.1% Tween 20

TVBE buffer

1 mM $NaHCO_3$

1 mM EDTA

0.1% (v/v) ethanol

0.01% Triton X-100

Methods

Cell culture

HEK and HeLa

HEK and HeLa were maintained in high glucose DMEM supplemented with 10% FCS and 1% glutamate. When a confluence of around 80% was met, cells were passaged into new flasks. For this, cells were washed with 10 mL PBS and then incubated for 5 minutes with 1 mL of trypsin at 37°C and 5% CO_2. Once cells detached from the surface, 9 mL of warm medium were added to the flask to stop the reaction and cells were recovered into a 15 mL tube. Cells were centrifuged for 5 minutes at 90 x g and the supernatant was discarded.

Here, if cryopreservation was necessary, cells were diluted in 10% DMSO culture medium and stored in cryotubes at -80°C. Otherwise, cells were diluted in 10 mL of culture medium, and in case counting was necessary, an aliquot of 10 µL was mixed 1:1 with 0.4% trypan blue stain, and the density was assessed with a cell counter (Logos biosystems). Then, cells were either seeded at a known density or passaged 1:10 to T75 flasks.

iPSCs

Induced pluripotent stem cells (iPSCs) were maintained in StemFlex medium. Cells were passaged twice a week, and every day after a passage the medium was changed. For passaging, cells were washed once with PBS-EDTA and then incubated with 1 mL PBS-EDTA at room temperature. The buffer was then carefully discarded and cells were resuspended in 1 mL of medium supplemented with the ROCK inhibitor thiazovivin (2 µM). When seeding with a known density was necessary, an aliquot of this suspension was mixed 1:1 with 0.4% trypsin, and measured with a cell counter. Then, the suspension was passaged at 1:6 on geltrex-coated 6-well plates and kept at 37ºC and 5% CO_2.

For cryopreservation, after the PBS-EDTA treatment, cells were detached with 10% DMSO StemFlex medium, supplemented with thiazovivin (2 µM). Then, cells were collected in cryotubes and stored at -80°C.

Differentiation of iPSCs into cardiomyocytes

Before the differentiation of iPSCs into cardiomyocytes (iPSC-CM), cells were passaged four times after recovery. At the start of the differentiation process, cells were kept in cardio differentiation medium. Additionally, on the days zero and two, CHIR9902 (4 µM) and IWP2 (5 µM) were used, respectively. From day number eight, beating was observable and the medium was changed to cardio culture medium. On

day number nine, cells were detached with 0.25% trypsin-EDTA and cardio digestion medium. Cells were kept at a density of 600,000 cells per well, on geltrex-coated 6-well plates. Then, the medium was changed to cardio selection medium for 2 days, after which cardio culture medium was used, and changed every two days. Experiments were performed on cells around 30 days after differentiation. The differentiation process was performed by Fatima Kanwal Baig as part of her laboratory rotation.

CRISPR-Cas9

A mutant HEK cell line lacking MDH1x was created through CRISPR-Cas9. For this, the following guide RNA (gRNA) was used:

crRNA AGTAACATCATTGTCTAGTCAGG (-)

First, the gRNA complex was formed with 1 µL of crRNA (100 µM) and 1 µL of tracRNA (100 µM) diluted in 98 µL of nuclease-free duplex buffer. The mix was then heated at 95ºC for 5 minutes and kept at room temperature. Afterwards, the RNP complex was formed, consisting of 1.5 µL of the gRNA complex, 1.5 µL of Cas9 (1 µM), 0.6 µL of Cas9 PLUS reagent, and 21.4 µL of Opti-MEM. Later, the RNP complex was incubated at room temperature for 5 minutes and prepared for transfection. For this, 25 µL of the RNP complex were mixed with 1.2 µL of CRISPRMAX transfection reagent and 23.8 µL of Opti-MEM, the solution was incubated for 20 minutes at room temperature. Then, 50 µL of the transfection complex were added to the well of a 96 well-plate. Over this, 100 µL of a suspension of cells (400,000 cells/mL) were added, and then incubated for 48 hours at 37ºC and 5% CO_2. Afterwards, cells were counted and seeded with a density of 0.5 cells per well, on 96-well plates.

Once cells achieved a confluence of about 80%, one sixth of the cells were passaged to a new well and the rest was used for DNA extraction using the DNeasy Blood & Tissue Kit (Qiagen). Then, the 3' region of MDH1, surrounding the first and second stop codon, was amplified with the following primers:

Forward	GGAAGTTTGTTGAAGGTCTCCC
Reverse	TGCACACTAACAGCATGACG

The program utilized for the polymerase chain reaction (PCR) was:

98 °C	3 min	
98°C	30 sec	32 cycles
62 °C	30 sec	
72 °C	30 sec	
72 °C	10 min	

Later, samples were sequenced with the Sanger method, using the BigDye Terminator v3.1 Cycle Sequencing Kit. For this, 10 ng of DNA were mixed with 0.5 µL of primer (10 µL), 2 µL of Big Dye buffer and 1 µL of sequencing Mix. The reaction consisted in 26 cycles of heating the sample at 96°C for 10 seconds, followed by an elongation step at 60°C for 4 minutes. Afterwards, the products (10µL) were cleaned with 220 µL of 100% ethanol, 120 µL of water and 10 µL of 3M sodium acetate (pH 4.6). Samples were vortexed and incubated for 15 minutes at room temperature, followed by 15 minutes of centrifugation at 14,000 rpm. The supernatant was discarded and the pellet washed once with 300 µL of 70% ethanol. Then, samples were centrifuged for 2 minutes at 14,000 rpm; the supernatant discarded and pellets left to dry for 10 minutes at 30°C. Pellets were then dissolved in 10 µL formamide. Finally, the sequencing itself was performed by Dr. Andreas Ohlenbusch of the department for Child and Adolescent Medicine, University Medical Center Göttingen. Additionally, iPSCs lacking MDH1x and LDHBx were acquired from the Stem Cell Unit, University Medical Center Göttingen.

Immunofluorescence

One day prior to the assay, 80,000 cells were seeded in 12-well plates containing poly-L-lysine (PLL)-coated glass covers of 18 mm in diameter and incubated overnight at 37°C and 5% CO_2. If necessary, cells were incubated with medium containing geneticin (100 µg/mL) for additional 24 hours. Next, cells were washed thrice with PBS and treated with wheat germ agglutinin (WGA) Alexa Fluor™ 633 (Invitrogen) diluted in HBSS (5 µg/mL) for ten minutes at 37°C. Then, cells were washed twice with PBS and fixed with paraformaldehyde (PFA) at room temperature for 30 minutes, or in the case of iPSC-CMs, one hour. Samples were then permeabilized with 0.5% (v/v) Triton X-100 in PBS for 5 minutes and blocked with 5% (w/v) bovine serum albumin (BSA) diluted in PBS, or 10% in the case of iPSC-CMs, for 30 minutes. Samples were then incubated with the primary antibodies diluted in 1% (w/v) BSA diluted in PBS for one hour at room temperature, or overnight at 4°C in the case of iPSC-CMs. The dilution of the antibodies is given in the following table:

Antibody	Host	Dilution	Cat. Number	Manufacturer
Anti-AGC1	Mouse	1:300	sc-271056	Santa Cruz
Anti-AGC1	Rabbit	1:300	SAB2103806	Sigma-Aldrich
Anti-AGC2	Rabbit	1:300	HPA018997	Sigma-Aldrich
Anti-COX4	Rabbit	1:300	mAb #4850	Cell Signaling Technology
Anti-LAMP1	Rabbit	1:300	ab24170	Abcam
Anti-LDHB	Mouse	1:300	MAB2732	Abnova
Anti-LDHB	Rabbit	1:300	14824-1-AP	Proteintech
Anti-MDH1	Rabbit	1:300	HPA027296	Sigma-Aldrich
Anti-MDH1	Mouse	1:300	ab55528	Abcam
Anti-OGC	Rabbit	1:300	HPA021167	Sigma-Aldrich
Anti-PEX14	Rabbit	1:300	10594-1-AP	Proteintech
Anti-PMP70	Mouse	1:200	SAB4200181	Sigma-Aldrich

Table 5 – Primary antibodies used in Immunofluorescence

Afterwards, samples were washed thrice with PBS and incubated with the secondary antibodies diluted in 1% (w/v) BSA for one hour at room temperature, or four hours in the case of iPSC-CMs (Table 6).

Antibody	Host	Dilution (iPSC-CM)	Cat. Number	Manufacturer
Anti-rabbit Cy3	Donkey	1:500 (1:1000)	705165147	Jackson ImmunoResearch
Anti-mouse Alexa488	Goat	1:500 (1:1000)	A-21053	Life Technologies
Anti-mouse Cy3	Donkey	1:500	715166150	Jackson ImmunoResearch
Anti-rabbit Alexa488	Donkey	1:500	711545152	Jackson ImmunoResearch

Table 6 – Secondary antibodies used in immunofluorescence

After the incubation, samples were washed thrice with PBS, the excess of PBS was collected with a tissue from the side of the coverslip, and the coverslips were placed on a cover slide with the mounting medium ProLong Gold Antifade with DAPI. After 24 hours of hardening in the dark at room temperature, the slides were ready for imaging or kept at 4°C for storage.

Imaging and image analysis

Images were taken with a Microscope Axio Observer 7 with Apotome.2, using a 63x objective (NA 1.4). Four channels per image were taken in most experiments, eGFP and Cy3 for the proteins of interest, DAPI for the nucleus, and TexasRed for the WGA633 staining the plasma membrane.

ROI selection

Through a self-developed macro in Fiji from imageJ (Schindelin et al., 2012), for some cell lines, these four channels were used to generate regions of interests (ROI) within images, marking each cell semi-automatically. Shortly, each channel was thresholded

individually, producing one mask per channel, these masks were combined creating a new mask containing the above-background information of all channels, which generally represented the whole cell. To make sure that the mask covered the whole cell, holes and irregularities were corrected manually. Then, the selection of all cells in an image was done with the function “Analyze Particles”, which selects all bodies with an area over 100 µm and adds them to the “ROI Manager”. Afterwards, the selected ROIs can be modified if necessary, and when the selection is confirmed by the user, the selection is saved as an independent file with the same name as the image, and the image is saved in the format TIFF. In cell lines that grew too close from each other, like iPSC and iPSC-CM, this step was skipped to avoid miscalculations, and instead, the whole image was taken in consideration for the analysis.

Colocalization analysis

Depending on the type of colocalization analysis employed, different macros were written for the second step in the analysis between the protein of interest and a peroxisomal marker. This second macro takes all the images and their corresponding ROI files from within a selected folder and analyze them in batch, creating an excel file with the values obtained from all the images.

For colocalization after geneticin treatment, the peroxisomal levels of MDH1 and LDHB were calculated by measuring the Pearson´s correlation coefficient (PCC) between the channel containing the POI and the channel containing the peroxisomal marker. This was done by thresholding the peroxisomal channel using the thresholding method “Moments”, and then feeding both channels into the JaCoP plugin (Bolte and Cordelières, 2006).

The same analysis was performed in HEK mutants lacking MDH1x and LDHBx, while for iPSCs a small difference was included. This is, the analysis was performed in the whole group of cells instead of in individual cells, due to their proximity.

For the analysis of the peroxisomal presence of the malate/aspartate shuttle (MAS) transporters, as well as the controls of this assay, Manders´ overlap coefficient (MOC) between the channel containing the POI and the channel containing the peroxisomal marker was calculated. For this, a mask was done of each channel by thresholding them with the automatic function “Moments”. Then, these masks were combined with their parent image, creating an image with the intensity information but without background. Both these images were fed into the plugin JaCoP of imageJ, and the MOC value was retrieved. In the case of HeLa cells, this was done in each cell individually, while for iPSC-CMs, this was done in the whole image.

Statistical analysis

In the case of PCC values, all data was first converted with the Fisher's z-transformation so it fits a normal distribution. Then, as for all the other data sets, the normal distribution was assessed using the Shapiro-Wilk test. In case the data set was distributed normally, Student's t-test was performed, on contrary; Mann-Whitney test was used.

siRNA transfection

For the transfection of HeLa cells with siRNA against AGC1, lipofectamine 3000 was used. First, cells were seeded on 6-well plates with a density of 1 million cells per well, and incubated for 24 hours at 37°C and 5% CO_2. In one tube, 7.5 µL of lipofectamine 3000 was diluted in 125 µL of Opti-MeM, while in another tube 75 pmol of siRNA was diluted in 125 µL of Opti-MeM. Then, 125 µL of each tube were combined in incubated at room temperature for 5 minutes. Afterwards, the mix was added to the sample containing freshly changed medium (2 mL) and samples were incubated for 48 hours at 37°C and 5% CO_2.

Western blot

For western blot analysis, 500,000 cells were seeded in 6-well plates and incubated overnight at 37°C and 5% CO_2. Then, cells were washed with PBS, and collected in 1 mL PBS using a cell scraper. Cells were then collected by centrifugation at 300 x g for 15 minutes, the supernatant discarded, and the pellet treated for 30 minutes with 20 µL of RIPA buffer while on ice, shaking regularly. Then, samples were centrifuged at 14,000 rpm for 15 minutes and 4°C. The supernatant was recovered and its protein concentration measured through BCA assay (Interchim).

Afterwards, 10 µg of the sample were diluted with 5 µL of 4x Lämmli buffer, and RIPA buffer until achieving a total volume of 10 µL. The preparation was heated at 96°C for 10 minutes, spun down and loaded into 12% acrylamide gel along with a protein standard. Samples were separated through electrophoresis for around 2 hours at 20 mA. Then, protein samples were transferred from the gel to a nitrocellulose membrane (0.45 µm) soaked in transfer buffer for 75 minutes at 65 mA. Then, membranes were shortly exposed to Ponceau-S solution and cleaned with water in order to check the correct transfer of the proteins from the gel. Additionally, membranes were cut to separate the protein of interest (POI) from the housekeeping. Afterwards, membranes were blocked with a 5% (w/v) milk in PBS-T for 30 minutes, while shaking. Membranes were then incubated overnight with primary antibodies diluted in 1% (w/v) milk in PBS-T at 4°C. The dilution and antibodies used are presented in the following table:

Antibody	Host	Dilution	Cat. Number	Manufacturer
Anti-MDH1	Rabbit	1:1000	HPA027296	Sigma-Aldrich
Anti-LDHB	Mouse	1:1000	MAB2732	Abnova
Anti-LDHB	Rabbit	1:1000	14824-1-AP	Proteintech
Anti-MDH1	Mouse	1:1000	ab55528	Abcam
Anti-GAPDH	Mouse	1:5000	G8795	Sigma-Aldrich
Anti-α-tubulin	Mouse	1:5000	T9026	Sigma-Aldrich
Anti-vinculin	Mouse	1:5000	V9131	Sigma-Aldrich

Table 7 – Primary antibodies used for western blot

Then, membranes were washed with PBS-T thrice for 5 minutes, and incubated for one hour with the secondary antibodies diluted in 1% (w/v) milk in PBS-T at room temperature. Depending on the primary antibody, the following secondary antibodies were used:

Antibody	Host	Dilution	Cat. Number	Manufacturer
Anti-rabbit HRP	Donkey	1:5000	111-035-003	Jackson ImmunoResearch
Anti-mouse HRP	Donkey	1:5000	715-035-150	Jackson ImmunoResearch

Table 8 – Secondary antibodies used for western blot

Afterwards, membranes were washed three times with PBS-T, and incubated with the peroxidase substrate Pierce™ ECL for one minute before visualization at the ECL imager (Chemostar). Images were analyzed using ImageJ. The protein of interest was normalized to its respective housekeeping and the control and the wild type was given the arbitrary value of 1.

Glutathione Assay

The glutathione (GSH) levels of cell lines was assessed with the GSH-Glo™ Glutathione Assay (Promega). This assay is based in the production of luciferin from a luciferin-derivative by the glutathione S-transferase (GST), in the presence of GSH. Light is generated by the enzyme luciferase through the use of luciferin, which is proportional to the original GSH levels. Shortly, cells were seeded with a density of 2,500 cells per well on dark 96-well plates and incubated at 37°C and 5% CO_2 for 24 hours. Then, the medium was extracted and 100 µL of GSH-Glo™ reagent were added per sample, samples were shortly mixed on a plate shaker and incubated for 30 minutes at room temperature. Afterwards, 100 µL of reconstituted Luciferin Detection Reagent was added to each sample, samples were shortly mixed on a plate shaker and incubated for 15 minutes at room temperature. Luminescence was measured and compared to a GSH-standard curve of known concentrations. Concentrations were normalized by total protein in µg and then statistically compared in GraphPad Prism. For assessing the normal distribution of the data, Shapiro-Wilk

test was used, and Mann-Whitney test for the analysis of significant differences between the groups.

Catalase Assay

For the analysis of catalase activity, 500,000 cells were seeded and incubated for 24 hours at 37°C and 5% CO_2. Then, cells were scrapped and collected through centrifugation at 5,000 rpm for 5 minutes at 4°C. The supernatant was discarded and samples were disrupted with a cannula syringe (0.4 x 20 mm) in 100 µL of TVBE buffer and kept on ice. Afterwards, samples were sonicated for 90 seconds in a bath sonicator. The protein concentration was estimated with BCA assay and 20 µg of protein were diluted in TVBE buffer up to 5 µL. The sample was then mixed with 5 µL of 1% Triton-X100 for measurement, while TVBE buffer alone was used as blank. Samples were kept for 5 minutes on ice, after which 100 µL of the catalase substrate were added. Samples were then incubated for exactly 15 minutes on ice, before 100 µL of the stopping solution were added. Finally, samples were incubated for 10 minutes at room temperature and measured at 410 nm. The assay was performed by Vishalini Venkatesan as part of her laboratory rotation.

The quantification was performed by a modification of the Beaufay method (Islinger et al., 2012). Here, the results are given in Beaufay units (BU), which originally describes the first order kinetic reaction of catalyzing 90% of the H_2O_2 present in 50 mL of reaction volume, in 1 minute. In this work, the total reaction volume was normalized by µg of total protein, following the formula:

$$[U/\mu g] = \left(\frac{\text{incubation volume}}{incubation\ time\ *\ \mu g\ sample}\right) * \log\left(\frac{OD\ blank}{OD\ sample}\right)$$

The statistical analysis was done in GraphPad Prism 8, normal distribution of the data was analyzed with Shapiro-Wilk test, while significant differences were assessed with Student's t-test.

Mitochondrial respiration

The mitochondrial respiration of intact cells was analyzed through a Cell Mito Stress test. First, cells were seeded with a density of 40,000 cells per well in 24-well Seahorse XF24 plates coated with Geltrex and incubated in supplemented StemFlex medium at 37ºC and 5% CO_2 for 4 days. Prior to the measurement, the XFe24 sensor cartridge was hydrated overnight with 1 mL of Seahorse XF calibrant solution per well. Then, the samples were washed with 1 mL of Seahorse XF RPMI medium supplemented with glucose (1 mM), and incubated for one hour at 37ºC. Three pockets of the cartridge were loaded with the drugs used in the Cell Mito Stress test. The cartridge and plate with the samples were mounted and inserted in the Seahorse

XFe24 Analyzer. This system measures the oxygen consumption rate (OCR) of the sample. First, since no extra component was added, the basal respiration was calculated. Then, oligomycin was injected for the inhibition of the ATP synthase (complex V), reaching a final concentration of 2.5 µM, blocking the ATP-linked respiration and thus decreasing the OCR. Afterwards, FCCP was injected achieving a final concentration of 200 nM, in this way uncoupling the proton gradient, and hence, stimulating mitochondrial OCR to its maximum. Finally, a mixture of the complex I and complex III inhibitors rotenone and antimycin A was injected to the sample, both with a final concentration of 0.5 µM, shutting down mitochondrial respiration completely and leaving active only residual, non-mitochondrial respiration. The raw data was acquired and analyzed with the Wave software from Agilent, while the statistical analysis was later performed with Graphpad Prism 8.

Metabolite quantification

The analysis of metabolites, particularly of the accumulation of fatty acids in the extracellular medium, was performed with a modified version of the CortecsT3 lipidomics method. For this, the use of methyl ester fatty acids was preferred due to their higher solubility, and to that the extra methyl group is readily lost once the fatty acid enters the cell (van de Beek et al., 2017). The experimental design was based in Violante et al., 2019, where the mitochondrial usage of shorter fatty acids is inhibited by blocking carnitine palmitoyltransferase (CPT2) with L-aminocarnitine (L-AC), in this way directing their catabolism towards peroxisomes. For this, cells were seeded in 24-well plates with a density of 200,000 cells per well and incubated with culture medium containing either methyl dodecanoate (C12, 120 µM), L-AC (200 µM), a combination of both, or 1% DMSO as control. After 72 hours of incubation, the extracellular medium was collected and the lipidomics assay was performed by Dr. Henry Klemp and Antony Grüness.

Shortly, the CortecsT3 lipidomics method was adapted from Narváez-Rivas and Zhang, 2016 and Rampler et al., 2018, with a shorter run period of 30 minutes due to a higher peak efficiency chromatographic column. As mobile phase A, 40% ammonium formate (10 mM) in water, with 60% acetonitrile and 0.1% formic acid was used. As mobile phase B, 90% isopropanol, 10% acetonitrile, 0.1% formic acid and ammonium formate (10 mM) was used. For the separation, 5 µL of sample was injected in a Water Cortecs UPCL T3 column with dimensions of 2.1 x 150 mm at 40°C. The gradient was kept with a flow of 0.3 mL/min for 35 minutes, with 35% mobile phase B, increasing linearly to 40%. Then, the gradient was linearly increased up to 43% in five minutes, after which was increased again to 50% in 0.1 minutes. The

gradient was then linearly increased up to 54% in a span of 12.4 minutes, followed by a one-minute jump to 70%. Afterwards, the gradient was increased up to 95% in the span of 6 minutes, and remained for three extra minutes. Finally, the column was equilibrated to 35% in the span of two minutes, and kept for 3 additional minutes. A Xevo G2-S mass spectrometer with an electrospray ionization (ESI) source in MS^E mode was used. The conditions of the mass spectrometer are depicted in Table 9.

Setting	Positive mode
ESI capillary voltage	0.8 kV
Cone voltage	25 V
Desolvation temperature	20 °C
Fragmentation	Ramp between 10V-40V
Mass range	50-800 Da
Source offset	80 V
Source temperature	150 °C

Table 9 – Mass spectrometer settings

Plasmid generation

For the generation of EGFP-tagged versions of AGC1, the AGC1 sequence was cloned from a plasmid containing the full sequence, and then inserted into the plasmids EGFP-N1 and EGFP-C1, which are able to produce a protein with a C- or N-terminal EGFP-tag, respectively. The amplification of AGC1 was done on 10 ng of the template, with KAPA polymerase with GC buffer according to the manufacturer's instructions. The primers used for the amplification of AGC1 were:

For using with EGFP-N1
Forward GCGCAAGCTTATGGCGGTCAAGGTGCAG
Backward GCGCACCGGTATCTGAGTGGCTGCCACTG

For using with EGFP-C1
Forward GCGCAAGCTTTAGCGGTCAAGGTGCAGACA
Backward GCGCGGTACCTCACTGAGTGGCTGCCAC

The polymerase chain reaction (PCR) program used was:

98 °C 3 min
98°C 30 sec
60 °C 30 sec } 28 cycles
72 °C 30 sec
72 °C 10 min

An aliquot of the samples was run on a 1% agarose gel at 100 V for 30 minutes and visualized on UV light. After confirmation of size, samples were purified with the High Pure PCR Product Purification Kit (Roche), according to the manufacturers' instructions. The final step of elution, instead of using elution buffer, was done in 20 µL of water. Then, 500 ng of the DNA fragments and plasmids were cleaved with 0.3

µL of the restriction enzymes HindIII-HF and AgeI in the case of EGFP-N1, while for EGFP-C1 HindIII-HF and KpnI were used. In all cases, 2 µl of CutSmart buffer was used. Digestion was done for 3 hours at 37°C. Additionally, 0.2 µL of KpnI were added to the reaction of EGFP-N1 for the last 30 minutes of reaction, while PstI was added in the case of EGFP-C1. Afterwards, fragments were run on a 1% agarose gel for 1 hour at 90 V and then extracted with the NucleoSpin Gel and PCR Clean-up kit. Then, the digested fragments of AGC1 were ligated with 50 ng of the digested EGFP-N1 and EGFP-C1 plasmids. For the ligation, the amount of insert was calculated as three times the molar mass of the vector in addition to 1 µL of T4 Ligase and 2 µL of ligase buffer in a total volume of 20 µL. The reaction was incubated for 1 hour at room temperature.

Then, *Escherichia coli* (*E. coli*) was transformed through heat shock. For this, 1 µL of the ligation product was added to 10 µL of competent *E. coli (*BIO*Blue)*. First, samples were kept on ice for 20 minutes, then were incubated for 45 seconds at 42°C, incubated for 2 minutes on ice, and finally added to 400 µL of LB medium. Samples were incubated on a shaker for 1 hour at 37°C, after which they were plated on LB-agar plates containing 50 µg/mL of kanamycin and kept overnight at 37°C. Afterwards, single colonies were picked and used to generate bacterial cultures in 3 mL of LB medium containing kanamycin for 24 hours at 37°C on a shaker.

After, the plasmid DNA was harvested from the bacterial cultures. For this, samples were centrifuged at 8,000 rpm for 1 minute, resuspended in 200 µL of buffer P1, and then 300 µL of buffer P2 were added. Samples were incubated for 5 minutes at room temperature, followed by addition of 300 µL of buffer P3. Then, samples were centrifuged for 10 minutes at 14,000 rpm, the supernatant was collected and 500 µL of isopropanol were added. Samples were centrifuged at 14,000 rpm for 20 minutes, washed with 70% ethanol, and dried for 10 minutes at 37°C. Later, samples were resuspended in 30 µL of water, and plasmids were sequenced as in the section “CRISPR-Cas9”. To confirm their integrity, several primers were used for the sequencing of each plasmid:

<u>For N1</u>

CMV primer	CGCAAATGGGCGGTAGGCGTG
OST 1940	GCGCAAGCTTATGGCGGTCAAGGTGCAG
OST 1941	GCGCACCGGTATCTGAGTGGCTGCCACTG
OST 2119	TCACACCAGGTTAGCTTCTCC
OST 2120	TGGCTCTGGCTCTGTTGTTG
OST 2121	AACTTCTCCAGCGGTGGTTT

For C1	
Citrine	AAATGTGGTATGGCTGATTATG
OST 1942	GCGCAAGCTTTAGCGGTCAAGGTGCAGACA
OST 1943	GCGCGGTACCTCACTGAGTGGCTGCCAC
OST 2119	TCACACCAGGTTAGCTTCTCC
OST 2120	TGGCTCTGGCTCTGTTGTTG
OST 2121	AACTTCTCCAGCGGTGGTTT

The plasmids for C- and N-terminal tagged AGC2 and OGC were done by Yelena Sargsyan as part of her laboratory rotation.

Transfections

For the transfection with AGC1, AGC2 and OGC plasmids, HeLa cells were seeded with a density of 80,000 cells per well on 12-well plates containing an 18 mm diameter glass coverslip, coated with PLL. Cells were incubated for 24 hours at 37ºC and 5% CO_2, and then transfected with Effectene transfection reagent, according to the manufacturers' instructions. Per well, 300 ng of plasmid were used, and cells were incubated with the transfection mix for 24 hours before fixation and imaging.

Proximity ligation assay

The closeness between the POIs and peroxisomes was analyzed by estimating the proximity of antibodies against a POI and a peroxisomal membrane protein. For this, proximity ligation assay (PLA) was used, which gives a signal when both antibodies are closer than 40 nm. First, HeLa cells were seeded in 24-well plates over glass coverslips coated with PLL. Cells were seeded with a ratio of 70,000 cells per well and incubated overnight at 37°C and 5% CO_2. Then, after washing thrice with PBS, cells were fixed with 4% PFA for 15 minutes, washed thrice with PBS again, followed by permeabilization with 0.05% (v/v) Triton X-100 for five minutes. Afterwards, samples were washed thrice with PBS, blocked with Duolink Blocking Solution for 30 minutes at 37°C in a humidity chamber, and incubated with the primary antibodies in the dilutions shown in Table 10. Primary antibodies were diluted in Duolink antibody diluent and samples were incubated for one hour at room temperature, either with each antibody alone as internal control, or in combination with PMP70, in order to assess their proximity with peroxisomes.

Antibody	Host	Dilution PLA	Dilution IF	Cat. Number	Manufacturer
Anti-AGC1	Rabbit	1:500	1:100	SAB2103806	Sigma-Aldrich
Anti-AGC2	Rabbit	1:500	1:100	HPA018997	Sigma-Aldrich
Anti-OGC	Rabbit	1:500	1:100	HPA021167	Sigma-Aldrich
Anti-PEX14	Rabbit	1:1500	1:100	10594-1-AP	Proteintech
Anti-PMP70	Mouse	1:750	1:100	SAB4200181	Sigma-Aldrich
Anti-H3K27me3	Rabbit	1:1500	1:100	AB_2561020	Active Motif
Anti-rabbit Cy3	Donkey		1:500	705165147	Jackson ImmunoResearch
Anti-mouse Alexa488	Goat		1:500	A-21053	Life Technologies

Table 10 – Antibodies for PLA

Then, samples were washed twice for 5 minutes with Wash Buffer A, and incubated with a 1:5 dilution of the PLA probes anti-mouse plus (DUO92001, Sigma-Aldrich) and anti-rabbit minus (DUO92005, Sigma-Aldrich) for one hour at 37°C in a humidity chamber. Samples were washed twice with Wash Buffer A for five minutes, and then incubated for 30 minutes at 37°C with the ligation solution. Later, after being washed twice for two minutes with Wash Buffer A, samples were incubated with the amplification solution for 100 minutes at 37°C. Afterwards, samples were immunostained as in the section “Immunofluorescence”, for the capture of the POI-fluorescence together with the PLA signal. Instead of ProlongGold, samples were mounted using Duolink in situ mounting medium, with DAPI. Coverslips were then fixed with nail polish to the slides and stored at -20°C. Samples were imaged as in the “Immunofluorescence” section, with the PLA signal at the far-red region, within the TexasRed area.

The quantification of proximity events was done in ImageJ semi-automatically. First, the ROIs were marked as in “ROI selection” in order to mark individual cells. Then, the proximity events were selected using Find Maxima, generating a mask where each peak of intensity is represented as one pixel. These pixels were then counted with Analyze particles, giving the events per cell. Considering that background dots are observed when an antibody is analyzed alone, the results of the antibodies alone was subtracted to each combination of antibodies. Then, the proximity negative control, H3, was set as zero, and the other combination of antibodies were scaled accordingly. The assay was performed by Dr. Christina James, excluding cell culture, imaging and data analysis.

Results

Peroxisomal presence of MDH1 and LDHB is inducible by geneticin

In order to perform their function, proteins need to be directed to specific parts of the cell. For instance, the transport of a protein into an organelle can be mediated by the presence of a targeting signal. In the case of peroxisomes, the most common targeting signal is the peroxisomal targeting signal 1 (PTS1), located at the C-terminal domain of the protein, which activates its import into peroxisomes (Gould et al., 1987; Lazarow and Fujiki, 1985). Additionally, some proteins are able to reach more than one compartment. One of the mechanisms by which they can achieve multiple localization is functional translational readthrough (FTR), that allows the incorporation of a targeting signal at the C-terminal portion of a protein (Schueren et al., 2014). This is particularly the case for MDH1 and LDHB, which possess a PTS1 between the first and second stop codon. This allows their transport into peroxisomes when FTR takes place, by translating their extended versions, MDH1x and LDHBx (Hofhuis et al., 2016; Schueren et al., 2014).

Since the ribosome is responsible for the level of FTR in response to the stop codon context around the stop codon, geneticin, an antibiotic that increases the errors during translation by the ribosome, can be used to increase the translation of MDH1x and LDHBx (Burke and Mogg, 1985; Schueren et al., 2014). For this, cells were treated with 100 µg/mL geneticin for 24 hours. Afterwards, cells were fixed and immunostained with an antibody against the peroxisomal membrane protein PEX14, which serves as peroxisomal marker, and co-stained with antibodies against MDH1 or LDHB.

Image analysis consisted in quantifying the Pearson's correlation coefficient (PCC) between the protein of interest (POI) and the peroxisomal protein PEX14. This is a way to measure peroxisomal colocalization of MDH1 and LDHB and its induction by geneticin treatment. The PCC is based on the covariance of two continuous variables, in this case, the intensity of MDH1, or LDHB, and PEX14 in any given pixel where both variables are above the threshold. PCC was quantified for each individual cell, yet since this analysis is non-parametric, the values were converted with Fisher's z-transformation. These newly converted values, PCC-Z, were used in the statistical analysis comparing treated and untreated cells.

As a result, it was observed that in both HEK and HeLa cells, MDH1 has higher colocalization with peroxisomes in cells treated with geneticin (Figure 4 A and C). In HEK cells, MDH1 shows an average PCC-Z of 0.215 in untreated cells, while in cells treated with geneticin it was 0.240, significantly higher than in untreated cells. In HeLa, the average PCC-Z between MDH1 and peroxisomes was 0.211 in untreated cells. In treated cells, with a value of 0.223, PCC-Z was significantly higher. The peroxisomal colocalization of LDHB in HEK cells, measured in terms of PCC-Z, was 0.177 in untreated cells and 0.186 for cells treated with geneticin, being significantly higher in treated cells in comparison to the control (Figure 4 B and C). In HeLa cells, an increase in the average PCC-Z from 0.143 to 0.156 was observed between the control and cells treated with geneticin, significantly higher in cells treated with geneticin (Figure 4 B and C). These results add evidence to the role of FTR as the mechanisms responsible for the transport of both LDHB and MDH1 into peroxisomes.

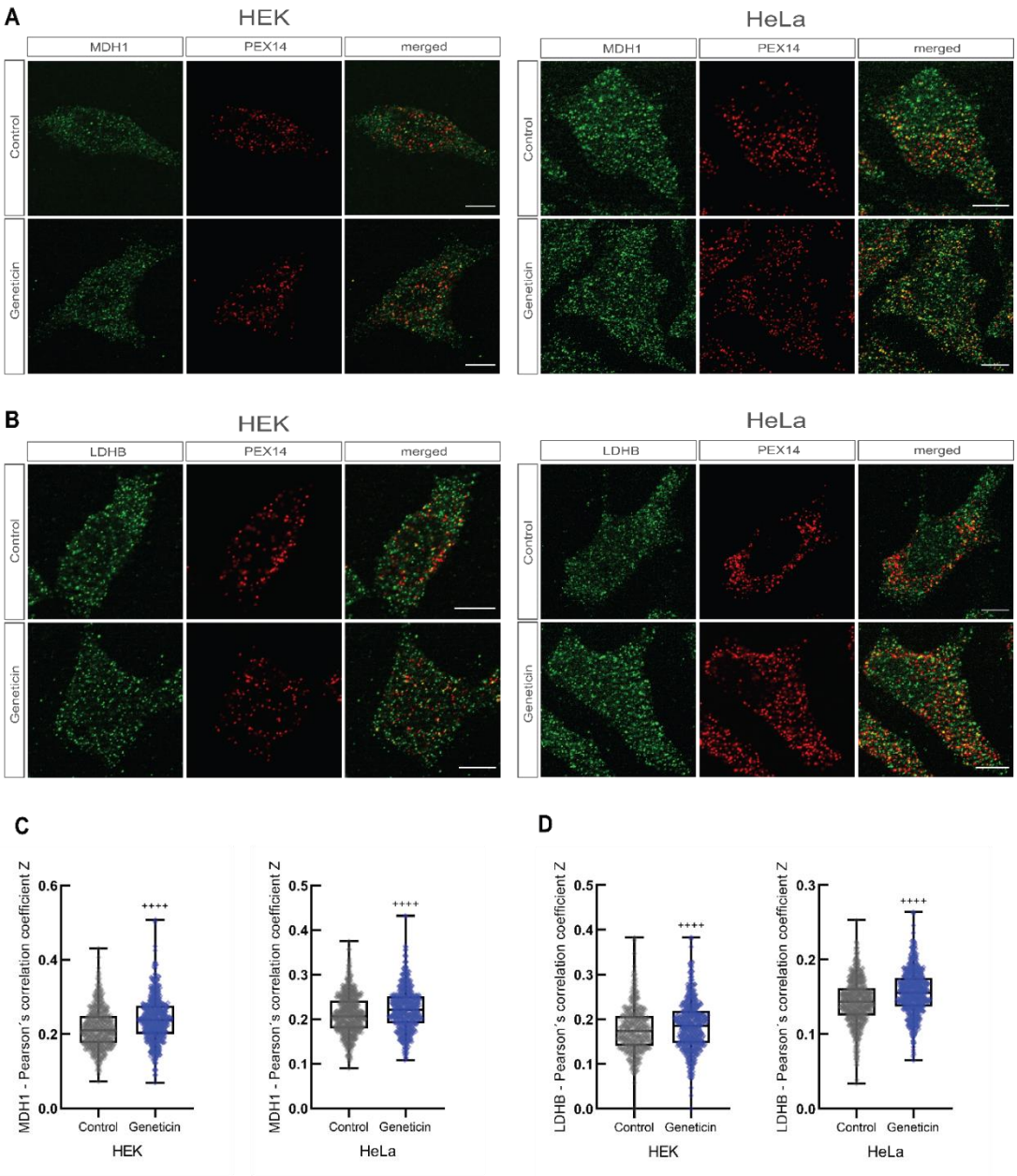

Figure 4 – Geneticin treatment induces the peroxisomal import of MDH1 and LDHB in in HEK and HeLa cells.
Cells were either treated for 24 hours with geneticin (100 µg/mL), or kept untreated as controls. Next, cells were fixed and immunostained against PEX14 together with MDH1, or LDHB. Representative images of HEK (left) and HeLa cells (right), stained against (**A**) MDH1 and PEX14, or (**B**) LDHB and PEX14. (**C**) Quantification of relative MDH1 after geneticin treatment in HEK and HeLa cells. (**D**) Quantification of peroxisomal LDHB in HEK and HeLa cells treated with geneticin. Around 500 cells from two independent experiments were quantified per condition. Images were used for the quantification of PCC. Data was converted with Fisher´s Z-transformation for statistical relevance and presented in the boxplots. Boxplots show the maximum and minimum data points on their upper and lower whisker, respectively. The first and third quartile are represented by the upper and lower line of the body of the boxplot, while the line in between shows the median. Normal distribution of the data was assessed with Shapiro-Wilk test and proven to be not normal, thus the statistical analysis was made with Mann-Whitney test. $^{++++}p \leq 0.0001$; $^{++}p \leq 0.01$. Scale bars represent 10 µm.

Generation of cells lacking MDH1x and LDHBx

Next, in order to have a model to assess the impact of MDH1x and LDHBx, cell lines lacking both of these proteins were generated. For HEK cells and induced pluripotent stem cells (iPSC), five nucleotides between the first and second stop codon of MDH1x were deleted (Figure 5A). This deletion produced a frameshift that erased the PTS1 at the C-terminal portion of MDH1x. In addition, an iPSC line lacking LDHBx (iPSC LDHBΔx) was produced. In this case, the cell line carried a heterozygous deletion of three nucleotides in one allele, and five nucleotides in the other. As a result, in both cases the deletion deleted the PTS1 by producing a reading frameshift (Figure 5A).

Afterwards, the impact of the mutations in the expression levels of the non-extended proteins was evaluated (Figure 5B). As a result, no difference in the relative levels of MDH1 was observed between the MDH1Δx mutant and wild type in HEK, nor iPSCs (Figure 5B). Likewise, no difference in relative LDHB levels were observed between the wild type and iPSC LDHBΔx (Figure 5B).

Since the mutation only affects MDH1x and LDHBx, but not the expression of MDH1 nor LDHB, these results support the use of the MDH1Δx and LDHBΔx cell lines for further assessment of the importance and effect of these two proteins.

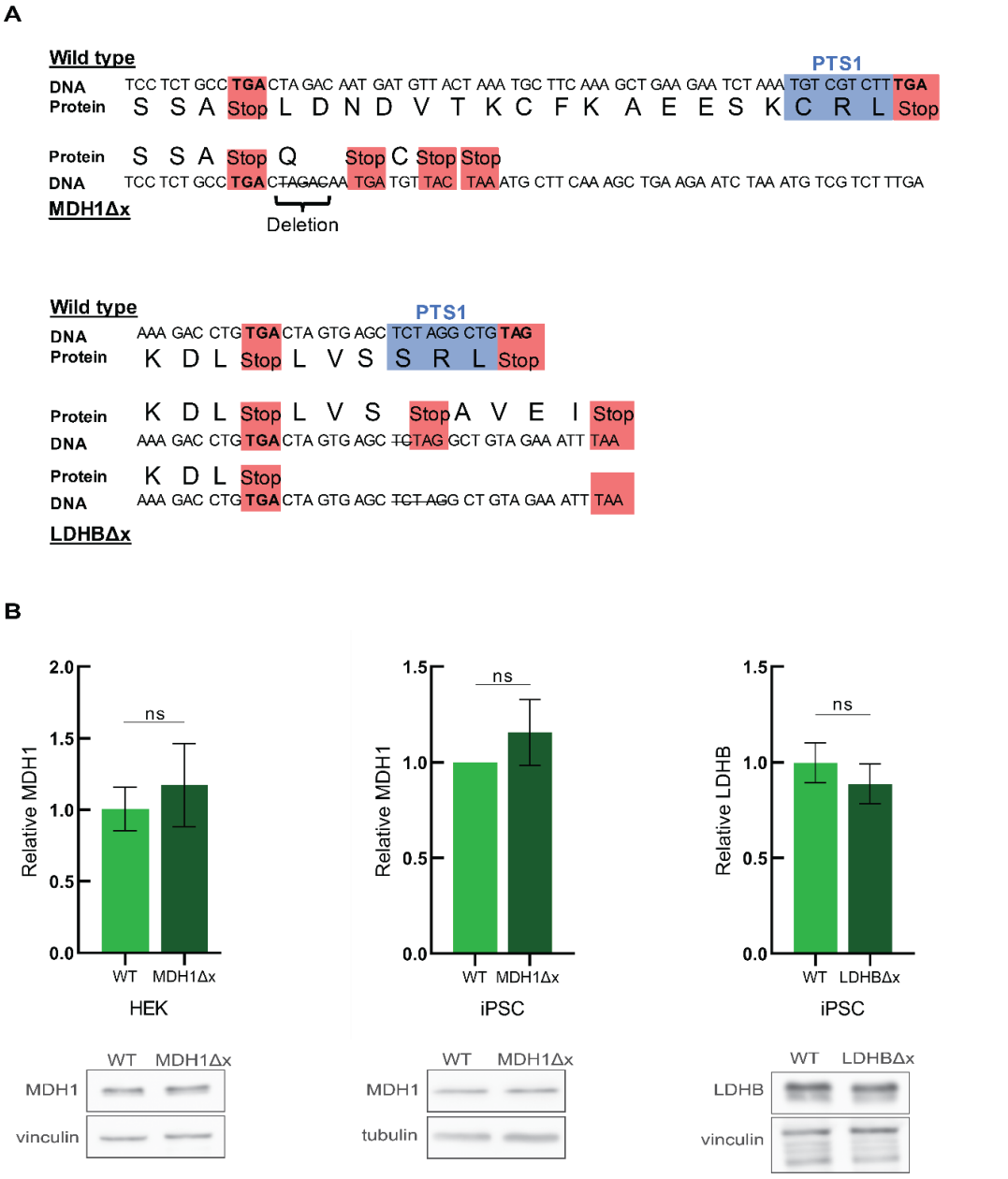

Figure 5 – Deletion of the MDH1 and LDHB extensions does not affect parent protein expression.
The extension of MDH1, which contains the PTS1, was disrupted in both HEK cells and iPSCs, as well as the extension of LDHB in iPSCs. (**A**) Representation of the C-terminal portion of both MDH1 and LDHB mutations. A deletion of five nucleotides between the first and second stop codon disrupts the PTS1 of MDH1 in both HEK and iPSC, while in addition, a compound heterozygous mutation was achieved for LDHB in iPSC. (**B**) The relative levels of MDH1 protein were measured by western blot in both HEK and iPSCs lacking MDH1x, as well as of LDHB in iPSCs lacking LDHBx. The results showed no difference between wild type and mutants. Three independent samples were measured per condition. Statistical analysis was performed using t-test. Whiskers show S.E.M. $^{ns}p>0.05$.

Deletion of MDH1x lowers the peroxisomal presence of MDH1 in HEK cells

Then, in order to see if the deletion of the extended portion of MDH1 has an effect on its peroxisomal presence, both HEK wild type and MDH1Δx cells were immunostained against MDH1 and a peroxisomal marker. The colocalization of both antigens was quantified with two set of antibodies, either mouse anti-human MDH1 together with rabbit anti-human PEX14, or rabbit anti-human MDH1 together with an antibody against 70 kDa peroxisomal membrane protein (PMP70), produced in mouse. In both cases, MDH1 showed the characteristic distribution of a cytosolic protein, very sparse in the cell, including regions where its signal overlaps with the peroxisomal marker (Figure 6A and B). As when cells were treated with geneticin, colocalization was quantified in terms of PCC-Z. When anti-MDH1 (mouse) was used, an average PCC-Z of 0.296 was observed in wild type, which is a value considered as moderate colocalization between two elements. The PCC-Z value of HEK MDH1Δx was significantly lower than the wild type, with a value of 0.269 (Figure 6A). A very similar result was observed when anti-MDH1 (rabbit) was used, with a PCC-Z of 0.209 for the wild type, and a significantly lower PCC-Z of 0.138 for the MDH1 mutant (Figure 6B). This shows, with two different sets of antibodies, that there is less presence of MDH1 in peroxisomes in mutant HEK lacking MDH1x.

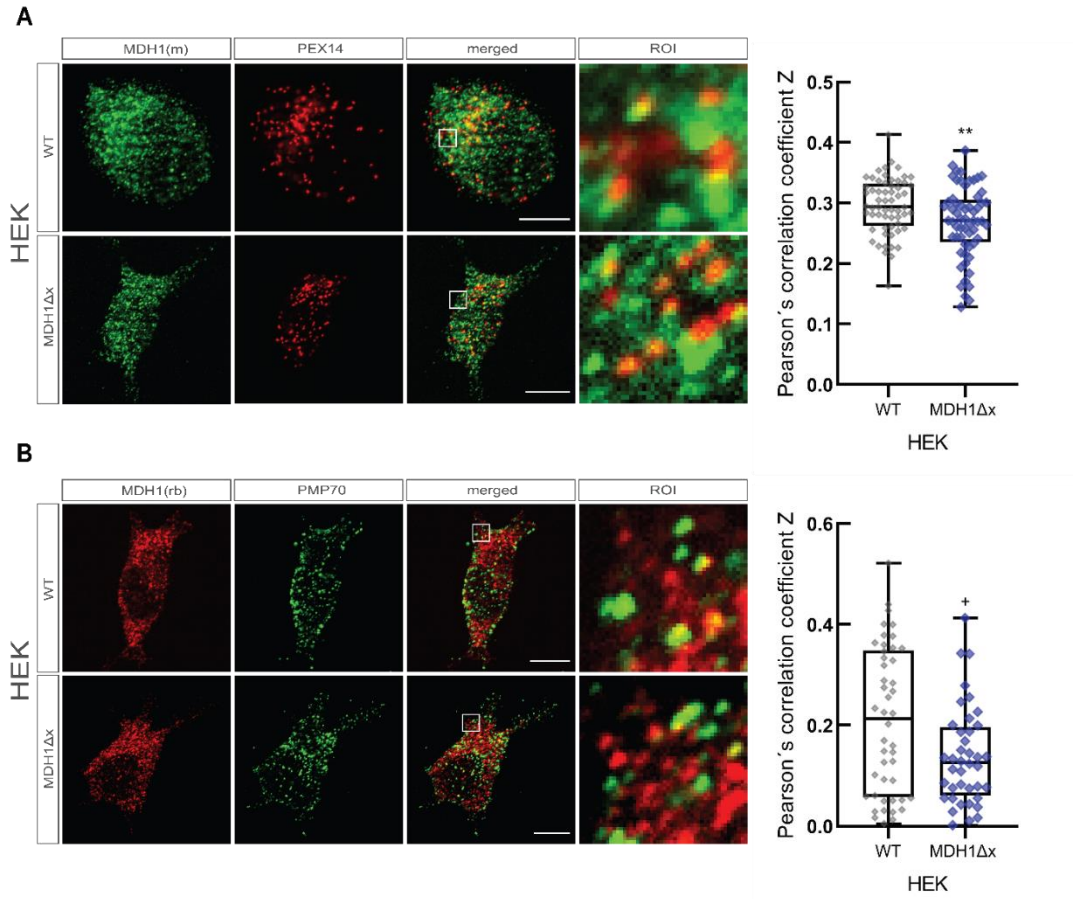

Figure 6 – MDH1 shows less peroxisomal colocalization in HEK cells lacking MDH1x.

Wild type and MDH1Δx HEK were immunostained against MDH1 and a peroxisomal marker. The colocalization levels between both markers were assessed using PCC after Fisher's z-transformation. Different combinations of antibodies showed a significantly reduced peroxisomal colocalization of MDH1: (**A**) mouse anti-human MDH1 co-stained with rabbit anti-human PEX14, and (**B**) rabbit anti-human MDH1 together with mouse anti-human PMP70. Statistical analysis was performed on PCC data after its conversion using Fisher's z-transformation, named PCC-Z. Converted data was then checked for normalization using Shapiro-Wilk test, resulting in a normal distribution for data in B, but not A. Mann-Whitney test was performed on A, while Student´s t-test was performed on B. The whiskers in the boxplot show the maximum and minimum. Upper and lower line of the boxplot body represent the first and third quartiles, while the line in between shows the median. Figures represent two independent experiments with a total of 80 cells in case A, and 50 cells in the case of B, per condition. $^{+}p \leq 0.05$; $^{**}p \leq 0.01$. Scale bars are 10 µm.

Lack of MDH1x in iPSCs decreases MDH1 presence in peroxisomes

Then, the peroxisomal localization of MDH1 in the iPSC mutants was tested in order to see if it was reduced, as it was the case for the HEK mutant. Both mutants were checked, lacking MDH1x and LDHBx, using two different set of antibodies: i) mouse anti-human MDH1 together with rabbit anti-human PEX14, and ii) rabbit anti-human MDH1 together with mouse anti-human PMP70. For measuring colocalization, correlation between both antibodies was assessed in terms of PCC. Then, Fisher's z-

transformation was used for converting the data into normally distributed data, and was afterwards analyzed statistically. Along with the results obtained in HEK, it was observed that MDH1 is dispersed across the whole cell, and that some overlap was noticed with the peroxisomal marker PEX14, and PMP70 (Figure 7A and B). Curiously, with rabbit anti-human MDH1, some accumulation of the protein was additionally observed, which was not present when mouse anti-human MDH1 was used (Figure 7A and B).

When cells were immunostained with mouse anti-human MDH1, an average PCC-Z of 0.200 was obtained in the wild type, while the average PCC-Z for MDH1Δx was 0.130; significantly lower than the wild type (Figure 7A). The same phenomenon was observed with rabbit anti-human MDH1, where the peroxisomal levels of MDH1 were significantly higher in wild type, with an average PCC-Z of 0.157, than in the MDH1Δx mutant, with an average PCC-Z of 0.101 (Figure 7B). These results agree with the model where the extension containing the PTS1 is responsible for the import of MDH1 into peroxisomes.

Additionally, the levels of peroxisomal MDH1 were assessed in the LDHBΔx mutant. In this case, when cells were immunostained mouse anti-human MDH1, the levels of peroxisomal MDH1 were higher in cells lacking LDHBx, with an average PCC-Z of 0.236 (Figure 7A). Likewise, when rabbit anti-human MDH1 was used, an average PCC-Z of 0.216 was obtained, significantly higher than the wild type (Figure 7B).

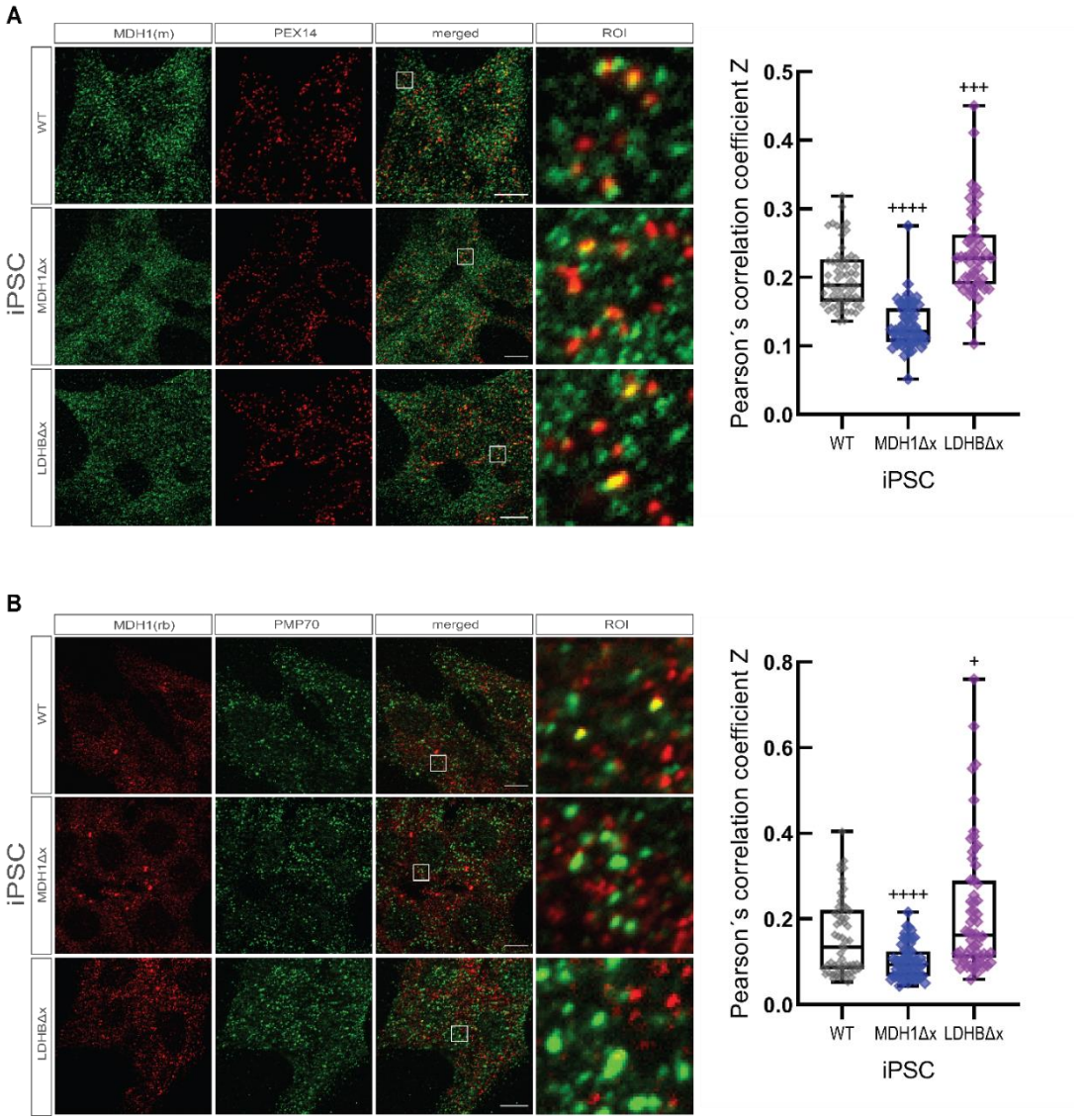

Figure 7 – MDH1 colocalizes less with peroxisomes in iPSCs lacking MDH1x.
Localization of MDH1 in peroxisomes was assessed in iPSCs lacking MDH1x, lacking LDHBx, and wild type. (**A**) Cells were immunostained with mouse anti-human MDH1 together with rabbit anti-human PEX14. The peroxisomal localization of MDH1 was significantly lower in iPSC mutant lacking MDH1x than in wild type, while in the LDHBΔx mutant it was higher than in the wild type. (**B**) Immunostaining with rabbit anti-human MDH1 together with mouse anti-human PMP70. The peroxisomal localization of MDH1 was also significantly lower in MDH1Δx, while the peroxisomal localization of MDH1 in LDHBΔx was higher than the wild type. Whiskers in the boxplot represent maximum and minimum data points. The upper and lower line of the boxplot‘s body represent the first and third quartiles, while the line in between illustrate the median. Two independent experiments were performed. PCC was calculated from a total of 50 images in the case of LDHBΔx immunostained against mouse anti-human MDH1, while 60 images were used for the rest of conditions. The data was converted with Fisher’s Z-transformation for statistical analysis (PCC-Z). Shapiro-Wilk test was used to assess the distribution of the data. Statistical analysis was done with Mann-Whitney test. $^{++++}p \leq 0.0001$; $^{+++}p \leq 0.001$; $^{+}p \leq 0.05$. Scale bars are 10 µm.

Effect of the lack of LDHBx in the presence of LDHB in peroxisomes of iPSCs

Next, the peroxisomal colocalization levels of LDHB were quantified in iPSC wild type, MDH1Δx and LDHBΔx (Figure 8). When cells were immunostained with mouse anti-human MDH1 together with rabbit anti-human PEX14, LDHB showed a very disperse and rather uniform signal all across the cell, with some peroxisomal overlap in the wild type, MDH1Δx and LDHBΔx (Figure 8A). When rabbit anti-human LDHB was used together with mouse anti-human PMP70, LDHB was also distributed across the whole cell, although the signal was more spotted and had higher background (Figure 8B).

Surprisingly, the peroxisomal colocalization of LDHB was significantly higher in the LDHBΔx mutant with both antibodies against LDHB. When mouse anti-human LDHB was used, an average PCC-Z of 0.163 was obtained for the wild type, while an average of 0.177 was obtained in the case of the LDHBΔx mutant (Figure 8A). Similar results were obtained when rabbit anti-human LDHB was used, where the peroxisomal colocalization levels of the wild type were 0.156, while the mutant LDHBΔx had an average PCC-Z of 0.287, significantly higher than the wild type (Figure 8B).

When the peroxisomal colocalization of LDHB was assessed in the MDH1Δx mutant, values were significantly lower than in the wild type, independently of the antibody used. With mouse anti-human LDHB, an average PCC-Z of 0.124 was obtained, while rabbit anti-human LDHB showed an average PCC-Z of 0.135 (Figure 8A and B). These results are unexpected, since an effect in the levels of peroxisomal LDHB are observed, when MDH1 is not present. One possible explanation would be that the lack of peroxisomal MDH1x, affects the transport of LDHB.

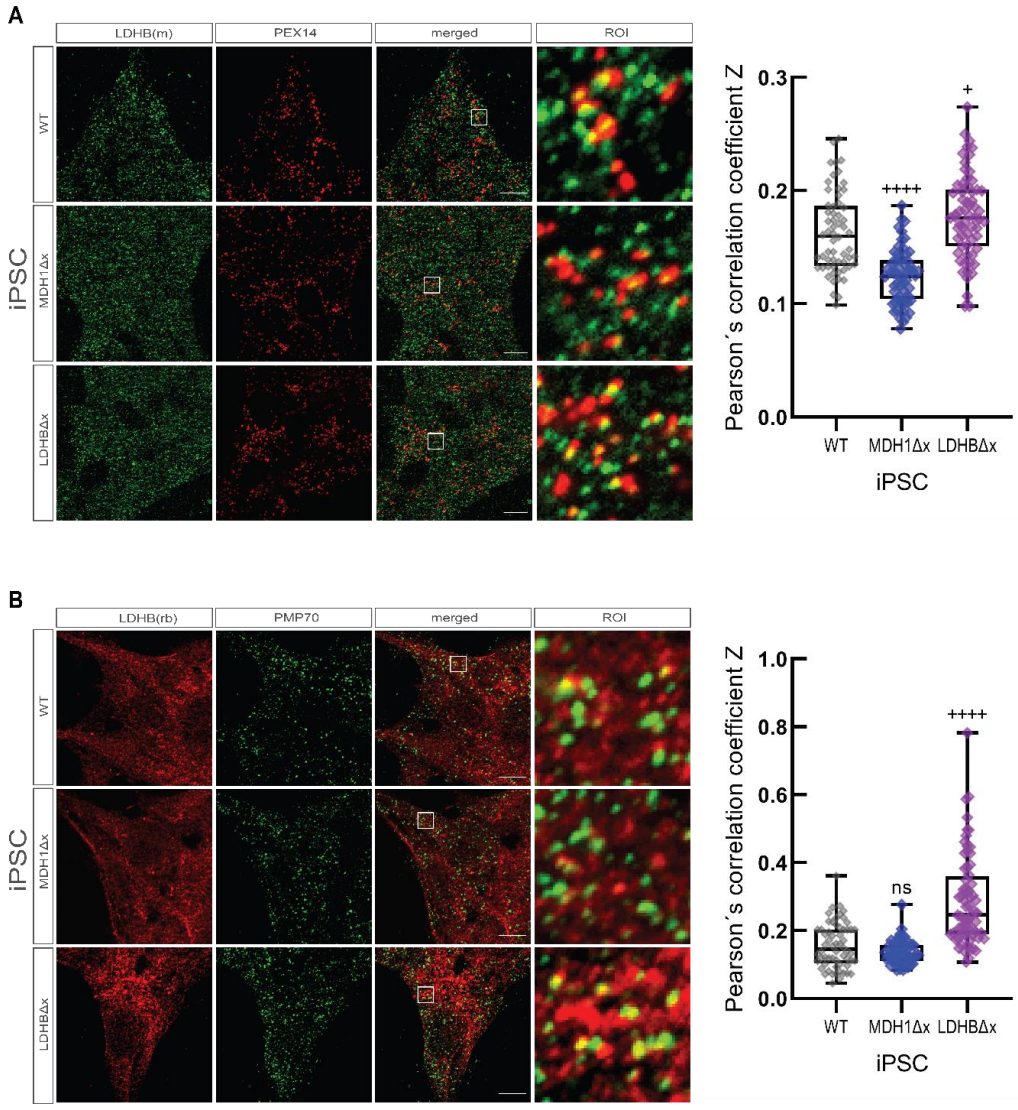

Figure 8 – Effect of LDHB colocalization with peroxisomes in cells lacking LDHBx.

The peroxisomal colocalization of LDHB in iPSC lacking MDH1, lacking LDHB, and wild type, was tested by immunostaining LDHB together with a peroxisomal membrane protein. Both experimental settings, either when cells were immunostained with (**A**) mouse anti-human LDHB together with rabbit anti-human PEX14, or (**B**) rabbit anti-human LDHB with mouse anti-human PMP70, showed less peroxisomal LDHB colocalization in the mutant MDH1Δx, when compared to wild type, while in the LDHBΔx mutant colocalization levels were higher than wild type. PCC was retrieved from a total of 60 images for wild type and MDH1Δx cells, while for LDHBΔx 63 and 68 images were used when immunostained with mouse and rabbit anti-human LDHB, respectively. Two independent experiments were performed. The boxplot's whiskers illustrate the maximum and minimum in each condition. The boxplot's body represents the first and third quartiles with the upper and lower line, while the middle line illustrates the median. Data was then converted with Fisher's z-transformation for further statistical analysis. Shapiro-Wilk test was used to assess the distribution of the data. Mann-Whitney test was performed in all data with the exception of the comparison between WT and MDH1Δx in (B), were t-test was used. $^{++++}p \leq 0.0001$; $^{+++}p \leq 0.001$; $^{*}p \leq 0.05$; $^{ns}p>0.05$. Scale bars are 10 µm.

ROS levels increase in iPSCs lacking MDH1x and LDHBx

Since peroxisomes are involved in H_2O_2 metabolism (Walker et al., 2018), ROS metabolism was indirectly assessed in the iPSC mutants. First, glutathione (GSH) levels were quantified in the iPSC-mutants and wild type under normal conditions. For the quantification of GSH, cells were harvested and lysed, and then the GSH levels were estimated with GSH-Glo™ Glutathione Assay from Promega. The assay is based in the conversion of a luciferin derivative into luciferin, by the action of glutathione S-transferase in the presence of GSH. Then, firefly luciferase oxidizes the luciferin creating light, which can be measured with a luminometer and used to calculate the original amount of GSH. For analysis, GSH levels were calculated in nanograms, normalized by the total protein levels in micrograms. This resulted in GSH levels of 910 ng/µg in the wild type, while in iPSCs lacking MDH1x and LDHBx, the levels were significantly higher. The MDH1Δx mutant had GSH levels of 1731 ng/µg, while the LDHBΔx mutant had 1404 ng/µg (Figure 9A).

Additionally, catalase activity was measured in the three iPSC lines with the method described in Islinger et al., 2012. Briefly, cells were collected and permeabilized with a buffer containing 0.2% (v/v) Triton X-100. Then, a solution containing H_2O_2 was added, so that the catalase present in the sample converts it into H_2O and O_2. The reaction was stopped with a solution containing titanyl sulphate ($TiOSO_4$), which forms a yellow complex with H_2O_2, and that can be measured and used for the estimation of catalase activity. Activity was measured in terms of units per milligram of total protein (U/mg), which represents the ability of catalase of causing the destruction of 90% of the substrate in one minute, in one milligram of protein sample.

Results showed that in both mutants, MDH1Δx and LDHBΔx, catalase activity is significantly higher than the wild type under normal conditions (Figure 9B). The wild type showed catalase activity of 11.52 U/mg, while the levels of MDH1Δx were 14.29 U/mg and the levels of LDHBΔx were 21.68 U/mg, 24% and 88% higher than the wild type, respectively (Figure 9B).

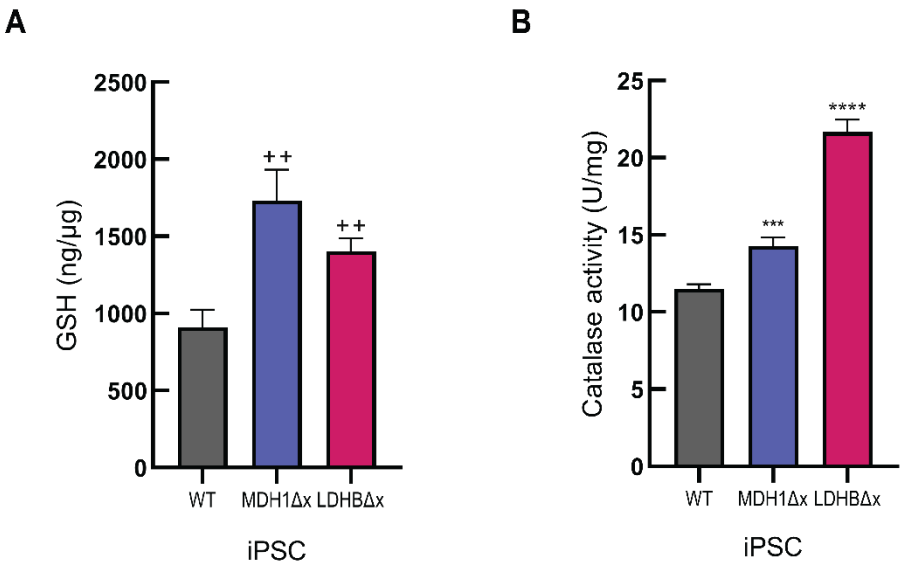

Figure 9 – iPSC mutants MDH1Δx and LDHBΔx show higher glutathione levels and catalase activity than wild type.
Cells were tested for oxidative stress under normal conditions. (**A**) Glutathione levels of both mutant cell lines, lacking either MDH1x or LDHBx had higher levels of GSH than wild type cells. (**B**) Catalase activity was measured higher in both mutants, MDH1Δx and LDHBΔx, when compared to wild type. Three independent experiments, with three replicates per condition were performed both in A and B. Data was tested for normal distribution with Shapiro-Wilk test. Statistical analysis was performed using Mann-Whitney test for A, and Student's t-test for B. $^{++}p \leq 0.01$; ****$p \leq 0.0001$; *$p \leq 0.05$. Whiskers indicate S.E.M. Experiments were done with the help of Vishalini Venkatesan.

Mitochondrial respiration in iPSC MDH1Δx and LDHBΔx

Since peroxisomes are known to communicate and cooperate with mitochondria (Fransen et al., 2017), it was assessed if the peroxisomal phenotype of iPSC MDH1Δx and LDHBΔx had an influence in mitochondrial respiration. For this, a Cell Mito Stress test from Agilent Seahorse was performed on the cells four days after seeding. The test consists in measuring the oxygen consumption rate (OCR) over time in a medium containing only one carbon source, in this case medium with glucose (1 mM) was used. Along the experiment, drugs are injected in the well to inhibit certain components of the mitochondrial machinery to recognize and compare different functions within mitochondrial respiration. At the start of the experiment, OCR was measured with medium alone, in order to assess the basal respiration (Figure 10A). This measurement already showed a difference between wild type and the mutants, with wild type showing a basal respiration of 362.2 pmol/min, significantly higher than MDH1Δx and LDHBΔx, with a basal respiration of 330.2 and 274.7 pmol/min, respectively (Figure 10B).

Then, oligomycin was added up to final concentration of 2.5 µM to inhibit ATP synthase, lowering respiration (Figure 10A). The difference between basal respiration and the respiration levels after oligomycin indicates the ATP-linked respiration, also named ATP production, namely the respiration reserved for the production of ATP through oxidative phosphorylation. For iPSC LDHBΔx, with an OCR of 236.6 pmol/min, a significantly lower ATP production than wild type (306.9 pmol/min) was observed, while the MDH1Δx mutant showed no difference with wild type (Figure 10B).

Next, cyanide-p-trifluoromethoxyphenylhydrazone (FCCP, 200 nM) was injected in order to uncouple mitochondrial respiration, resulting in an increase in mitochondrial respiration to its maximum rate (Figure 10A). The maximum respiration showed to be the same for iPSC wild type, MDH1Δx and LDHBΔx, as well as the spare respiration capacity, which represents the difference between maximum and basal respiration (Figure 10B). Finally, a mixture of rotenone and antimycin A was added, both with a final concentration of 0.5 µM, in order to shut down mitochondrial respiration, leaving the residual respiration of proteins not related with mitochondrial respiration (Figure 10A). From this, the residual non-mitochondrial oxygen consumption is calculated, which was significantly lower for MDH1Δx (62.42 pmol/min) than wild type (77.5 pmol/min), while no difference was observed between the LDHBΔx and wild type (Figure 10B). Importantly, the values of non-mitochondrial respiration represent the baseline over which all previous values are calculated. Additionally, with the difference between the non-mitochondrial respiration and the respiration after oligomycin, the proton leak was estimated, which was significantly lower in LDHBΔx (49.9 pmol/min) than in wild type (55.3 pmol/min), while no significant difference was observed between MDH1Δx and wild type (Figure 10B). Overall, small but significant differences were observed in mitochondrial respiration between wild type and cells lacking MDH1x or LDHBx, like in the case of basal respiration. This supports the interdependence between peroxisomes and mitochondria, and suggest an influence of the peroxisomal shuttling systems over mitochondria metabolism.

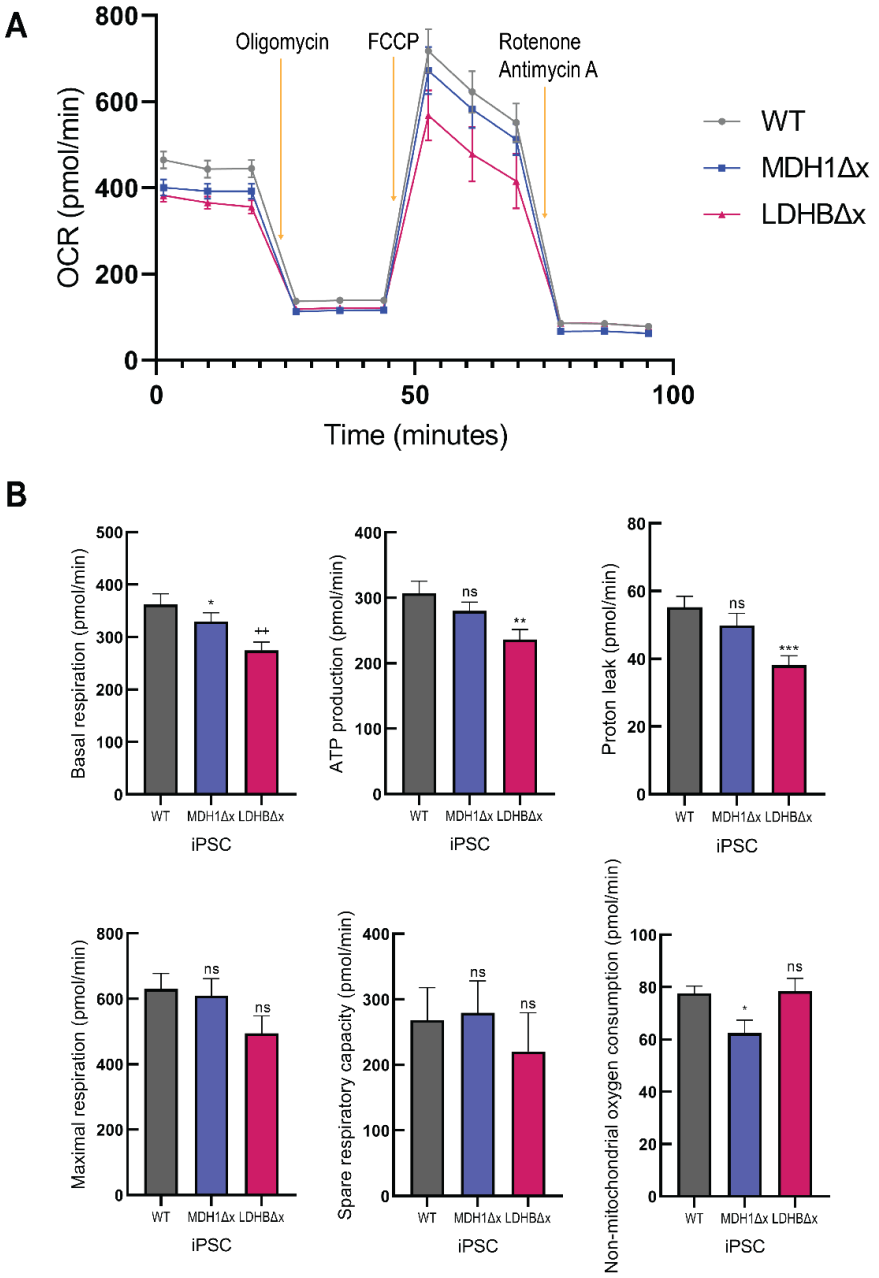

Figure 10 – The lack of peroxisomal MDH1 and LDHB has small but significant effects on mitochondrial respiration.
Mitochondrial respiration of the iPSCs lacking MDH1x and LDHBx was measured with Seahorse Cell Mito Stress test. (**A**) Oxygen consumption rate was measured under 1 mM glucose as basal respiration, then oligomycin (2.5 µM) was added for the inhibition on ATP synthase, afterwards FCCP (200 nM) was injected for the measurement of maximal respiration, and finally, a mixture of rotenone (0.5 µM) and antimycin A (0.5 µM) was added to shut down mitochondrial respiration. (**B**) The mutants show differences in mitochondria respiration when compared to the wild type. Lower levels of basal respiration are seen in both iPSC MDH1Δx and LDHBΔx, lower non-mitochondrial consumption in the case of MDH1Δx, and lower ATP production and proton leak in the case of LDHBΔx alone. Non-mitochondrial consumption is taken as the baseline for each measurement. Four independent experiments were performed. Data distribution was assessed by Shapiro-Wilk test. Statistical analysis was performed with Student t-test: ****p ≤ 0.0001; ***p ≤ 0.001; **p ≤ 0.01; *p ≤ 0.05; ^{ns}p>0.05. Whiskers are S.E.M.

Fatty acid metabolism in cells lacking MDH1Δx

Next, it was assessed if the lack of MDH1 in peroxisomes had an effect in the metabolism of fatty acids. For this, an experiment based on Violante et al., 2019, was performed. Shortly, cells were incubated with dodecanoic acid (C12:0, 120 µM) and treated with L-aminocarnitine (L-AC, 200 µM), which inhibits the carnitine palmitoyltransferase II (CPT2) at the mitochondria, hence forcing the catabolism of fatty acids towards peroxisomes instead of mitochondria. After 3 days of treatment, the medium was collected and analyzed with the CortecsT3 lipidomics method. As a result, when no C12:0 nor drugs were added, no differences in the levels of C10:0 and C12:0 were observed between HEK wild type and MDH1Δx (Figure 11A and B).

When cells were incubated with C12:0, no significant changes were observed between wild type and MDH1Δx in the measurement of C10:0, nor C12:0, although a tendency to increase was observed in both cases (Figure 11A and B). The same situation was observed when L-AC was used for the inhibition of Carnitine O-palmitoyltransferase 2 (CPT2), and with this, the mitochondrial import of fatty acids, a non-significant increase was observed in C10:0 and C12:0 (Figure 11A and B).

Finally, cells treated with a mix of C12:0 and L-AC were tested, resulting in no significant difference between the wild type and MDH1Δx in the levels of both C10:0 and C12:0 (Figure 11A).

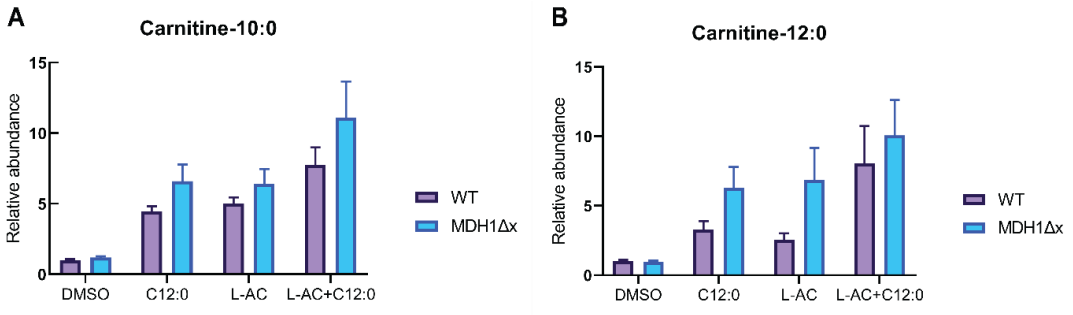

Figure 11 – Catabolism of dodecanoic acid in cells lacking MDH1x.
Fatty acid metabolism was assessed in HEK cells lacking MDH1x, as well as in wild type. Cells were treated either with dodecanoic acid (C12:0), with L-aminocarnitine (L-AC) for the inhibition of CPT2 in mitochondria, with both C12:0 and L-AC for inducing the metabolism of fatty acids into peroxisomes, or with DMSO as control. After 72 hours of treatment, cell media was collected and metabolites detected with the CortecsT3 lipidomics method. (**A**) When measuring the levels of carnitine-C10:0, no significant difference was found between the wild type and MDH1Δx in the DMSO control, when L-AC was used, when incubated with C12:0, nor when C12:0 was added together with L-AC. (**B**) When carnitine-C12:0 was measured in the medium, no significant difference was observed between the wild type and MDH1Δx in the control, when L-AC or C12:0 were added independently, nor together. Three independent experiments were made, each with three replicates per condition. Data distribution was assessed with Shapiro-Wilk test. When data had normal distribution, t-test was used to compare MDH1Δx to wild type, otherwise, Mann-Whitney test was used.

Expression of AGC1, AGC2 and OGC with fluorescent tags indicates their presence in peroxisomes

As MDH1x is expected to work as part of a peroxisomal malate aspartate shuttle (MAS), the membrane carriers of MAS were also investigated for their peroxisomal presence. The transporters involved in MAS are the aspartate-glutamate carrier 1 (AGC1), aspartate-glutamate carrier 2 (AGC2) and the 2-oxoglutarate/malate carrier (OGC) (Bisaccia et al., 1988; Palmieri et al., 2001). For this, constructs of each transporter were developed, containing an EGFP either at the N- or C-terminal portion of the protein. Transporters were overexpressed in HeLa cell for 24 hours, fixed, and their distribution evaluated.

As a result, all proteins with the EGFP-tag at the N-termini showed a distribution that resembles mitochondria, and in addition, they presented some round-shaped structures (Figure 12A, white arrows). The same pattern was observed when the tag was at the C-terminal domain of the proteins, a mitochondria-like distribution in addition to some small round structures (Figure 12B, white arrows).

Then, in order to test if the proteins were transported mainly to mitochondria, the EGFP-tagged proteins were expressed together with a mitochondrial marker, mito-BFP, in addition to the peroxisomal marker ruby-PTS1, in order to assess if the small round structures corresponded to peroxisomes. Indeed, the main distribution of all

EGFP-tagged proteins was mitochondrial, and in addition to this, it was observed that peroxisomes showed three dispositions towards the EGFP-tagged proteins. Some peroxisomes overlapped with the EGFP-proteins only, while were distant from mitochondria (Figure 12C, yellow arrows). Other peroxisomes overlapped with the EGFP signal, but were also very close to mitochondria, which made it difficult to know with certainty that the overlap was between our EGFP-proteins and peroxisomes, or rather because peroxisomes were close to mitochondria (Figure 12C, magenta arrows). The third situation was when peroxisomes did not overlap neither with mitochondria, nor the EGFP-tagged proteins (Figure 12C, white arrows).

For AGC1, the three previously described conditions were observed, both for cells transfected with the EGFP tag at the C-terminal (AGC1-EGFP, Figure 12C-a and b), and at the N-terminal (EGFP-AGC1, Figure 12C-c and d). In the case of AGC2, two of the three scenarios were found when the EGFP-tag was at the N-terminus (EGFP-AGC2). On the one hand, peroxisomes that did not overlap with anything were observed, and on the other hand, peroxisomes that were close to mitochondria, for which is difficult to assess if the overlap with EGFP-AGC2 is due to their closeness to mitochondria instead of real overlap (Figure 12C-e and f). Nevertheless, all three conditions were observed when the tag was at the C-terminal end of AGC2 (AGC2-EGFP, Figure 12C-g and h). Finally, when EGFP-tagged OGC was expressed in HeLa, the three peroxisomal situations were observed with both versions of OGC, tagged either at the N- or C-termini (EGFP-OGC and OGC-EGFP). Interestingly, a particularly high overlap between peroxisomes and OGC was found, independently of the tag's position (Figure 12C-i, j, k and l).

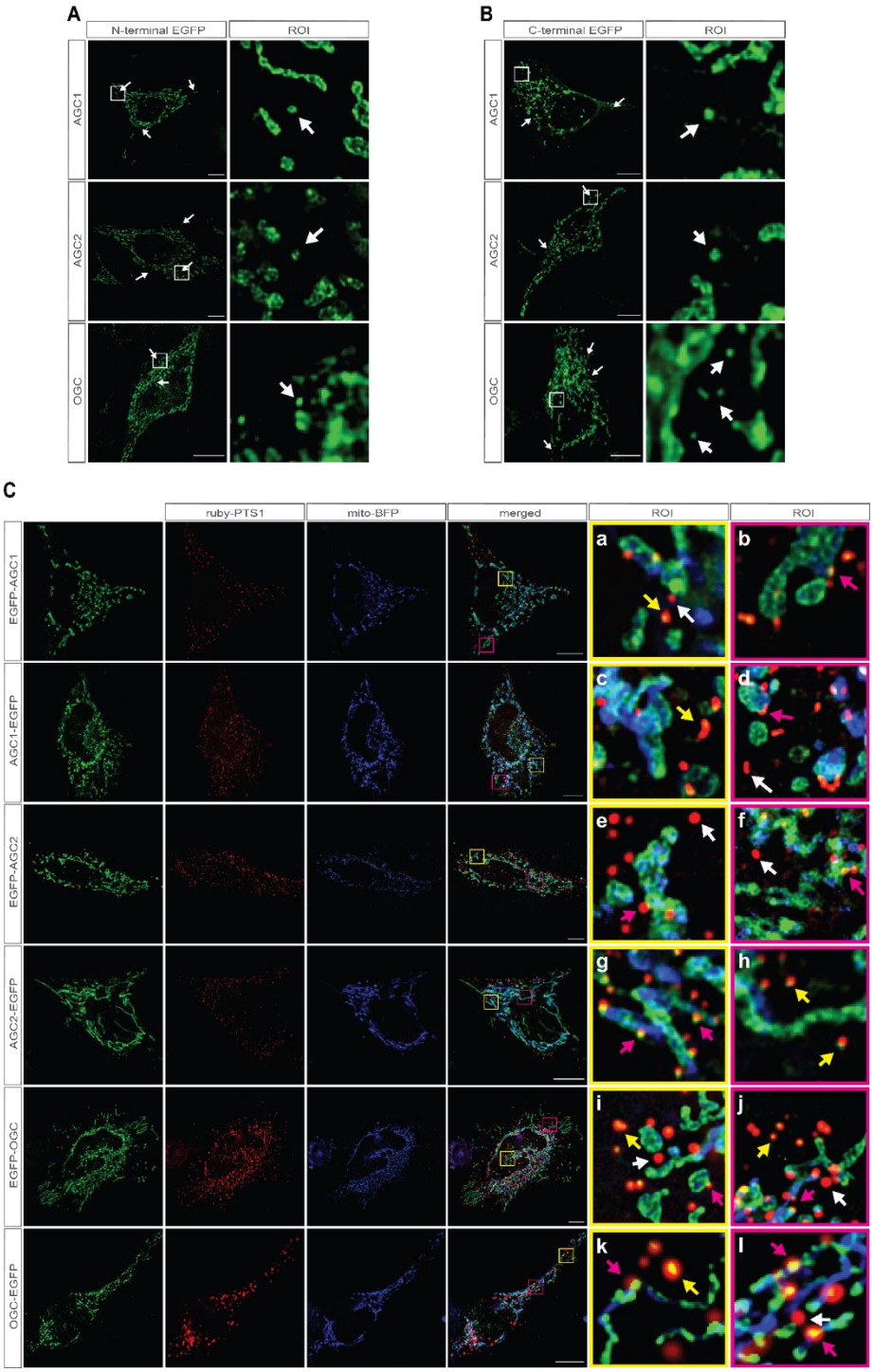

Figure 12 – Plasmid-borne expression of AGC1, AGC2 and OGC demonstrates their presence at the peroxisome of HeLa cells.
HeLa cells were transfected for 24 hours with EGFP-tagged AGC1, AGC2 and OGC, to assess their distribution. (**A**) N-terminal tagged AGC1, AGC2 and OGC show mitochondria-like distribution, together with some small structures (white arrows). (**B**) C-terminal tagged AGC1, AGC2 and OGC also show structures resembling mitochondria in addition to dotty structures. (**C**) Triple transfection consisting in AGC1, AGC2, or OGC, together with the peroxisomal marker ruby-PTS1 and the mitochondrial marker mito-BFP. Peroxisomes show three distinct configurations: no overlap with any other marker (white arrows), overlap with mitochondria nor the protein of interest (magenta arrows), or overlap with the protein of interest alone (yellow arrows). Scale bars are 10 µm.

Validation of antibodies against AGC1

Next it was determined which antibody against AGC1 was more suitable for immunofluorescence. For this, AGC1 was knocked down for 72 hours, and its relative expression estimated with mouse and rabbit anti-human AGC1 (Figure 13A). Independently of the antibody used, a reduction of around 85% was appreciated in the expression from AGC1, validating the use of both antibodies in western blot.

Next, since they were produced in different species, HeLa cells were immunostained with both antibodies against AGC1. Surprisingly, the signal from both antibodies did not overlapped considerably with each other, which could mean that one of the antibodies, or both in the worst case, is/are not suitable for immunofluorescence (Figure 13B).

Then, HeLa cells were transfected with the EGFP-AGC1 construct. After 24 hours of incubation, cells were immunostained against AGC1, with rabbit and mouse anti-human AGC1. As a result, the signal from the rabbit anti-human AGC1 overlapped nicely with the signal from the overexpressed protein, in addition to having more signal spread in the cell. Nevertheless, mouse anti-human AGC1 just had a very disperse distribution in the cell, but failed to overlap with EGFP-AGC1 (Figure 13C).

Finally, these findings were confirmed by repeating the previous experiment, this time transfecting HeLa cells with AGC1-EGFP instead of EGFP-AGC1. As a result, mouse anti-human AGC1 showed the same lack of overlap with AGC1-EGFP, so this antibody was excluded from further analyses (Figure 13D).

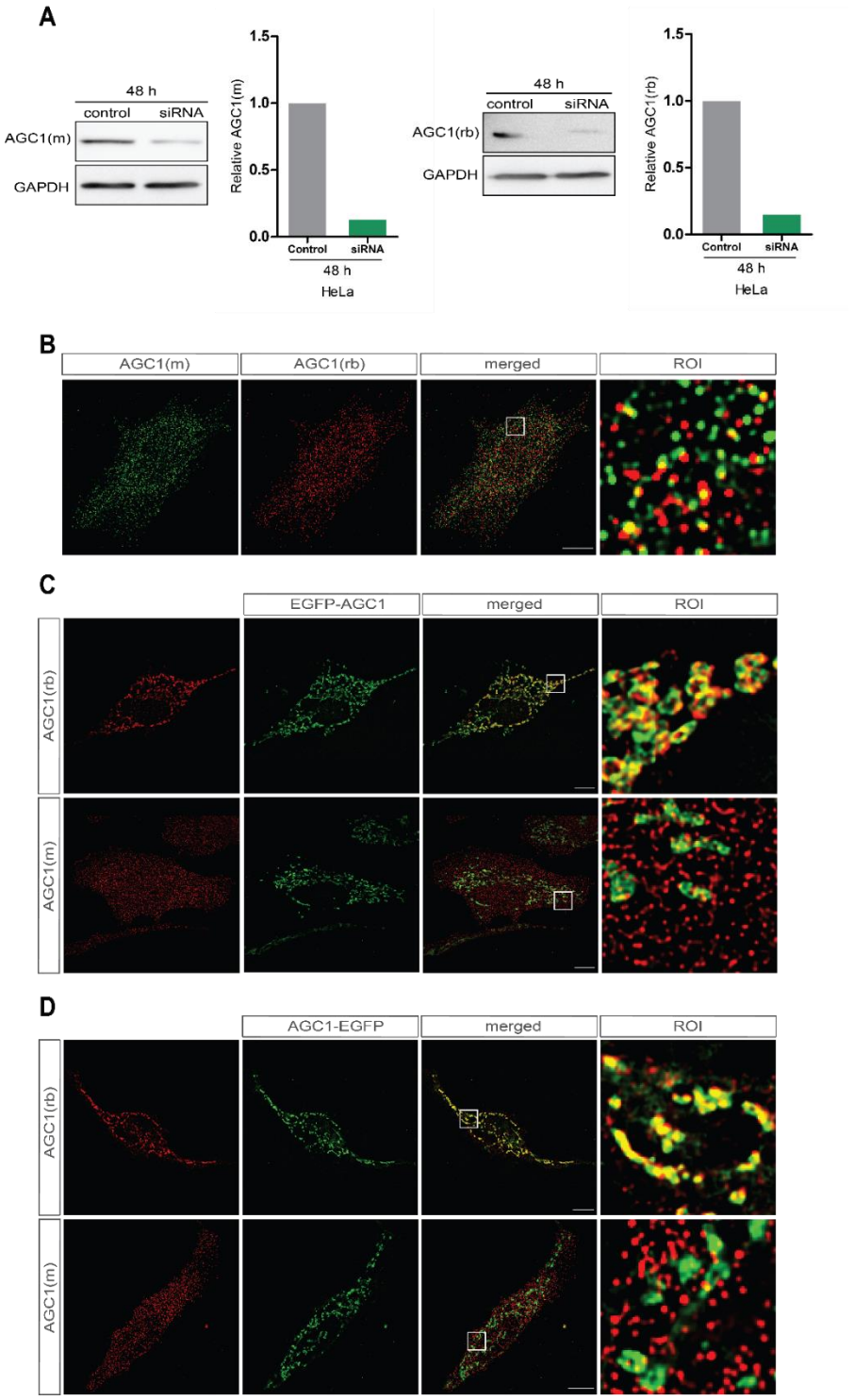

Figure 13 – Antibodies produced in rabbit and mouse against AGC1 are suitable for western blot, but only anti-AGC1 (rabbit) for immunofluorescence.
Validation of antibodies against AGC1. (**A**) HeLa cells were treated with siRNA against AGC1 for 48 hours, then protein levels were analyzed by western blot showing a reduction in AGC1 expression both with mouse anti-human AGC1 (left), as with rabbit anti-human AGC1 (right). (**B**) Immunofluorescence using both antibodies against AGC1 together. (**C**) HeLa cells were transfected with N-terminal EGFP-tagged AGC1, and after 24 hours immunostained with both antibodies against AGC1. (**D**) HeLa cells transfected with C-terminal EGFP-tagged AGC1 were immunostained with rabbit or mouse anti-human AGC1. Scale bars are 10 µm.

The same methodology was used for the validation of the antibodies against AGC2 and OGC. The EGFP-tagged versions of AGC2 and OGC were overexpressed and then immunostained against the same proteins. In this case, rabbit anti-human AGC2 overlapped quite nicely with both N- and C-terminal proteins. Similarly, rabbit anti-human OGC showed a good overlap with both tagged proteins.

Additionally, in all cases we see that the detection with antibodies gives, on top of the overlapping signal, additional signal spread across the cell. This signal might be the endogenous non-tagged protein, present for example in peroxisomes not reached by the overexpression of tagged protein. Altogether, the validity of the antibodies rabbit anti-human AGC1, AGC2 and OGC for their usage in immunofluorescence could be confirmed.

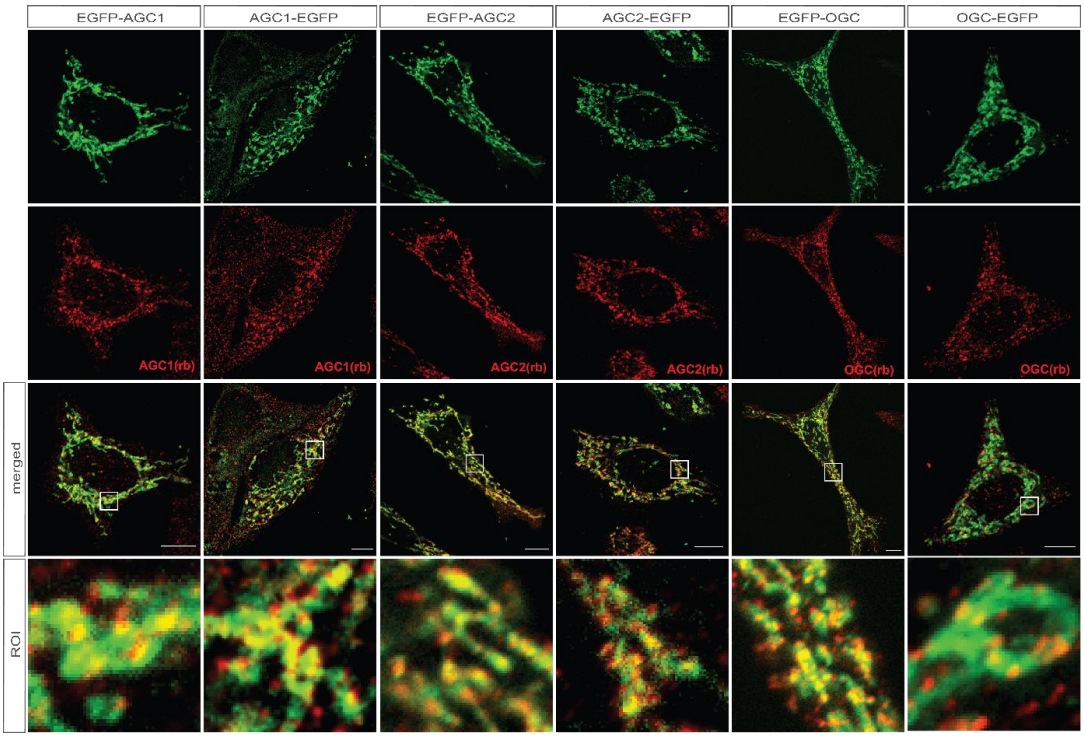

Figure 14 – Antibodies against AGC1, AGC2 and OGC were validated with their GFP-tagged counterparts.
HeLa cells were transfected with plasmids containing C- or N-terminal EGFP-tagged AGC1, AGC2, or OGC. After the transfection, cells were incubated for 24 hours and immunostained against rabbit anti-human AGC1, AGC2, or OGC, respectively. Scale bars are 10 µm.

Assessment of the peroxisomal localization of MAS transporters in HeLa

The peroxisomal localization of AGC1, AGC2, and OGC was then assessed in cells under normal conditions. For this, HeLa cells were immunostained with the previously validated antibodies against AGC1, AGC2, and OGC, together with mouse anti-human PMP70, a peroxisomal membrane protein that functions as a peroxisomal marker.

Since the MAS transporters are expected to reside mainly in mitochondria, Manders' overlap coefficient (MOC) was preferred for the measurement of colocalization. Manders' coefficient estimates how much of the peroxisomal signal is overlapped by the signal of the POI. This value goes from zero to one, zero being no colocalization, and one being 100% overlap.

Also, before measuring the peroxisomal colocalization of AGC1, AGC2 and OGC, three other proteins were selected as internal references of the colocalization method. The first one, lysosomal-associated membrane protein 1 (LAMP1), a lysosomal membrane protein used as a negative control. The second, PEX14, a peroxisomal membrane protein used as a positive control. The last one, cytochrome c oxidase polypeptide IV (COX4), a mitochondrial membrane protein, was used to assess the normal overlap of mitochondria with peroxisomes. The later was used as a threshold, over which an expected mitochondrial protein, is said to also localize in peroxisomes.

For LAMP1, the antibody's signal was distributed across the whole cell, with some bigger structures in the area of the nucleus (Figure 14A). When quantified, the average colocalization with peroxisomes was 0.084. This represents the lowest colocalization between peroxisomes and a protein that is not expected to be present in the peroxisomal membrane (Figure 14B). COX4 showed a mitochondria-like distribution (Figure 14A). The average colocalization of COX4 with peroxisomes had a value of 0.169, which represents normal colocalization levels between peroxisomes and mitochondria (Figure 14B). Finally, PEX14 showed high overlap with peroxisomes across the whole cell (Figure 14A). The colocalization of PEX14 with peroxisomes had an average of 0.688, being the highest colocalization levels between two proteins to be expected with this method (Figure 14B).

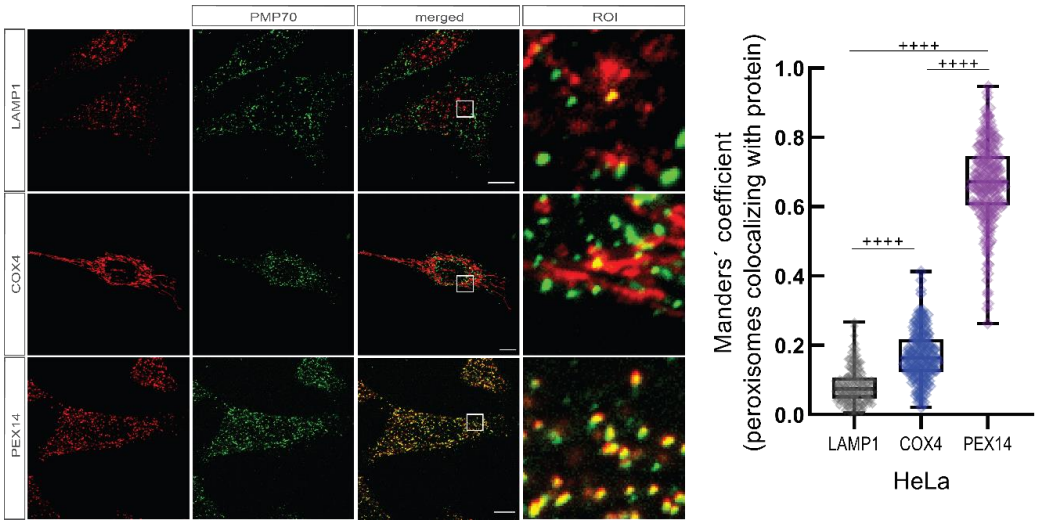

Figure 15 – LAMP1, COX4 and PEX14 serve as peroxisomal colocalization controls in HeLa cells.
HeLa cells were immunostained against LAMP1, COX4, or PEX14, together with PMP70. Colocalization between both markers is expressed as Manders' coefficient, which represents the portion of peroxisomes overlapped by our protein of interest. The lysosomal membrane protein, LAMP1, shows colocalization levels of 0.084, the mitochondrial protein COX4 has colocalization levels of 0.169, and the peroxisomal protein PEX14 of 0.668. The whiskers of the boxplot illustrate the maximum and minimum data point in each condition. The boxplot's upper and lower line illustrate the first and third quartiles, and the line in the middle represents the median. Two experiments were done with a total of approximately 200 cells per condition. Data distribution was assessed with Shapiro-Wilk test, and statistical analysis was done with Mann-Whitney test. $^{++++}p \leq 0.0001$. Scale bars are 10 µm.

Then, the peroxisomal colocalization of AGC1, AGC2 and OGC was assessed, in comparison with the peroxisomal colocalization levels of COX4.

When immunostained, AGC1 showed a quite sparse distribution in the cell, in addition to some overlap with the peroxisomal signal (Figure 16A). The quantification of the peroxisomal AGC1 showed colocalization levels of 0.238, in terms of average MOC. This value is significantly higher than random mitochondrial-peroxisome colocalization, given by COX4, suggesting the presence of AGC1 in peroxisomes, in addition to mitochondria (Figure 16B). For AGC2, the distribution follows a mitochondria-like shape, with visible overlap with peroxisomes in some regions (Figure 16A). The peroxisomal colocalization of AGC2 was 0.219, significantly higher than the peroxisomal colocalization levels of COX4, suggesting the presence of AGC2 in peroxisomes (Figure 16B). Finally, the distribution in the cell of OGC was quite similar to the distribution of AGC1, with a signal spread across the whole cell (Figure 16A). Also, the colocalization levels of OGC were significantly higher than COX4, with an average value of 0.361, suggesting its presence in the peroxisomal membrane, together with AGC1 and AGC2 (Figure 16B).

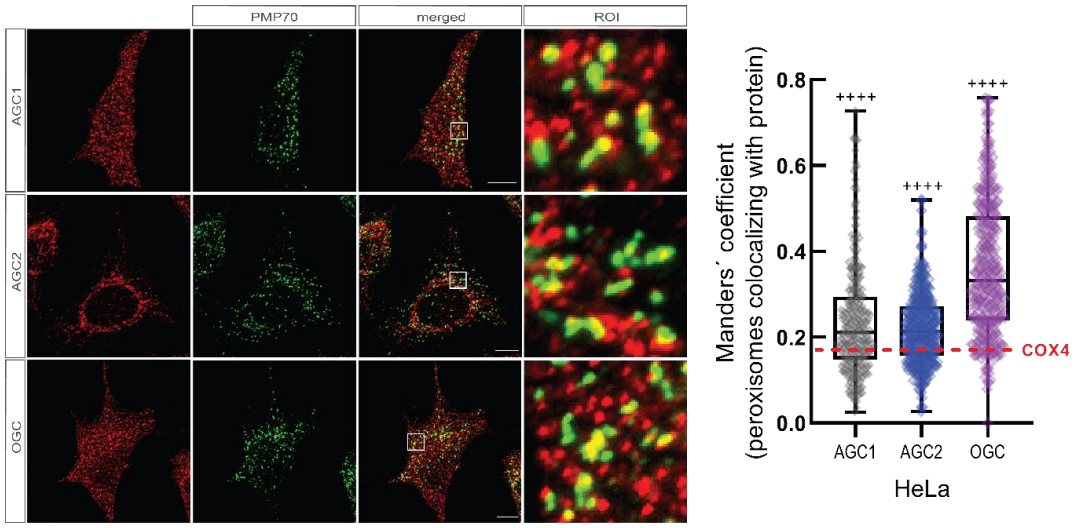

Figure 16 – AGC1, AGC2 and OGC are present in peroxisomes of HeLa cells.
HeLa cells were immunostained against AGC1, AGC2, or OGC, together with PMP70 as a peroxisomal marker. Colocalization between both proteins was assessed with Manders' coefficient, which represents the portion of peroxisomes which overlaps with the POI. The colocalization levels of the three proteins were significantly higher than the colocalization levels of COX4 (0.169), with an average of 0.238 in the case of AGC1, 0.219 for AGC2, and 0.361 for OGC. The boxplot's whiskers show the maximum and minimum. The body represents the first and third quartiles in the upper and lower line, while the middle line represents the median. Two independent experiments were conducted, with around 260 cells per condition. Data distribution was assessed with Shapiro-Wilk test, and statistical analysis was performed with Mann-Whitney test. $^{++++}p \leq 0.0001$. Scale bars are 10 µm.

Evaluation of the peroxisomal presence of MAS transporters in iPSC-CM

Next, considering that some patients with peroxisomal diseases show a cardiac phenotype, together with the reliance of fatty acids in the adult heart (Goldberg et al., 2012; Koh et al., 2001; Wanders and Komen, 2007), the presence of the MAS transporters was assessed in cardiac cells, specifically in cardiomyocytes derived from iPSCs (iPSC-CM).

As before with HeLa cells, the peroxisomal levels of LAMP1, COX4, and PMP70 were determined and used as reference. LAMP1 was distributed all over the cell, in addition to two accumulations in the nuclear area of the cell. Such accumulations were not present in HeLa (Figure 17B). When quantified, the average peroxisomal colocalization of LAMP was 0.072, value that represents the colocalization of a protein that is not present in the peroxisomal membrane (Figure 17B). When cells were immunostained against COX4, the signal had a nice mitochondria-like distribution, as previously seen in HeLa (Figure 17A). The peroxisomal localization of COX4 had an

average of 0.141, which acts as a threshold over which a presumably mitochondrial protein should be also present in peroxisomes (Figure 17B). Finally, the signal of PEX14 showed a nice overlap with peroxisomes (Figure 17A). The colocalization levels of PEX14 had a mean value of 0.788, which represents the highest expectable colocalization between two proteins with this method (Figure 17B).

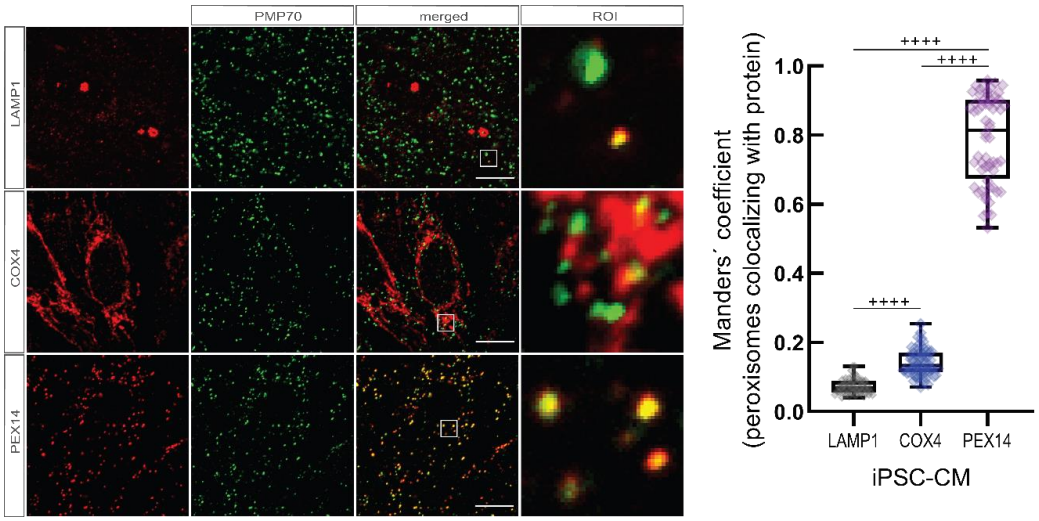

Figure 17 – LAMP1, COX4 and PEX14 serve as controls for peroxisomal colocalization in iPSC-CMs.
iPSC-CMs were immunostained with antibodies against PMP70 together with the lysosomal protein LAMP1, the mitochondrial protein COX4, or the peroxisomal protein PEX14. Colocalization between the components was analyzed in terms of Manders' coefficient, which represents the portion of peroxisomes overlapped by the protein of interest. The mean peroxisomal localization of LAMP1 is 0.072, of COX4 is 0.141, and 0.788 in the case of PEX14. The whiskers of the boxplot illustrate the maximum and minimum in the cohort. The upper and lower lines of the boxplot show the first and third quartiles, while the middle line depicts the median. Two independent experiments were performed, with a total of 60 pictures per condition. The distribution of the data was assessed with Shapiro-Wilk test and the statistical analysis with Mann-Whitney test. $^{++++}p \leq 0.0001$. Scale bars are 10 µm.

Then, the peroxisomal localization of AGC1, AGC2, and OGC was tested. When iPSC-CMs were immunostained against AGC1, the AGC1 signal showed a widespread distribution in the cell, with some overlap with peroxisomes (Figure 18A). The colocalization levels of AGC1 were significantly lower than the colocalization levels of COX4, with a mean colocalization value of 0.096, suggesting that AGC1 is not present in the peroxisomes of iPSC-CMs (Figure 18B). AGC2 showed a mitochondria-like distribution in the cell, with some overlap with the peroxisomal signal (Figure 18A). The average of peroxisomal localization was significantly higher than the threshold, with a mean value of 0.257, suggesting the presence of AGC2 in peroxisomes (Figure 18B). Finally, as it was the case for AGC1, the OGC signal was

also distributed in the whole cell, showing some small overlap with peroxisomes (Figure 18A). The colocalization levels of OGC were also significantly lower than the threshold COX4, with an average of 0.078, suggesting the absence of OGC in peroxisomes of iPSC-CMs (Figure 18B).

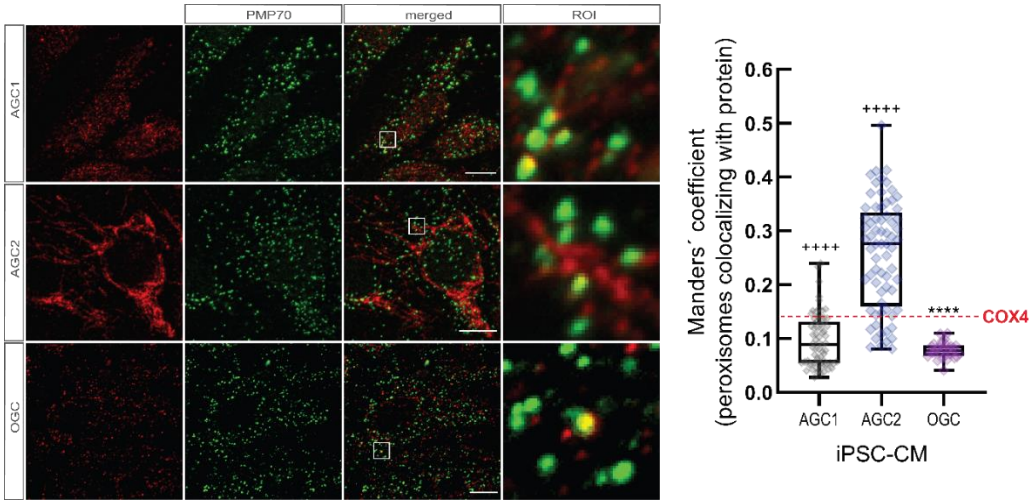

Figure 18 – AGC2 is present in the peroxisomes of iPSC-CMs.
iPSC-derived cardiomyocytes were immunostained against PMP70, together with AGC1, AGC2, or OGC. Colocalization between the proteins was assessed with Manders' coefficient, which corresponds to the portion of peroxisomes covered by the protein of interest. Only AGC2, with an average of 0.257, showed higher colocalization levels than the control COX4 (0.141), while both AGC1 and OGG, with an average of 0.096 and 0.078 respectively, showed lower colocalization levels than COX4. The whiskers of the boxplot show the minimum and maximum, while the body shows the first quartile, median, and third quartile, in the upper, middle, and lower line. Two independent experiments were conducted with a total of around 60 pictures per condition. Distribution of data was analyzed with Shapiro-Wilk test. Statistical analysis was performed with Mann-Whitney test for AGC1 and AGC2, while Student's t-test was used for OGC. $^{++++}p \leq 0.0001$; ****$p \leq 0.0001$. Scale bars are 10 µm.

Proximity between peroxisomal marker and AGC1, AGC2 and OGC supports their presence in peroxisomes

Then, since the colocalization analysis showed the presence of AGC1, AGC2 and OGC in peroxisomes of HeLa cells (Figure 16), the proximity between these proteins and PMP70 was assessed using a proximity ligation assay (Duolink, Sigma-Aldrich). The assay is based in the recognition of the primary antibodies by two independent probes. When these probes are closer than 40 nm, ligation produces a circular DNA, which is then amplified and detected with a fluorescent probe. The amplification is observed under the microscope as a highly fluorescent dot. The different dots represent an independent proximity event between the antibodies, which can be quantified per cell (Figure 19A). Additionally, the proximity events given by each

antibody by itself were measured and subtracted from the events when both antibodies were together. As a negative control, an antibody against the histone H3, trimethylated at the lysine 27, was utilized, and as positive control, PEX14 was used. As a result, the proximity events of H3 were presented as zero, while the values of the others conditions were scaled accordingly (Figure 19B). The proximity events of AGC1 were significantly higher than the negative control, with an average of 5.5 contacts per cell. The same situation was observed for AGC2, where 9.38 proximity events were observed per cell, significantly higher than H3. In the case of OGC, 11.23 proximity events were observed per cell in average. Finally, the positive control PEX14 showed 56.13 proximity events per cell. These results confirm the presence of AGC1, AGC2 and OGC in peroxisomes of HeLa cells, as previously seen through quantifying colocalization.

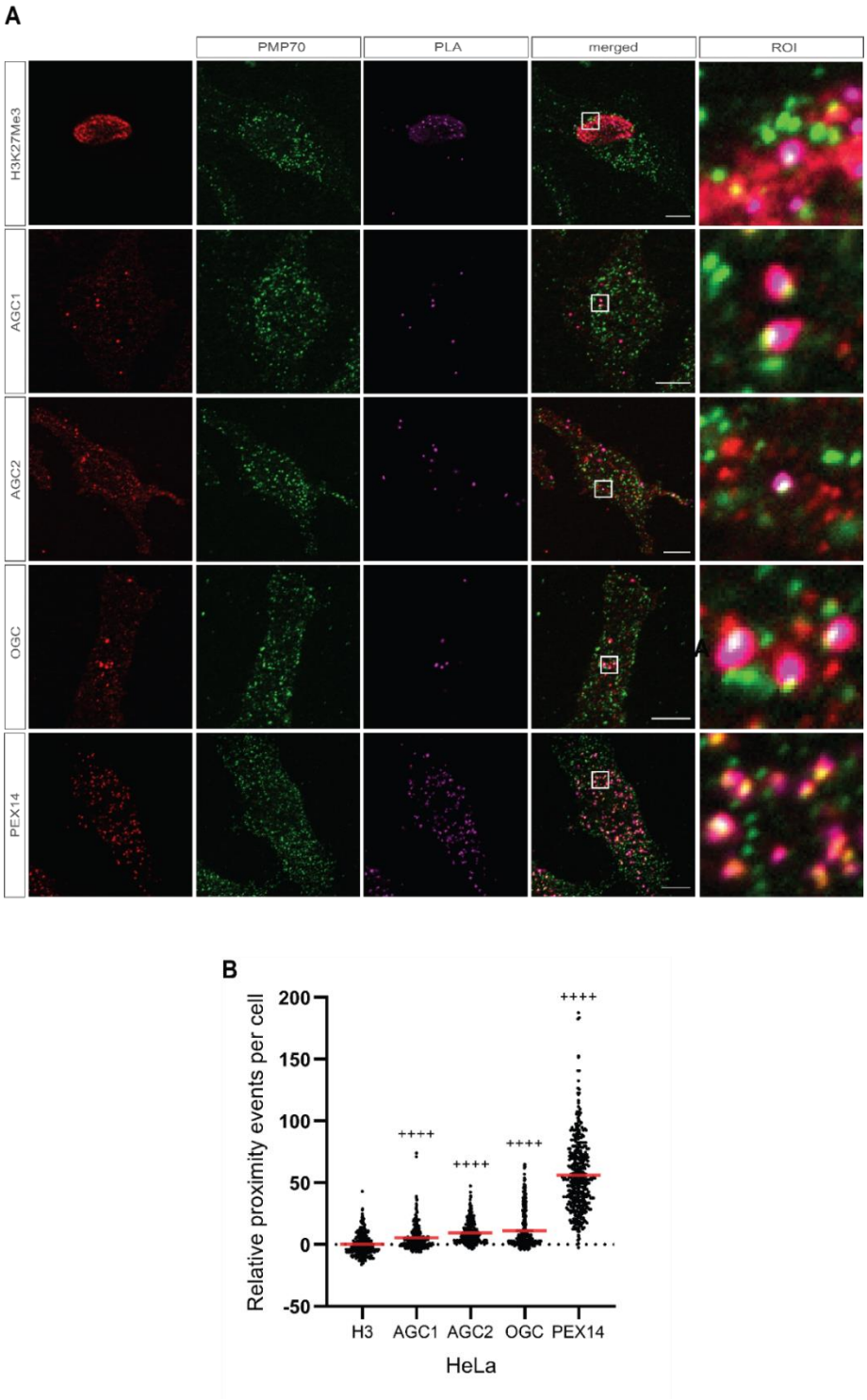

Figure 19 – Proximity between MAS transporters and PMP70 adds evidence to their presence in peroxisomes.
HeLa cells were fixed and the proximity between the POI and the peroxisomal membrane protein PMP70 was measured with the proximity ligation assay Duolink In Situ (Sigma-Aldrich). Cells were marked against mouse anti-human PMP70 together with either rabbit anti-human AGC1, AGC2, OGC, H3, or PEX14, followed by image acquisition under the microscope. For quantification, the signal representing proximity was assessed both with combined antibodies, as with single antibodies. The negative control H3 was given the value 0, and the other values were scaled accordingly. Normal distribution of the data was analyzed with Shapiro-Wilk test, and statistical analysis was performed with Mann-Whitney test. $^{++++}p \leq 0.0001$. Scale bars are 10 µm.

Discussion

Since the discovery of the extended malate dehydrogenase 1 (MDH1x) and lactate dehydrogenase B (LDHBx), it has been known that these proteins are capable to reach peroxisomes. The extensions, added by the means of translational readthrough, contain a PTS1 at the C-terminus, allowing their import into peroxisomes (Hofhuis et al., 2016; Schueren et al., 2014). Nevertheless, their function within the peroxisomal lumen remains unclear.

It has been hypothesized that the presence of both MDH1x and LDHBx in peroxisomes may play a role in the oxidation of NADH within peroxisomes as part of shuttling systems, where the necessary metabolites are transported across the peroxisomal membrane through membrane carriers. In addition, since MDH1 and LDHB form dimers and tetramers in the cytosol, respectively, and the peroxisomal transport mechanism is able to import fully folded oligomers, MDH1x and LDHBx should be able to piggy-back non-extended isomers into the peroxisomal lumen, thereby increasing the intraperoxisomal pool even further (Hall et al., 1992; Thoms, 2015).

Induction of readthrough leads to higher import of MDH1 and LDHB into peroxisomes

For MDH1x and LDHBx, their expression depends on the readthrough levels during translation of MDH1 and LDHB, respectively. It has been demonstrated that around 4% of MDH1, and 1.6% of LDHB undergoes this process (Hofhuis et al., 2016; Schueren et al., 2014). Therefore, in this study, it was determined if increasing the readthrough likelihood would lead to an increase in the translation of MDH1x and LDHBx, and with this, of their peroxisomal presence. To achieve this, HEK and HeLa cells were treated for 24 hours with the aminoglycoside geneticin, also known as G418, which induces ribosomal readthrough at the stop codon (Burke and Mogg, 1985). After the incubation, cells were fixed and immunostained against MDH1 or LDHB, and PEX14.

For the analysis of peroxisomal localization, the fluorescent signal of PEX14 was thresholded, while for MDH1 and LDHB, the intensity information of the whole cell was used. This was done because thresholding would leave much of the pixel information out of the analysis, since both are, in contrast to PEX14, mainly cytosolic proteins. The interaction of both signals was analyzed in terms of Pearson's correlation coefficient (PCC), which determines the linear relation between two variables. Then, PCC values were converted with Fisher's z-transformation into an

almost normally distributed measurement, named PCC-Z, which was then used for the statistical analysis of the different groups.

The incubation with geneticin resulted in an induction of peroxisomal presence of MDH1 in both HEK and HeLa, showed by an increase in colocalization. This goes in line with the findings of Hofhuis et al., 2016, where the levels of MDH1x were measured by introducing a Venus/hRluc dual reporter containing full-length MDH1 in HeLa cells. Interestingly, they observed an increase in readthrough of over three fold after treatment with geneticin, from 4.3% to 13.1%, while the changes observed in the present work look considerably smaller. Nevertheless, it is important to consider that while in Hofhuis et al., 2016, the levels of translation readthrough were measured, in this work, the levels of peroxisomal MDH1 caused by the increase in FTR are showed, opening the question of why is there a difference between both data sets. One possibility is that even when the FTR process increases the levels of PTS1-containing MDH1, and with this its import into peroxisomes, other mechanisms play a role in the average levels of MDH1 within peroxisomes. For example, by regulating its export through ubiquitination which could lead to an export of MDH from the peroxisomes (Williams, 2014). On top of this, being PCC a non-linear measurement, it is difficult to estimate how much higher, or how far apart, is one PCC value from the other, even when the differences are a significant.

A similar situation was observed for LDHB, where while a significant increase in the peroxisomal PCC levels was observed both in HEK and HeLa cells, the difference seems rather small compared to the effect produced by geneticin in the work of Schueren et al., 2014. Here, they observed an increase in FTR from 1.55% to 4.38% in LDHB after treatment with geneticin, using a Venus/hRluc dual reporter system.

With this, not only an indirect confirmation of previous observations showing that geneticin increases translation of MDH1x and LDHBx was obtained, but also that both proteins have higher presence in peroxisomes after readthrough induction. Importantly, it is still unknown what kind of regulation mechanisms are involved in both the expression and activity of MDH1x and LDHBx. For MDH1, it has been described that post-translational acetylation plays a role in its activity, but not in its expression (Zhao et al., 2010). In the case of LDHB, it was recently shown that Aurora-A, a mitosis-related kinase, promotes NAD^+ regeneration by increasing LDHB activity in cancer cells (Cheng et al., 2019).

Deletion of its extension reduces the peroxisomal import of MDH1, but not of LDHB

Then, as the influence of readthrough in the peroxisomal presence of MDH1 and LDHB was confirmed, cell lines lacking the extended proteins MDH1x and LDHBx were engineered in order to have a system to analyze the importance of these proteins in peroxisomes, and by extension, of the peroxisomal malate/aspartate (pMAS) and lactate/pyruvate shuttles (pLS).

For MDH1, the extension translated by means of readthrough comprises 57 nucleotides, ending with a PTS1 adjacent to the second stop codon (Hofhuis et al., 2016). In order to prevent MDH1 to reach peroxisomes, the region after the first stop codon was targeted with CRISPR-Cas9 in both HeLa cells and iPSCs. This resulted in a deletion of five nucleotides, starting at the second position after the first stop codon and provoking a frameshift that prevents the translation of the PTS1 signal. Additionally, due to the frameshift, a set of three stop codons was now present almost immediately after the first stop codon, meaning that even when readthrough occurs, it only adds one additional amino acid, but not a PTS1.

In the case of LDHB, the extension after the first stop codon is only 18 nucleotides long, from which the nine last nucleotides correspond to the PTS1 at the C-termini (Schueren et al., 2014). Through CRISPR-Cas9, a heterozygous mutation was achieved in iPSC, starting at the tenth nucleotide after the first stop codon. In one of the alleles, a deletion of five nucleotides was obtained, while in the other allele, a deletion of three nucleotides was achieved. In both cases, the deletion led to a frameshift, deleting the PTS1 signal at the end of the extension.

Since changes in the mRNA can cause instability, affecting the protein expression (Chamary et al., 2006), it was assessed if these mutations had an effect in the total protein amount of MDH1 and LDHB, through western blot. No differences were observed in the relative amounts of MDH1 in HEK MDH1Δx cells, nor in iPSC MDH1Δx, when compared to their respective wild type. Likewise, no differences were observed in the relative LDHB amount in iPSC LDHBΔx, when compared to wild type. However, in spite of the lack of PTS1 in both MDH1x and LDHBx, it is important to notice that these extended proteins are likely still being translated, and that the deletions might have an effect in the translation and stability of their respective proteins. For example, these mutations might have an influence on the readthrough levels, because they are in the region of the stop codon context. This is especially true for MDH1Δx, where the mutation starts at the second position after the stop

codon, a position which has been shown to be relevant for inducing readthrough (Schueren et al., 2014; Wangen and Green, 2020). Additionally, it is not known if these extended mutated proteins are to be degraded, or kept in the cytosol. The lack of a reduction in the levels of MDH1 and LDHB in the mutants suggests that the extended versions of MDH1 and LDHB in mutants are not degraded, or that the reduction is so small that is not measurable by this method. Altogether, the development of cell lines lacking MDH1x and LDHBx, while keeping unaffected the expression of MDH1 and LDHB, will help to assess their function and relevance in peroxisomes.

Later, the peroxisomal localization levels of MDH1 were measured in HEK MDH1Δx in terms of Pearson's correlation coefficient (PCC) through the analysis of immunofluorescence experiments. As in geneticin experiments, the PCC values were converted with Fisher's z-transformation for statistical analysis. Interestingly, even though a significant reduction in the peroxisomal levels of MDH1 was observed independently of the antibodies used, a higher decrease was observed when rabbit anti-human MDH1 was used. This difference might be due to the characteristics of the antibodies against PMP70 and PEX14, which do not overlap completely with each other, as it was observed later when used as control in the proximity ligation assay. This might also address the higher dispersion of the data obtained when rabbit anti-human MDH1 was used, in comparison to the results acquired with mouse anti-human MDH1.

Overall, these results support the PTS1 at the C-terminal region of MDH1 as a cause in the import of MDH1 into peroxisomes. Nevertheless, it is important to point out the limitations of this method. For example, with the current method is impossible to know if peroxisomes are completely free of MDH1, or if the import is only reduced. This is because any cytosolic protein, as MDH1 and LDHB, will randomly colocalize with peroxisomes to a certain extent. This means that a PCC-Z of zero is not likely, underestimating the real change in colocalization between wild type and mutant.

Then, the peroxisomal presence of MDH1 was assessed in the iPSC-mutants, both lacking the extension at MDH1 and LDHB. As done previously with HEK cells, colocalization was measured in terms of PCC and converted into PCC-Z for statistical analysis. The mutation at the extension of MDH1x, in iPSC MDH1Δx, resulted in a decrease in PCC-Z, indicating a reduction in the presence of MDH1 in peroxisomes thanks to the lack of PTS1-containing MDH1. This reduction was independent of the antibody used (Figure 7A), presenting a reduction of 0.0056 in PCC-Z with mouse anti-human MDH1, while a 0.007 decrease was observed when rabbit anti-human MDH1 was used (Figure 7B). Interestingly, the peroxisomal localization of MDH1 was

also altered in the iPSC LDHBΔx. An increase of 0.0079 in PCC-Z was observed when the analysis was performed using mouse anti-human MDH1 (Figure 7A), while an increase of 0.0056 was observed when rabbit anti-human MDH1 was used (Figure 7B). This might be due to a compensatory effect by MDH1, when LDHB is not present in peroxisomes. MDH1 might supply support for the lack of NADH oxidation. However, this would be assuming that both proteins are present in peroxisomes in this cell type, and that their processes are regulated together. As it was the case with HEK, these results support the presence of MDH1 in peroxisomes, imported due to the presence of a hidden PTS1 signal translated by FTR.

Surprisingly, when the levels of peroxisomal LDHB were assessed in iPSCs, the levels were higher in cells lacking LDHBx than in wild type. These results are contradictory with the premise that LDHBx is imported in peroxisomes solely by its PTS1 extension. In this respect, it has been already showed by Schueren et. al, 2014, that LDHB can acquire a PTS1 signal through FTR, and the increase of peroxisomal LDHB through the induction of readthrough has also been demonstrated in this work. Since the genetic background of iPSC LDHBΔx was confirmed, it is possible that LDHB is imported into peroxisomes by more than one mechanism. Also, the fact that one of the measurements on the MDH1Δx mutants showed lower levels of LDHB in peroxisomes, suggests a joint import mechanism, where the lack of PTS1 signal in LDHB is compensated in a mechanism involving MDH1, while in MDH1Δx mutants, less import of peroxisomal LDHB is observed. In future studies, more research on the dependency of LDHB on MDH1 has to be done, but this objective escapes the focus of this thesis.

Lack of MDH1x and LDHBx increase ROS levels in iPSCs

Peroxisomes are known for harboring a vast array of metabolic pathways, many of which produce reactive oxygen species like H_2O_2. Nonetheless, the same species are mainly reduced within peroxisomes by enzymes like catalase, glutathione peroxidase and peroxiredoxin V (Wanders and Waterham, 2006). Since the lack in MDH1x and LDHBx could have an effect in the redox levels, due to the lack in NAD^+ within peroxisomes, glutathione (GSH) levels and catalase activity were measured.

In the case of GSH levels, iPSCs showed an increase of 90.2% and 54.3% in cells lacking MDH1x and LDHBx, respectively. These results suggest a cellular mechanism in response to increased basal redox levels, to which cells increase its reduction capacity by increasing its GSH levels. The tripeptide GSH importance lays in its participation against ROS, acting as a potent antioxidant in the detoxification of peroxides through catalysis in a process mediated by GSH peroxidase (GPx)

(Townsend et al., 2003). Although is mainly present in the cytosol, peroxisomes also show glutathione peroxidase activity (Morel et al., 2004). Additionally, oxidants are capable to promote the expression of GSH through response elements (Moinova and Mulcahy, 1998; Wild et al., 1998). Therefore, the increase in GSH is likely a direct response to the increased ROS levels within peroxisomes, and maybe the whole cell, due to the lack of MDH1x and LDHBx.

Furthermore, considering that the lack of MDH1x and LDHBx might result in lack of NAD^+, two peroxisomal pathways may be impaired and, as a consequence, be involved in the increase of oxidative stress: α- and β-oxidation. In β-oxidation, NAD^+ is required for the conversion of 3-hydroxyacil into beta-ketoacyl-CoA by the 3-hydroxyacil-CoA dehydrogenase activity of one of the peroxisomal bifunctional enzymes (PBE), L-PBE and D-PBE (Wanders and Waterham, 2006). The importance of PBE can be appreciated by the severe symptoms of its deficiency, which include hypotonia, elevated VLCFA and bile acid in plasma, uncontrolled seizures in the case of L-PBE deficiency, and accumulation of DHCA, THCA and pristanic acid in DBP deficiency (Wanders, 2004). Thus, the increase in oxidative stress and GSH may be due to the limited availability of NAD^+. In α-oxidation, NAD^+ is necessary for the conversion of pristanal into pristanic acid by an enzyme with pristanal dehydrogenase activity, presumably fatty aldehyde dehydrogenase (FALDH) (Ashibe et al., 2007; Jansen et al., 2001). Mutations in FALDH lead to the presentation of the Sjörgen-Larsson Syndrome, a disease characterized by accumulation of LCFA alcohols, together with mental and physical handicap (Lloyd et al., 2007; Rizzo et al., 1999). Nevertheless, FALDH exists in two forms produced by alternative splicing, the peroxisomal FALDH-V and FALDH-N, which resides in the ER (Ashibe et al., 2007). Additionally, it has been shown that when overexpressed, FALDH-V has a protective effect against the oxidative damage produced by phytanic acid (Ashibe et al., 2007). All things considered, it is likely that a decrease in the available NAD^+ is responsible for a decline in the action of FALDH, increasing oxidative stress and with this the GSH levels.

When catalase activity was measured in iPSCs lacking MDH1x and LDHBx, an increase of 24% and 88.2% was observed, respectively, suggesting a response to higher production of H_2O_2. Catalase is widely responsible for the control of H_2O_2 levels (Mueller et al., 1997), as it decomposes H_2O_2 into O_2 and H_2O with an impressively high rate constant of around $10^{7}\ _{M}{}^{-1}\ s^{-1}$ (Young, 2001). Since the iPSC mutants MDH1Δx and LDHBΔx lack a protein expected to participate in the oxidation of NADH, the increase observed in catalase activity might be due to decreased availability of

NAD^+ within peroxisomes, as previously observed with GSH. A protein that might be involved in this process is xanthine dehydrogenase (XDH), the rate-limiting enzyme of purine catabolism, responsible of the conversion of xanthine into urate while reducing NAD^+ into NADH (Frederiks and Vreeling-Sindelárová, 2002; McManaman and Bain, 2002; Pritsos, 2000). Interestingly, when NAD^+ is widely available, XDH will opt for NAD^+ as an electron acceptor, but once the xanthine/NAD^+ reaction has gone to completion, the NADH produced can be consumed through the NADH oxidase activity of XDH, producing superoxide, contributing to redox and increasing catalase activity (Harris and Massey, 1997; Sanders et al., 1997). Additionally, XDH can be converted into xanthine oxidase (XOD), which also mediates the conversion of xanthine into uric acid, but with O_2 as electron donor, producing H_2O_2 in the process (Della Corte et al., 1969). In both cases, the lack of NAD^+ could increase superoxide production by enzymes like XDH, increasing catalase activity in cells lacking MDH1x and LDHBx.

Deletion of MDH1x and LDHBx has an effect on mitochondrial respiration

Over the past years, the importance of the connection between organelles has become evident by the way they work together, and peroxisomes are no exception of this collaboration. For example, interaction of peroxisomes with ER contemplate the biosynthesis of ether-phospholipids, glycosyl phosphatidyl inositol (GPI)-anchored proteins and polyunsaturated fatty acids, processes which are divided between both organelles (Braverman and Moser, 2012; Kanzawa et al., 2012; Sprecher and Chen, 1999). Moreover, interaction between lipid droplets and peroxisomes implies an exchange in lipids between both organelles. Although the molecular basis of this interaction remains elusive, indirect evidence supports this connection, like the enlargement of lipid droplets when β-oxidation is defective (Schrader et al., 2015).

Particularly interesting is the connection between peroxisomes and mitochondria. Many elements advocate for a rich connection between these two organelles, like their closeness, evidenced for decades by spatial proximity through microscopy, also by the fact that they share fission machinery elements, and that they coordinate their abundance through shared transcriptional regulatory mechanisms (reviewed in Fransen et al., 2017). Additionally, one tethering complex has been reported, containing both peroxisomal and mitochondrial targeting signal in opposite terminal regions (Fan et al., 2016). More importantly, peroxisomes are intertwined with mitochondria through several metabolic processes. For example, β-oxidation of fatty acids takes place in both organelles, shorter fatty acids are preferably metabolized in

mitochondria (reviewed in Wanders et al., 2010), while larger and branched fatty acids are metabolized in peroxisomes (Van Veldhoven, 2010). Additionally, mitochondria and peroxisomes are important participants in the redox balance and homeostasis of the cell (Nordgren and Fransen, 2014). This not only individually, but it is known that changes in catalase activity affect the redox state of mitochondria (Barbosa et al., 2013). Also, one of the most important redox scavengers in mitochondria is GSH (Murphy, 2012). Thus, as changes were observed in both these redox parameters, in addition to the wide connection between peroxisomes and mitochondria, mitochondrial respiration was assessed in iPSCs lacking MDH1x and LDHBx.

As a result, a statistically significant increase in basal respiration was observed in iPSCs lacking MDH1x and LDHBx. Wild type cells showed a basal respiration of 362.2 pmol/min, in MDH1Δx mutants mitochondrial respiration was 8.8% lower, while in LDHBΔx mutants the decrease in respiration was of 24.2%. Basal respiration comprises mainly two processes, the respiration involved in ATP synthesis and in proton leak (Divakaruni et al., 2014). Thus, the low basal respiration might be due to one, or both of these processes.

ATP-linked respiration, also referred as ATP production, can be affected by processes like the intrinsic ATP demand of the cell, impaired ATP synthesis levels, or by the substrate supply and oxidation. The ATP production levels were not significantly lower in MDH1Δx cells than in wild type, although a tendency was observed. For LDHBΔx cells, a significant decrease was observed in ATP production, which seems to contribute to lower levels in basal respiration.

The proton leak-linked respiration corresponds to the portion of protons that cross back the mitochondrial inner membrane without being used for ATP synthesis (Jastroch et al., 2010, p. 10). This might represent a change in the membrane conductance for the LDHBΔx mutant, since no changes were observed in the maximal respiration after the uncoupler FCCP was used (Divakaruni and Brand, 2011). As for MDH1Δx, a small decrease was observed in proton leak, yet is not significant. Hence, it seems that for both mutants is the sum of changes in both ATP production and leak proton that lead to a decrease in basal respiration, being more prominent in the case of iPSC LDHBΔx.

Additionally, the levels of non-mitochondrial oxygen consumption were significantly lower in cells lacking MDH1x, a 19.5% lower than wild type. This may involve two different scenarios, first, a difference in the number of cells, which is unlikely the case since cells lacking MDH1Δx show the same growing pattern as wild type, or second,

differences in cytoplasmic oxidases, which might be a result of higher redox levels, as shown in the GSH and catalase assays.

Overall, the lack of MDH1x and LDHBx in iPSCs had a small effect in mitochondrial respiration, as seen in basal respiration. This might be due to an overall effect in the redox state of the cell, as well as for a more direct interaction between peroxisomes and mitochondria, although both options are at this point just speculation.

Peroxisomes in HeLa contain AGC1, AGC2 and OGC, while only AGC2 is present in peroxisomes of iPSC-CMs

For oxidizing NADH within peroxisomes, the pMAS needs carriers to transport metabolites across the peroxisomal membrane. In mitochondria, this is performed by three proteins, AGC1 and AGC2 that mediate the exchange of aspartate and glutamate, and OGC, responsible for the exchange of 2-oxoglutarate and malate (reviewed in Palmieri, 2004).

The distribution of AGC1, AGC2 and OGC was assessed through the expression of their EGFP-tagged versions in HeLa cells, showing the mitochondrial and peroxisomal presence of these proteins with the help of a mitochondrial an peroxisomal marker. Interestingly, even considering the overexpression of AGC1, AGC2 and OGC, not all peroxisomes showed presence of these proteins, suggesting that the import of these proteins might be reserved for a subpopulation of peroxisomes. Additionally, it is known that when peroxisomes are isolated in subpopulations from different fractions, each subpopulation presents distinct matrix and membrane proteins, suggesting the presence of specialized peroxisomes (Islinger et al., 2012; Völkl et al., 1999). These subpopulations of peroxisomes, as suggested in Shai et al., 2016, could also be an answer for interaction between peroxisomes and different organelles, which could be the case of peroxisomes containing AGC1, AGC2 and OGC.

After validating the use of the antibodies against the MAS transporters, the presence in peroxisomes of AGC1, AGC2 and OGC was quantified in HeLa cells. Two important points were taken in consideration for the quantification of the peroxisomal colocalization of the MAS transporters: the basal proximity between peroxisomes and mitochondria, and the natural presence in mitochondria from the MAS transporters (Bisaccia et al., 1988; Hicks and Fahimi, 1977; Palmieri et al., 2001). Due to these factors, much of the colocalization between peroxisomes and the MAS transporters is expected to come from the overlap between mitochondria and peroxisomes. To avoid this, the measurement was performed from the perspective of the peroxisomes

alone, quantifying colocalization through the Manders´ overlap coefficient (MOC). MOC represents the portion of peroxisomal signal overlapped by the POI signal, after thresholding. Its value oscillates between zero, when there is no overlap, and one, for total overlap. However, with this method is necessary to have a reference to use as threshold, over which a mitochondrial protein can be expected to reside also in peroxisomes. For this, the colocalization between COX4, a mitochondrial membrane protein, and PMP70 was assessed in HeLa cells. The peroxisomal localization of COX4 showed an average of 0.169 in terms of MOC, which will be used as threshold for assessing the peroxisomal presence of AGC1, AGC2 and OGC. In addition to the mitochondrial control, two other controls were selected. As negative control, the peroxisomal localization of the lysosomal membrane protein LAMP1 was used, giving an average of 0.084. As positive control, the peroxisomal localization of PEX14 was measured, giving an average value of 0.688, representing the highest expectable value with this method. These findings go in line with the work of Valm et al., 2017, in COS-7 cells, where they showed that around 10% of peroxisomes are in contact with lysosomes, while around 20% are in contact with mitochondria.

The peroxisomal colocalization analysis of AGC1, AGC2 and OGC showed that all three proteins are significantly over the threshold set by COX4 in HeLa cells. The peroxisomal levels of OGC, with an average value of 0.361, are higher than both AGC1 and AGC2, with colocalization values of 0.238 and 0.219, respectively. This goes in line with the composition of the pMAS, since the transport aspartate and glutamate can be divided between AGC1 and AGC2, while OGC would be the only responsible for the transport of 2-oxoglutarate through the peroxisomal membrane, explaining the difference in colocalization between them. Nevertheless, the presence of both isoforms of AGC in peroxisomes could also be explained by the presence of two subtypes of peroxisomes, which contain either AGC1 or AGC2, together with OGC. Interestingly, the expression levels of AGC1, AGC2 and OGC seem to be independent of their expression levels in the cell, as seen from the information obtained from www.proteomicsdb.org (Schmidt et al., 2018). Here, expression values are presented as median protein expression (MPE) and calculated through the approach of intensity-based absolute quantification (Schwanhäusser et al., 2011). The expression levels of AGC2 are the highest (MPE = 6.02), relatively to AGC1 (MPE = 4.76) and OGC (MPE = 5.37), which suggests an import mechanism independent of the total expression in the cell.

As the adult human heart gets between 60 and 80% of its energy from fatty acids (Goldberg et al., 2012), peroxisomes and the presence of pMAS might be also play a

role in cardiac metabolism. The importance of peroxisomes is also highlighted by the cardiac phenotype of patients with adult Refsum´s disease, which present symptoms that expand from tachycardia to cardiac insufficiency (Koh et al., 2001; Wanders and Komen, 2007). For analysis of pMAS in cardiac cells, human induced pluripotent cells differentiated into cardiomyocytes (iPSC-CM) were used.

As done with HeLa, prior to quantifying the peroxisomal localization levels of AGC1, AGC2 and OGC, the peroxisomal presence of the controls LAMP1, COX4 and PEX14 was estimated. The values obtained for the controls in iPSC-CMs were similar as in HeLa, with a MOC of 0.072 for LAMP1, the lysosomal membrane protein used as a negative control. For COX4, a value of 0.141 was obtained, which acts as the threshold for peroxisomal presence of the MAS proteins, while for PEX14, an average value of 0.788 was calculated.

Then, the peroxisomal levels of AGC1, AGC2 and OGC were calculated. Strikingly, only AGC2 showed an average colocalization over the threshold, with a value of 0.257, while both AGC1 and OGC showed values barely over LAMP1, with an average of 0.096 and 0.078 respectively. In terms of function, the lack of AGC1 should not represent a problem, since AGC2 would be able to cover for the transport of aspartate and glutamate in pMAS. Notably, AGC1 is known to be highly expressed in the heart, while AGC2 is more present in liver (Amoedo et al., 2016). This would suggest, yet again, for an import mechanism of these proteins into peroxisomes that functions independently of the total expression of each protein.

Nevertheless, the lack of peroxisomal OGC presents itself as a problem for the presence of pMAS. Alternatively, another protein could cover for the transport of 2-oxoglutarate and malate, like the dicarboxylate carrier (DIC, SLC25A10), able to exchange oxaloacetate, malate, or 2-oxoglutarate against inorganic phosphate (Pi) (Mizuarai et al., 2005). Other candidates for substituting OGC could be 2-oxodicarbolxylate carrier (ODC, SLC25A21), a transporter able to counter exchange metabolites like 2-oxoadipate and 2-oxoglutarate, among others (Fiermonte et al., 2001). Or the uncoupling protein 2 (UCP2, SLC25A8), which can transport malate, oxaloacetate or aspartate, in exchange for phosphate and a proton (Vozza et al., 2014). Or perhaps UCP5 (SLC25A14) and UCP6 (SLC25A30), both able to transport malate in exchange for succinate, phosphate, sulfate, and thiosulfate (Gorgoglione et al., 2019). Nonetheless, it is important to notice that the replacement of OGC by any of the abovementioned carriers might not be as practical as OGC for the exchange of electrons.

Lastly, as a confirmation of the presence of the MAS transporters in peroxisomes of HeLa cells, a proximity ligation assay (PLA) was performed, which produces a fluorescent signal at the sites where the antibodies against the POI and the peroxisomal marker are at a distance of 40 nm or less.

All three MAS transporters showed significantly higher contact sites than the negative control, going in line with the colocalization results measuring MOC, where OGC showed the highest peroxisomal colocalization of the three transporters. Interestingly, the values of AGC1 and AGC2 are further from each other than in the colocalization assay. Nevertheless, such a difference may be due to the distribution of the transporters throughout the peroxisomal membrane, considering that peroxisomes size oscillates between 0.1 and 1 µm in diameter (Grabenbauer et al., 2000), and that the resolution of the PLA is around 40 nm. This means that even though there is certainly close contact between PMP70 and both AGC1 and AGC2, the distribution of the two latter within the peroxisome might differ. Additionally, it cannot be completely ruled out that some of the contact sites are given by closeness between the peroxisomal marker and the MAS proteins residing in the mitochondrial membrane, even though the mMAS transporters are part of the inner membrane of mitochondria.

Furthermore, there is the question of how do these membrane proteins reach peroxisomes. One appealing transport mechanism involves mitochondrial-derived vesicles. Said vesicles have been shown to import the membrane mitochondria-anchored protein ligase (MAPL) into a subgroup of peroxisomes (Neuspiel et al., 2008). Another possibility, is that these proteins are already part of pre-peroxisomes derived for mitochondria, which mature when fused with pre-peroxisomes from ER (Sugiura et al., 2017). Nevertheless, the production of pre-peroxisomes derived from mitochondria has only been shown in cells lacking PEX3, where their production is the result of the restauration of PEX3 in the cell, not being certain if this process occurs also under normal conditions.

Altogether, this work presents evidence of the presence of MDH1 and LDHB in peroxisomes of HeLa and HEK cells, by inducing their import with geneticin treatment. Additionally, the occurrence of MDH1 in peroxisomes was confirmed by mutating the region after the first stop codon, deleting MDH1x in both HEK cells and iPSCs. This was not the case for LDHB, since the deletion of LDHBx caused an increase in peroxisomal LDHB by unknown mechanisms. Also, evidence of the peroxisomal localization of the mitochondrial proteins AGC1, AGC2 and OGC was provided by comparing peroxisomal colocalization, as well as through PLA, adding proof to the existence of a pMAS in charge of the oxidation of NADH. Nevertheless, for iPSC-CMs

only one transporter was recognized to be in peroxisomes, AGC2. This opens the question of whether other carriers are involved in the process, or if the presence of pMAS is dependent on the cell type.

References

Agrimi, G., Russo, A., Scarcia, P., Palmieri, F., 2012. The human gene SLC25A17 encodes a peroxisomal transporter of coenzyme A, FAD and NAD+. *Biochem J* 443, 241–247. https://doi.org/10.1042/BJ20111420

Amoedo, N.D., Punzi, G., Obre, E., Lacombe, D., De Grassi, A., Pierri, C.L., Rossignol, R., 2016. AGC1/2, the mitochondrial aspartate-glutamate carriers. *Biochim Biophys Acta*. 2016 Oct; 1863, 2394–2412. https://doi.org/10.1016/j.bbamcr.2016.04.011

Antonenkov, V.D., Hiltunen, J.K., 2012. Transfer of metabolites across the peroxisomal membrane. *Biochim Biophys Acta*. 2012 Sep; 1822, 1374–1386. https://doi.org/10.1016/j.bbadis.2011.12.011

Antonenkov, V.D., Sormunen, R.T., Hiltunen, J.K., 2004. The rat liver peroxisomal membrane forms a permeability barrier for cofactors but not for small metabolites in vitro. *J. Cell. Sci*. 117, 5633–5642. https://doi.org/10.1242/jcs.01485

Ashibe, B., Hirai, T., Higashi, K., Sekimizu, K., Motojima, K., 2007. Dual Subcellular Localization in the Endoplasmic Reticulum and Peroxisomes and a Vital Role in Protecting against Oxidative Stress of Fatty Aldehyde Dehydrogenase Are Achieved by Alternative Splicing. *J Biol Chem*. 2007 Jul 13;282, 20763–20773. https://doi.org/10.1074/jbc.M611853200

Barbosa, M.R., Sampaio, I.H., Teodoro, B.G., Sousa, T.A., Zoppi, C.C., Queiroz, A.L., Passos, M.A., Alberici, L.C., Teixeira, F.R., Manfiolli, A.O., Batista, T.M., Cappelli, A.P.G., Reis, R.I., Frasson, D., Kettelhut, I.C., Parreiras-e-Silva, L.T., Costa-Neto, C.M., Carneiro, E.M., Curi, R., Silveira, L.R., 2013. Hydrogen peroxide production regulates the mitochondrial function in insulin resistant muscle cells: Effect of catalase overexpression. *Biochim Biophys Acta*. 2013 Oct; 1832, 1591–1604. https://doi.org/10.1016/j.bbadis.2013.04.029

Baumgart, E., Fahimi, H.D., Stich, A., Völkl, A., 1996. L-lactate dehydrogenase A4- and A3B isoforms are bona fide peroxisomal enzymes in rat liver. Evidence for involvement in intraperoxisomal NADH reoxidation. *J. Biol. Chem*. 271, 3846–3855.

Bersch, K., Lobos Matthei, I., Thoms, S., 2018. Multiple Localization by Functional Translational Readthrough, in: del Río, L.A., Schrader, M. (Eds.), Proteomics of Peroxisomes. *Subcell Biochem.* 2018;89:201–219. https://doi.org/10.1007/978-981-13-2233-4_8

Bisaccia, F., Indiveri, C., Palmieri, F., 1988. Purification and reconstitution of two anion carriers from rat liver mitochondria: The dicarboxylate and the 2-oxoglutarate carrier. *Biochim Biophys Acta.* 1988 Apr 22; 933, 229–240. https://doi.org/10.1016/0005-2728(88)90030-8

Bolte, S., Cordelières, F.P., 2006. A guided tour into subcellular colocalization analysis in light microscopy. *J Microsc* 224, 213–232. https://doi.org/10.1111/j.1365-2818.2006.01706.x

Braverman, N., Steel, G., Obie, C., Moser, A., Moser, H., Gould, S.J., Valle, D., 1997. Human PEX7 encodes the peroxisomal PTS2 receptor and is responsible for rhizomelic chondrodysplasia punctata. *Nat. Genet*. 15, 369–376. https://doi.org/10.1038/ng0497-369

Braverman, N.E., Moser, A.B., 2012. Functions of plasmalogen lipids in health and disease. *Biochim. Biophys. Acta* 1822, 1442–1452. https://doi.org/10.1016/j.bbadis.2012.05.008

Brocard, C., Hartig, A., 2006. Peroxisome targeting signal 1: is it really a simple tripeptide? *Biochim. Biophys. Acta* 1763, 1565–1573. https://doi.org/10.1016/j.bbamcr.2006.08.022

Brown, L.-A., Baker, A., 2008. Shuttles and cycles: transport of proteins into the peroxisome matrix (review). *Mol. Membr. Biol.* 25, 363–375. https://doi.org/10.1080/09687680802130583

Burke, J.F., Mogg, A.E., 1985. Suppression of a nonsense mutation in mammalian cells *in vivo* by the aminoglycoside anthiotics G–418 and paromomycin. *Nucl Acids Res* 13, 6265–6272. https://doi.org/10.1093/nar/13.17.6265

Chamary, J.V., Parmley, J.L., Hurst, L.D., 2006. Hearing silence: non-neutral evolution at synonymous sites in mammals. *Nat Rev Genet* 7, 98–108. https://doi.org/10.1038/nrg1770

Cheng, A., Zhang, P., Wang, B., Yang, D., Duan, X., Jiang, Yongliang, Xu, T., Jiang, Ya, Shi, J., Ding, C., Wu, G., Sang, Z., Wu, Q., Wang, H., Wu, M., Zhang, Z., Pan, X., Pan, Y., Gao, P., Zhang, H., Zhou, C., Guo, J., Yang, Z., 2019. Aurora-A mediated phosphorylation of LDHB promotes glycolysis and tumor progression by relieving the substrate-inhibition effect. *Nat Commun* 10, 5566. https://doi.org/10.1038/s41467-019-13485-8

Chornyi, S., IJlst, L., van Roermund, C.W.T., Wanders, R.J.A., Waterham, H.R., 2021. Peroxisomal Metabolite and Cofactor Transport in Humans. *Front. Cell Dev. Biol.* 8, 613892. https://doi.org/10.3389/fcell.2020.613892

De Bellis, M., Pisani, F., Mola, M.G., Rosito, S., Simone, L., Buccoliero, C., Trojano, M., Nicchia, G.P., Svelto, M., Frigeri, A., 2017. Translational readthrough generates new astrocyte AQP4 isoforms that modulate supramolecular clustering, glial endfeet localization, and water transport. *Glia* 65, 790–803. https://doi.org/10.1002/glia.23126

De Duve, C., Baudhuin, P., 1966. Peroxisomes (microbodies and related particles). *Physiol Rev*. 46, 323–357. https://doi.org/10.1152/physrev.1966.46.2.323

Della Corte, E., Gozzetti, G., Novello, F., Stirpe, F., 1969. Properties of the xanthine oxidase from human liver. *Biochim Biophys Acta*. 191, 164–166. https://doi.org/10.1016/0005-2744(69)90327-1

Divakaruni, A.S., Brand, M.D., 2011. The Regulation and Physiology of Mitochondrial Proton Leak. *Physiology (Bethesda)* 26, 192–205. https://doi.org/10.1152/physiol.00046.2010

Divakaruni, A.S., Paradyse, A., Ferrick, D.A., Murphy, A.N., Jastroch, M., 2014. Analysis and Interpretation of Microplate-Based Oxygen Consumption and pH Data, *Methods Enzymol.* pp. 309–354. https://doi.org/10.1016/B978-0-12-801415-8.00016-3

Dodt, G., Gould, S.J., 1996. Multiple PEX genes are required for proper subcellular distribution and stability of Pex5p, the PTS1 receptor: evidence that PTS1 protein import is mediated by a cycling receptor. *J Cell Biol*. 135, 1763–1774. https://doi.org/10.1083/jcb.135.6.1763

Fan, J., Li, X., Issop, L., Culty, M., Papadopoulos, V., 2016. ACBD2/ECI2-Mediated Peroxisome-Mitochondria Interactions in Leydig Cell Steroid Biosynthesis. *Mol Endocrinol*. 30, 763–782. https://doi.org/10.1210/me.2016-1008

Farrell, S.O., Fiol, C.J., Reddy, J.K., Bieber, L.L., 1984. Properties of purified carnitine acyltransferases of mouse liver peroxisomes. *J Biol Chem*. 259, 13089–13095. https://doi.org/10.1016/S0021-9258(18)90661-7

Felmlee, M.A., Jones, R.S., Rodriguez-Cruz, V., Follman, K.E., Morris, M.E., 2020. Monocarboxylate Transporters (SLC16): Function, Regulation, and Role in Health and Disease. *Pharmacol Rev* 72, 466–485. https://doi.org/10.1124/pr.119.018762

Felsenstein, K.M., Goff, S.P., 1988. Expression of the gag-pol fusion protein of Moloney murine leukemia virus without gag protein does not induce virion formation or proteolytic processing. *J. Virol*. 62, 2179–2182.

Ferdinandusse, S., Denis, S., IJlst, L., Dacremont, G., Waterham, H.R., Wanders, R.J., 2000. Subcellular localization and physiological role of alpha-methylacyl-CoA racemase. *J. Lipid Res*. 41, 1890–1896.

Ferdinandusse, S., Mulders, J., IJlst, L., Denis, S., Dacremont, G., Waterham, H.R., Wanders, R.J.A., 1999. Molecular Cloning and Expression of Human Carnitine Octanoyltransferase: Evidence for Its Role in the Peroxisomal β-Oxidation of Branched-Chain Fatty Acids. *Biochem Biophys Res Commun*. 263, 213–218. https://doi.org/10.1006/bbrc.1999.1340

Fiermonte, G., Dolce, V., Palmieri, L., Ventura, M., Runswick, M.J., Palmieri, F., Walker, J.E., 2001. Identification of the Human Mitochondrial Oxodicarboxylate Carrier. *J Biol Chem*. 276, 8225–8230. https://doi.org/10.1074/jbc.M009607200

Fransen, M., Lismont, C., Walton, P., 2017. The Peroxisome-Mitochondria Connection: How and Why? *Int J Mol Sci*. 18, 1126. https://doi.org/10.3390/ijms18061126

Fransen, M., Nordgren, M., Wang, B., Apanasets, O., 2012. Role of peroxisomes in ROS/RNS-metabolism: Implications for human disease. *Biochim Biophys Acta*. 1822, 1363–1373. https://doi.org/10.1016/j.bbadis.2011.12.001

Frederiks, W.M., Vreeling-Sindelárová, H., 2002. Ultrastructural localization of xanthine oxidoreductase activity in isolated rat liver cells. *Acta Histochem*. 104, 29–37. https://doi.org/10.1078/0065-1281-00629

Freitag, J., Ast, J., Bölker, M., 2012. Cryptic peroxisomal targeting via alternative splicing and stop codon read-through in fungi. *Nature* 485, 522–525. https://doi.org/10.1038/nature11051

Fujiki, Y., Abe, Y., Imoto, Y., Tanaka, A.J., Okumoto, K., Honsho, M., Tamura, S., Miyata, N., Yamashita, T., Chung, W.K., Kuroiwa, T., 2020. Recent insights into peroxisome biogenesis and associated diseases. *J Cell Sci*. 133, jcs236943. https://doi.org/10.1242/jcs.236943

Goldberg, I.J., Trent, C.M., Schulze, P.C., 2012. Lipid Metabolism and Toxicity in the Heart. Cell Metab. 15, 805–812. https://doi.org/10.1016/j.cmet.2012.04.006

Gorgoglione, R., Porcelli, V., Santoro, A., Daddabbo, L., Vozza, A., Monné, M., Di Noia, M.A., Palmieri, L., Fiermonte, G., Palmieri, F., 2019. The human uncoupling proteins 5 and 6 (UCP5/SLC25A14 and UCP6/SLC25A30) transport sulfur oxyanions, phosphate and dicarboxylates. *Biochim Biophys Acta Bioenerg*. 1860, 724–733. https://doi.org/10.1016/j.bbabio.2019.07.010

Gould, S.G., Keller, G.A., Subramani, S., 1987. Identification of a peroxisomal targeting signal at the carboxy terminus of firefly luciferase. *J. Cell Biol*. 105, 2923–2931.

Gould, S.J., Keller, G.-A., Hosken, N., Wilkinson, J., Subramani, S., 1989. A conserved tripeptide sorts proteins to peroxisomes. *J Cell Biol*. 108, 1657–1664.

Grabenbauer, M., Sätzler, K., Baumgart, E., Fahimi, H.D., 2000. Three-dimensional ultrastructural analysis of peroxisomes in HepG2 cells. Absence of peroxisomal reticulum but evidence of close spatial association with the endoplasmic reticulum. *Cell Biochem. Biophys*. 32 Spring, 37–49.

Gronemeyer, T., Wiese, S., Ofman, R., Bunse, C., Pawlas, M., Hayen, H., Eisenacher, M., Stephan, C., Meyer, H.E., Waterham, H.R., Erdmann, R., Wanders, R.J., Warscheid, B., 2013. The Proteome of Human Liver Peroxisomes: Identification of Five New Peroxisomal Constituents by a Label-Free Quantitative Proteomics Survey. *PLoS ONE* 8, e57395. https://doi.org/10.1371/journal.pone.0057395

Hall, M.D., Levitt, D.G., Banaszak, L.J., 1992. Crystal structure of Escherichia coli malate dehydrogenase. Journal of Molecular Biology 226, 867–882. https://doi.org/10.1016/0022-2836(92)90637-Y

Harrell, L., Melcher, U., Atkins, J.F., 2002. Predominance of six different hexanucleotide recoding signals 3' of read-through stop codons. *Nucleic Acids Res.* 30, 2011–2017.

Harris, C.M., Massey, V., 1997. The Oxidative Half-reaction of Xanthine Dehydrogenase with NAD; Reaction Kinetics and Steady-state Mechanism. *J Biol Chem*. 272, 28335–28341. https://doi.org/10.1074/jbc.272.45.28335

He, D., Barnes, S., Falany, C.N., 2003. Rat liver bile acid CoA:amino acid N-acyltransferase. *J Lipid Res*. 44, 2242–2249. https://doi.org/10.1194/jlr.M300128-JLR200

Hicks, L., Fahimi, H.D., 1977. Peroxisomes (microbodies) in the myocardium of rodents and primates. A comparative Ultrastructural cytochemical study. *Cell Tissue Res*. 175, 467–481.

Hofhuis, J., Schueren, F., Nötzel, C., Lingner, T., Gärtner, J., Jahn, O., Thoms, S., 2016. The functional readthrough extension of malate dehydrogenase reveals a modification of the genetic code. *Open Biol*. 6, 160246. https://doi.org/10.1098/rsob.160246

Hunt, M.C., Rautanen, A., Westin, M.A.K., Svensson, L.T., Alexson, S.E.H., 2006. Analysis of the mouse and human acyl-CoA thioesterase (ACOT) gene clusters shows that convergent, functional evolution results in a reduced number of human peroxisomal ACOTs. *FASEB J*. 20, 1855–1864. https://doi.org/10.1096/fj.06-6042com

Islinger, M., Abdolzade-Bavil, A., Liebler, S., Weber, G., Völkl, A., 2012. Assessing Heterogeneity of Peroxisomes: Isolation of Two Subpopulations from Rat Liver. *Methods Mol Biol*. pp. 83–96. https://doi.org/10.1007/978-1-61779-959-4_6

Jansen, G.A., van den Brink, D.M., Ofman, R., Draghici, O., Dacremont, G., Wanders, R.J.A., 2001. Identification of Pristanal Dehydrogenase Activity in Peroxisomes: Conclusive Evidence That the Complete Phytanic Acid α-Oxidation Pathway Is Localized in Peroxisomes. *Biochem Biophys Res Commun*. 283, 674–679. https://doi.org/10.1006/bbrc.2001.4835

Jansen, G.A., Wanders, R.J.A., 2006. Alpha-Oxidation. *Biochim Biophys Acta*. 1763, 1403–1412. https://doi.org/10.1016/j.bbamcr.2006.07.012

Jastroch, M., Divakaruni, A.S., Mookerjee, S., Treberg, J.R., Brand, M.D., 2010. Mitochondrial proton and electron leaks. *Essays Biochem*. 47, 53–67. https://doi.org/10.1042/bse0470053

Jones, J.M., Morrell, J.C., Gould, S.J., 2000. Identification and Characterization of HAOX1, HAOX2, and HAOX3, Three Human Peroxisomal 2-Hydroxy Acid Oxidases. *J Biol Chem*. 275, 12590–12597. https://doi.org/10.1074/jbc.275.17.12590

Jones, J.M., Nau, K., Geraghty, M.T., Erdmann, R., Gould, S.J., 1999. Identification of Peroxisomal Acyl-CoA Thioesterases in Yeast and Humans. *J Biol Chem*. 274, 9216–9223. https://doi.org/10.1074/jbc.274.14.9216

Kanzawa, N., Shimozawa, N., Wanders, R.J.A., Ikeda, K., Murakami, Y., Waterham, H.R., Mukai, S., Fujita, M., Maeda, Y., Taguchi, R., Fujiki, Y., Kinoshita, T., 2012. Defective lipid remodeling of GPI anchors in peroxisomal disorders, Zellweger syndrome, and rhizomelic chondrodysplasia punctata. *J Lipid Res*. 53, 653–663. https://doi.org/10.1194/jlr.M021204

Kemp, S., Theodoulou, F.L., Wanders, R.J., 2011. Mammalian peroxisomal ABC transporters: from endogenous substrates to pathology and clinical significance: Mammalian peroxisomal ABC transporters. *Br J Pharmacol*. 164, 1753–1766. https://doi.org/10.1111/j.1476-5381.2011.01435.x

Kirkby, B., Roman, N., Kobe, B., Kellie, S., Forwood, J.K., 2010. Functional and structural properties of mammalian acyl-coenzyme A thioesterases. *Prog Lipid Res*. 49, 366–377. https://doi.org/10.1016/j.plipres.2010.04.001

Koh, J.T., Choi, H.H., Ahn, K.Y., Kim, J.U., Kim, J.H., Chun, J.-Y., Baik, Y.H., Kim, K.K., 2001. Cardiac Characteristics of Transgenic Mice Overexpressing Refsum Disease Gene-Associated Protein within the Heart. *Biochem Biophys Res Commun.* 286, 1107–1116. https://doi.org/10.1006/bbrc.2001.5510

Lametschwandtner, G., Brocard, C., Fransen, M., Van Veldhoven, P., Berger, J., Hartig, A., 1998. The difference in recognition of terminal tripeptides as peroxisomal targeting signal 1 between yeast and human is due to different affinities of their receptor Pex5p to the cognate signal and to residues adjacent to it. *J. Biol. Chem*. 273, 33635–33643.

Lazarow, P.B., Fujiki, Y., 1985. Biogenesis of peroxisomes. *Annu. Rev. Cell Biol*. 1, 489–530. https://doi.org/10.1146/annurev.cb.01.110185.002421

Le, A., Cooper, C.R., Gouw, A.M., Dinavahi, R., Maitra, A., Deck, L.M., Royer, R.E., Vander Jagt, D.L., Semenza, G.L., Dang, C.V., 2010. Inhibition of lactate dehydrogenase A induces oxidative stress and inhibits tumor progression. *Proc Natl Acad Sci U S A*. 107, 2037–2042. https://doi.org/10.1073/pnas.0914433107

Legakis, J.E., Koepke, J.I., Jedeszko, C., Barlaskar, F., Terlecky, L.J., Edwards, H.J., Walton, P.A., Terlecky, S.R., 2002. Peroxisome Senescence in Human Fibroblasts. *Mol Biol Cell*. 13, 4243–4255. https://doi.org/10.1091/mbc.e02-06-0322

Léon, S., Goodman, J.M., Subramani, S., 2006. Uniqueness of the mechanism of protein import into the peroxisome matrix: Transport of folded, co-factor-bound and oligomeric proteins by shuttling receptors. *Biochim Biophys Acta*. 1763, 1552–1564. https://doi.org/10.1016/j.bbamcr.2006.08.037

Lloyd, M.D., Boardman, K.D.E., Smith, A., van den Brink, D.M., Wanders, R.J.A., Threadgill, M.D., 2007. Characterisation of recombinant human fatty aldehyde dehydrogenase: Implications for Sjögren-Larsson syndrome. *J Enzyme Inhib Med Chem*. 22, 584–590. https://doi.org/10.1080/14756360701425360

Loughran, G., Chou, M.-Y., Ivanov, I.P., Jungreis, I., Kellis, M., Kiran, A.M., Baranov, P.V., Atkins, J.F., 2014. Evidence of efficient stop codon readthrough in four mammalian genes. *Nucleic Acids Res*. https://doi.org/10.1093/nar/gku608

McCaughan, K.K., Brown, C.M., Dalphin, M.E., Berry, M.J., Tate, W.P., 1995. Translational termination efficiency in mammals is influenced by the base following the stop codon. *Proc Natl Acad Sci U S A*. 92, 5431–5435.

McClelland, G.B., Khanna, S., González, G.F., Eric Butz, C., Brooks, G.A., 2003. Peroxisomal membrane monocarboxylate transporters: evidence for a redox shuttle system? *Biochem Biophys Res Commun*. 304, 130–135. https://doi.org/10.1016/S0006-291X(03)00550-3

McGroarty, E., Hsieh, B., Wied, D.M., Gee, R., Tolbert, N.E., 1974. Alpha hydroxy acid oxidation by peroxisomes. *Arch Biochem Biophys*. 161, 194–210. https://doi.org/10.1016/0003-9861(74)90251-3

McManaman, J.L., Bain, D.L., 2002. Structural and Conformational Analysis of the Oxidase to Dehydrogenase Conversion of Xanthine Oxidoreductase. *J Biol Chem*. 277, 21261–21268. https://doi.org/10.1074/jbc.M200828200

Mindthoff, S., Grunau, S., Steinfort, L.L., Girzalsky, W., Hiltunen, J.K., Erdmann, R., Antonenkov, V.D., 2016. Peroxisomal Pex11 is a pore-forming protein homologous to TRPM channels. *Biochim Biophys Acta*. 1863, 271–283. https://doi.org/10.1016/j.bbamcr.2015.11.013

Mizuarai, S., Miki, S., Araki, H., Takahashi, K., Kotani, H., 2005. Identification of Dicarboxylate Carrier Slc25a10 as Malate Transporter in de Novo Fatty Acid Synthesis. *J Biol Chem*. 280, 32434–32441. https://doi.org/10.1074/jbc.M503152200

Moinova, H.R., Mulcahy, R.T., 1998. An Electrophile Responsive Element (EpRE) Regulates β-Naphthoflavone Induction of the Human γ-Glutamylcysteine Synthetase Regulatory Subunit Gene. *J Biol Chem*. 273, 14683–14689. https://doi.org/10.1074/jbc.273.24.14683

Morel, F., Rauch, C., Petit, E., Piton, A., Theret, N., Coles, B., Guillouzo, A., 2004. Gene and Protein Characterization of the Human Glutathione S-Transferase

Kappa and Evidence for a Peroxisomal Localization. *J Biol Chem*. 279, 16246–16253. https://doi.org/10.1074/jbc.M313357200

Morita, M., Imanaka, T., 2012. Peroxisomal ABC transporters: Structure, function and role in disease. *Biochim Biophys Acta*. 1822, 1387–1396. https://doi.org/10.1016/j.bbadis.2012.02.009

Mueller, S., Riedel, H.D., Stremmel, W., 1997. Direct evidence for catalase as the predominant H2O2 -removing enzyme in human erythrocytes. *Blood*. 90, 4973–4978.

Murphy, M.P., 2012. Mitochondrial Thiols in Antioxidant Protection and Redox Signaling: Distinct Roles for Glutathionylation and Other Thiol Modifications. *Antioxid Redox Signal*. 16, 476–495. https://doi.org/10.1089/ars.2011.4289

Namy, O., Hatin, I., Rousset, J.P., 2001. Impact of the six nucleotides downstream of the stop codon on translation termination. *EMBO Rep*. 2, 787–793. https://doi.org/10.1093/embo-reports/kve176

Narváez-Rivas, M., Zhang, Q., 2016. Comprehensive untargeted lipidomic analysis using core–shell C30 particle column and high field orbitrap mass spectrometer. *J Chromatogr A*. 1440, 123–134. https://doi.org/10.1016/j.chroma.2016.02.054

Neuspiel, M., Schauss, A.C., Braschi, E., Zunino, R., Rippstein, P., Rachubinski, R.A., Andrade-Navarro, M.A., McBride, H.M., 2008. Cargo-selected transport from the mitochondria to peroxisomes is mediated by vesicular carriers. *Curr Biol*. 18, 102–108. https://doi.org/10.1016/j.cub.2007.12.038

Nordgren, M., Fransen, M., 2014. Peroxisomal metabolism and oxidative stress. *Biochimie.* 98, 56–62. https://doi.org/10.1016/j.biochi.2013.07.026

Osmundsen, H., 1982. Factors which can influence beta-oxidation by peroxisomes isolated from livers of clofibrate treated rats. Some properties of peroxisomal fractions isolated in a self-generated Percoll gradient by vertical rotor centrifugation. *Int J Biochem*. 14, 905–914.

Palmieri, F., 2004. The mitochondrial transporter family (SLC25): physiological and pathological implications. *Pflugers Arch*. 447, 689–709. https://doi.org/10.1007/s00424-003-1099-7

Palmieri, L., Pardo, B., Lasorsa, F.M., del Arco, A., Kobayashi, K., Iijima, M., Runswick, M.J., Walker, J.E., Saheki, T., Satrústegui, J., Palmieri, F., 2001. Citrin and aralar1 are Ca2+-stimulated aspartate/glutamate transporters in mitochondria. *EMBO J*. 20, 5060–5069. https://doi.org/10.1093/emboj/20.18.5060

Pellicoro, A., van den Heuvel, F.A.J., Geuken, M., Moshage, H., Jansen, P.L.M., Faber, K.N., 2007. Human and rat bile acid-CoA:amino acid *N* -acyltransferase are liver-specific peroxisomal enzymes: Implications for intracellular bile salt transport. *Hepatology*. 45, 340–348. https://doi.org/10.1002/hep.21528

Poirier, Y., Antonenkov, V.D., Glumoff, T., Hiltunen, J.K., 2006. Peroxisomal β-oxidation—A metabolic pathway with multiple functions. *Biochim Biophys Acta*. 1763, 1413–1426. https://doi.org/10.1016/j.bbamcr.2006.08.034

Pritsos, C.A., 2000. Cellular distribution, metabolism and regulation of the xanthine oxidoreductase enzyme system. *Chem Biol Interact*. 129, 195–208. https://doi.org/10.1016/S0009-2797(00)00203-9

Rachubinski, R.A., Subramani, S., 1995. How proteins penetrate peroxisomes. *Cell*. 83, 525–528. https://doi.org/10.1016/0092-8674(95)90091-8

Rampler, E., Criscuolo, A., Zeller, M., El Abiead, Y., Schoeny, H., Hermann, G., Sokol, E., Cook, K., Peake, D.A., Delanghe, B., Koellensperger, G., 2018. A Novel Lipidomics Workflow for Improved Human Plasma Identification and Quantification Using RPLC-MSn Methods and Isotope Dilution Strategies. *Anal Chem*. 90, 6494–6501. https://doi.org/10.1021/acs.analchem.7b05382

Rhodin, J.A.G., 1954. Correlation of ultrastructural organization : and function in normal and experimentally changed proximal convoluted tubule cells of the mouse kidney: an electron microscopic study. Dept. of Anatomy, Karolinska Institutet, Stockholm.

Rizzo, W.B., Carney, G., Lin, Z., 1999. The Molecular Basis of Sjögren-Larsson Syndrome: Mutation Analysis of the Fatty Aldehyde Dehydrogenase Gene. *Am J Hum Genet*. 65, 1547–1560. https://doi.org/10.1086/302681

Roermund, C.W.T., Visser, W.F., IJlst, L., Cruchten, A., Boek, M., Kulik, W., Waterham, H.R., Wanders, R.J.A., 2008. The human peroxisomal ABC half transporter ALDP functions as a homodimer and accepts acyl–CoA esters. *FASEB J*. 22, 4201–4208. https://doi.org/10.1096/fj.08-110866

Rokka, A., Antonenkov, V.D., Soininen, R., Immonen, H.L., Pirilä, P.L., Bergmann, U., Sormunen, R.T., Weckström, M., Benz, R., Hiltunen, J.K., 2009. Pxmp2 Is a Channel-Forming Protein in Mammalian Peroxisomal Membrane. *PLoS ONE.* 4, e5090. https://doi.org/10.1371/journal.pone.0005090

Sanders, S.A., Eisenthal, R., Harrison, R., 1997. NADH Oxidase Activity of Human Xanthine Oxidoreductase. Generation of Superoxide Anion. *Eur J Biochem*. 245, 541–548. https://doi.org/10.1111/j.1432-1033.1997.00541.x

Schindelin, J., Arganda-Carreras, I., Frise, E., Kaynig, V., Longair, M., Pietzsch, T., Preibisch, S., Rueden, C., Saalfeld, S., Schmid, B., Tinevez, J.-Y., White, D.J., Hartenstein, V., Eliceiri, K., Tomancak, P., Cardona, A., 2012. Fiji: an open-source platform for biological-image analysis. *Nat Methods.* 9, 676–682. https://doi.org/10.1038/nmeth.2019

Schmidt, T., Samaras, P., Frejno, M., Gessulat, S., Barnert, M., Kienegger, H., Krcmar, H., Schlegl, J., Ehrlich, H.-C., Aiche, S., Kuster, B., Wilhelm, M., 2018. ProteomicsDB. *Nucleic Acids Res*. 46, D1271–D1281. https://doi.org/10.1093/nar/gkx1029

Schrader, M., Costello, J.L., Godinho, L.F., Azadi, A.S., Islinger, M., 2016. Proliferation and fission of peroxisomes — An update. *Biochim Biophys Acta*. 1863, 971–983. https://doi.org/10.1016/j.bbamcr.2015.09.024

Schrader, M., Godinho, L.F., Costello, J.L., Islinger, M., 2015. The different facets of organelle interplay—an overview of organelle interactions. *Front Cell Dev Biol*. 3. https://doi.org/10.3389/fcell.2015.00056

Schueren, F., Lingner, T., George, R., Hofhuis, J., Dickel, C., Gärtner, J., Thoms, S., 2014. Peroxisomal lactate dehydrogenase is generated by translational readthrough in mammals. *Elife*. 3, e03640. https://doi.org/10.7554/eLife.03640

Schueren, F., Thoms, S., 2016. Functional Translational Readthrough: A Systems Biology Perspective. *PLoS Genet*. 12, e1006196. https://doi.org/10.1371/journal.pgen.1006196

Schwanhäusser, B., Busse, D., Li, N., Dittmar, G., Schuchhardt, J., Wolf, J., Chen, W., Selbach, M., 2011. Global quantification of mammalian gene expression control. *Nature*. 473, 337–342. https://doi.org/10.1038/nature10098

Shai, N., Schuldiner, M., Zalckvar, E., 2016. No peroxisome is an island - Peroxisome contact sites. *Biochim Biophys Acta*. 1863, 1061–1069. https://doi.org/10.1016/j.bbamcr.2015.09.016

Singh, I., 1996. Mammalian Peroxisomes: Metabolism of Oxygen and Reactive Oxygen Species. *Ann NY Acad Sci*. 804, 612–627. https://doi.org/10.1111/j.1749-6632.1996.tb18648.x

Smith, J.J., Aitchison, J.D., 2013. Peroxisomes take shape. *Nat Rev Mol Cell Biol*. 14, 803–817. https://doi.org/10.1038/nrm3700

Sprecher, H., Chen, Q., 1999. Polyunsaturated fatty acid biosynthesis: a microsomal-peroxisomal process. *Prostaglandins Leukot Essent Fatty Acids*. 60, 317–321. https://doi.org/10.1016/S0952-3278(99)80006-4

Sugiura, A., Mattie, S., Prudent, J., McBride, H.M., 2017. Newly born peroxisomes are a hybrid of mitochondrial and ER-derived pre-peroxisomes. *Nature*. 542, 251–254. https://doi.org/10.1038/nature21375

Thoms, S., 2015. Import of proteins into peroxisomthat's the es: piggybacking to a new home away from home. *Open Biol*. 5, 150148. https://doi.org/10.1098/rsob.150148

Townsend, D.M., Tew, K.D., Tapiero, H., 2003. The importance of glutathione in human disease. *Biomed Pharmacother*. 57, 145–155. https://doi.org/10.1016/S0753-3322(03)00043-X

Valm, A.M., Cohen, S., Legant, W.R., Melunis, J., Hershberg, U., Wait, E., Cohen, A.R., Davidson, M.W., Betzig, E., Lippincott-Schwartz, J., 2017. Applying systems-level spectral imaging and analysis to reveal the organelle interactome. *Nature*. 546, 162–167. https://doi.org/10.1038/nature22369

van de Beek, M.-C., Ofman, R., Dijkstra, I., Wijburg, F., Engelen, M., Wanders, R., Kemp, S., 2017. Lipid-induced endoplasmic reticulum stress in X-linked adrenoleukodystrophy. *Biochim Biophys Acta*. 1863, 2255–2265. https://doi.org/10.1016/j.bbadis.2017.06.003

van Roermund, C.W.T., IJlst, L., Wagemans, T., Wanders, R.J.A., Waterham, H.R., 2014. A role for the human peroxisomal half-transporter ABCD3 in the oxidation of dicarboxylic acids. *Biochim Biophys Acta*. 1841, 563–568. https://doi.org/10.1016/j.bbalip.2013.12.001

van Roermund, C.W.T., Visser, W.F., IJlst, L., Waterham, H.R., Wanders, R.J.A., 2011. Differential substrate specificities of human ABCD1 and ABCD2 in peroxisomal fatty acid β-oxidation. *Biochim Biophys Acta*. 1811, 148–152. https://doi.org/10.1016/j.bbalip.2010.11.010

Van Veldhoven, P.P., 2010. Biochemistry and genetics of inherited disorders of peroxisomal fatty acid metabolism. *J Lipid Res*. 51, 2863–2895. https://doi.org/10.1194/jlr.R005959

van der Zand, A., Gent, J., Braakman, I., Tabak, H.F., 2012. Biochemically Distinct Vesicles from the Endoplasmic Reticulum Fuse to Form Peroxisomes. *Cell*. 149, 397–409. https://doi.org/10.1016/j.cell.2012.01.054

Violante, S., Achetib, N., Roermund, C.W.T., Hagen, J., Dodatko, T., Vaz, F.M., Waterham, H.R., Chen, H., Baes, M., Yu, C., Argmann, C.A., Houten, S.M., 2019. Peroxisomes can oxidize medium- and long-chain fatty acids through a pathway involving ABCD3 and HSD17B4. *FASEB J*. 33, 4355–4364. https://doi.org/10.1096/fj.201801498R

Visser, W.F., van Roermund, C.W.T., Waterham, H.R., Wanders, R.J.A., 2002. Identification of human PMP34 as a peroxisomal ATP transporter. *Biochem Biophys Res Commun*. 299, 494–497. https://doi.org/10.1016/S0006-291X(02)02663-3

Völkl, A., Mohr, H., Fahimi H., D., 1999. Peroxisome Subpopulations of the Rat Liver: Isolation by Immune Free Flow Electrophoresis. *J Histochem Cytochem*. 47, 1111–1117. https://doi.org/10.1177/002215549904700902

Vozza, A., Parisi, G., De Leonardis, F., Lasorsa, F.M., Castegna, A., Amorese, D., Marmo, R., Calcagnile, V.M., Palmieri, L., Ricquier, D., Paradies, E., Scarcia, P., Palmieri, F., Bouillaud, F., Fiermonte, G., 2014. UCP2 transports C4 metabolites out of mitochondria, regulating glucose and glutamine oxidation. *Proc Natl Acad Sci U S A.* 111, 960–965. https://doi.org/10.1073/pnas.1317400111

Walker, C.L., Pomatto, L.C.D., Tripathi, D.N., Davies, K.J.A., 2018. Redox Regulation of Homeostasis and Proteostasis in Peroxisomes. *Physiol Rev*. 98, 89–115. https://doi.org/10.1152/physrev.00033.2016

Walton, P.A., Hill, P.E., Subramani, S., 1995. Import of stably folded proteins into peroxisomes. *Mol Biol Cell*. 6, 675–683.

Wanders, R.J.A., 2004. Metabolic and molecular basis of peroxisomal disorders: A review. *Am J Med Genet*. 126A, 355–375. https://doi.org/10.1002/ajmg.a.20661

Wanders, R.J.A., Komen, J.C., 2007. Peroxisomes, Refsum's disease and the alpha- and omega-oxidation of phytanic acid. *Biochem Soc Trans*. 35, 865–869. https://doi.org/10.1042/BST0350865

Wanders, R.J.A., Ruiter, J.P.N., IJlst, L., Waterham, H.R., Houten, S.M., 2010. The enzymology of mitochondrial fatty acid beta-oxidation and its application to follow-up analysis of positive neonatal screening results. *J Inherit Metab Dis.* 33, 479–494. https://doi.org/10.1007/s10545-010-9104-8

Wanders, R.J.A., Waterham, H.R., 2006. Biochemistry of mammalian peroxisomes revisited. *Annu Rev Biochem*. 75, 295–332. https://doi.org/10.1146/annurev.biochem.74.082803.133329

Wangen, J.R., Green, R., 2020. Stop codon context influences genome-wide stimulation of termination codon readthrough by aminoglycosides. *Elife*. 9, e52611. https://doi.org/10.7554/eLife.52611

Watkins, P.A., Ellis, J.M., 2012. Peroxisomal acyl-CoA synthetases. *Biochim Biophys Acta*. 1822, 1411–1420. https://doi.org/10.1016/j.bbadis.2012.02.010

Wiese, S., Gronemeyer, T., Ofman, R., Kunze, M., Grou, C.P., Almeida, J.A., Eisenacher, M., Stephan, C., Hayen, H., Schollenberger, L., Korosec, T., Waterham, H.R., Schliebs, W., Erdmann, R., Berger, J., Meyer, H.E., Just, W., Azevedo, J.E., Wanders, R.J.A., Warscheid, B., 2007. Proteomics characterization of mouse kidney peroxisomes by tandem mass spectrometry and protein correlation profiling. *Mol Cell Proteomics*. 6, 2045–2057. https://doi.org/10.1074/mcp.M700169-MCP200

Wild, A.C., Gipp, J.J., Mulcahy, R.T., 1998. Overlapping antioxidant response element and PMA responseelement sequences mediate basal and β-naphthoflavone-induced expression of the human γ-glutamylcysteine synthetase catalytic subunit gene. *Biochem J*. 332, 373–381. https://doi.org/10.1042/bj3320373

Williams, C., 2014. Going against the flow: A case for peroxisomal protein export. *Biochim Biophys Acta*. 1843, 1386–1392. https://doi.org/10.1016/j.bbamcr.2014.04.009

Yoshinaka, Y., Katoh, I., Copeland, T.D., Oroszlan, S., 1985. Murine leukemia virus protease is encoded by the gag-pol gene and is synthesized through suppression of an amber termination codon. *Proc Natl Acad Sci U S A*. 82, 1618–1622.

Young, I.S., 2001. Antioxidants in health and disease. *J Clin Pathol*. 54, 176–186. https://doi.org/10.1136/jcp.54.3.176

Zhao, S., Xu, W., Jiang, W., Yu, W., Lin, Y., Zhang, T., Yao, J., Zhou, L., Zeng, Y., Li, H., Li, Y., Shi, J., An, W., Hancock, S.M., He, F., Qin, L., Chin, J., Yang, P., Chen, X., Lei, Q., Xiong, Y., Guan, K.-L., 2010. Regulation of Cellular Metabolism by Protein Lysine Acetylation. *Science*. 327, 1000–1004. https://doi.org/10.1126/science.1179689.

Acknowledgments

Here I would like to thank all the people that made possible this work. First, I would like to thank Prof. Sven Thoms for supervising me along this exciting project. Without your support and understanding this would not have been possible.

I would also like to thank my committee members, Prof. Ralph Kehlenbach and Prof. Michael Müller, for their critical view and always-helpful suggestions. Additionally, I would like to extent my gratitude to Dr. Laura Zelarayán-Behrend, Prof. Tiago Outeiro and Dr. Dieter Klopfenstein, for being part of my examination board.

I would also like to show my gratitude to Dr. Julia Hofhuis for her constant help in the analysis and discussion of data, as well as during the writing process.

To Dr. Kristina Bersch I would like to express my gratitude for her assistance in the generation of plasmids, and her help during my arrival in the research group.

I would also like to thank the scientists whose work was indispensable for this project. I would like to thank Yelena Sargsyan for her work generating the AGC2 and OGC plasmids, Vishalini Venkatesan for the catalase activity and GSH measurements, and Fatima Kanwal Baig and Maya Walper for the iPSC-differentiation. For their assistance in the experiments involving mitochondrial respiration, I would like to extend a big thank you to Dr. Norman Liaw and Branimir Berečić, to Dr. Henry Klemp and Antony Grüness for the measurements involving fatty acids, and for her help in the design and realization of the PLA assays, I would like to thank Dr. Christina James.

In addition, I would like to express my gratitude to Prof. Jutta Gärtner, for having me in the Department of Child and Adolescent Health, as well as to the whole department for being always willing to help.

A big thank you to the Molecular Medicine program and everyone involved, as well as the GGNB team, for their assistance and help during the whole PhD process.

Finally, I would like to thank my family and friends for their support and love. I am very lucky to have you.